UNIVERSITÀ CAMPUS BIO-MEDICO DI ROMA

Dottorato di Ricerca in Ingegneria Biomedica - XXIV ciclo

ENGINEERING HUMAN MULTILAYER TISSUES: APPLICATIONS IN VASCULAR AND ORTHOPEDIC FIELDS

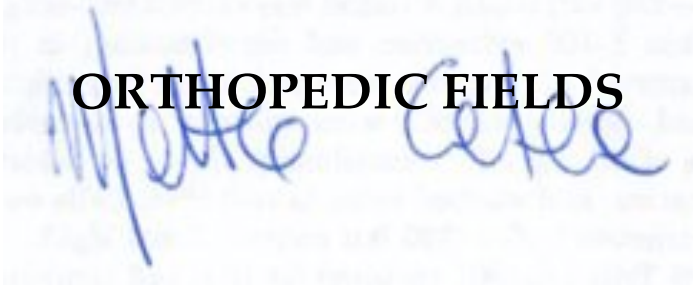

Candidate

Matteo Centola, M Eng

Supervisor

Prof. Marcella Trombetta

Co-supervisor

Alberto Rainer, PhD

Academic year 2010-2011

Engineering human multilayer tissues

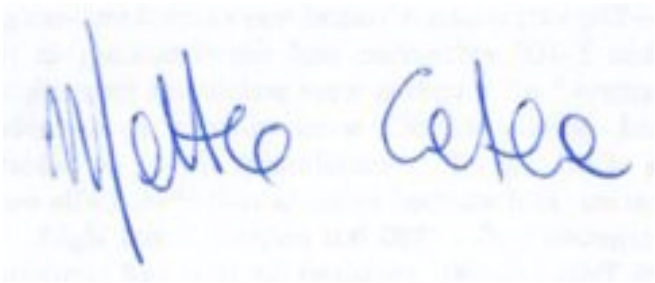

Alla mia famiglia, punto di riferimento insostituibile, fonte di amore inesauribile. Vi porto sempre con me.

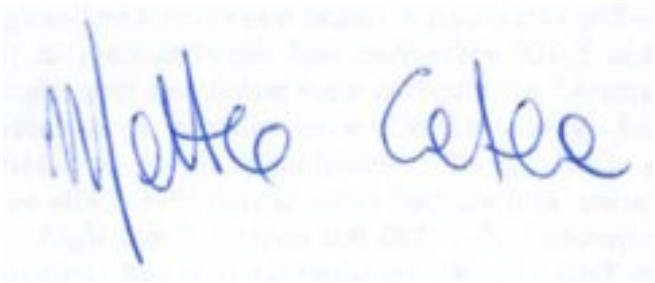

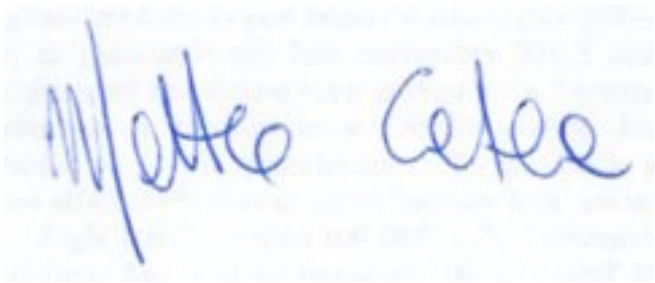

Summary

Abstract

This PhD thesis sets in tissue engineering (TE), a discipline which, starting from the principles of biology, medicine and engineering, it aims to restore, maintaining, or enhancing tissue and organ function. TE is performed following mainly three approaches: genetic engineering, cell therapy and scaffold/cells construct. The present work is focused on the latter approach, aiming to propose a change in its paradigm. In fact, TE by scaffold/cells construct develops in few consecutive steps, i.e. tissue harvesting, cell expansion in plastic, cell seeding onto a scaffold namely forming a so-called tissue engineering constructs (TECs), in vitro conditioning of TEC, and the final implantation into the donor site. However, targeting clinical translation, this strategy poses several constraints, especially in terms of economic burden, which still limits the definitive entrance of TE in clinics.To surmount this problem, hereby we propose a possible alternative way to repair or regenerate tissues presenting a multilayer architecture, with particular regard to blood vessels and articular cartilage. In particular, we propose a "one-step" approach, where the in vitro preconditioning of the constructs is not needed since the scaffold itself will provide the proper biochemical stimuli to the cells seeded therein. In our settings the differentiating factors are released from the scaffold, so driving the differentiation as well as the maturation of freshly-isolated constructs. Matching the neo extracellular matrix production time by seeded cells with polymer-based scaffold degradation time, it is possible to regenerate tissues directly in vivo, dramatically shortening times and costs, and also avoiding double-hospitalization.
We hypothesize that this *off-the-shelf* devices could simplify logistical issues surrounding transfer of tissue-engineered constructs into the clinical arena, reduce the need for large and expensive GMP tissue engineering facilities and minimize operator handling, with the likely final result of reducing the cost of engineered grafts.

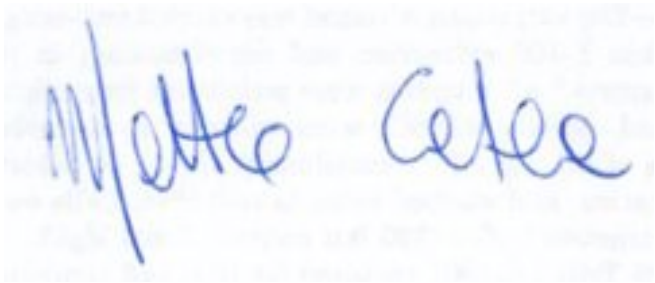

1. Introduction

The replacement of tissues has been from time one of the hidden dreams of human being. This vision started to become reality only about two decades ago, when an emerging field called tissue engineering (TE) originates from reconstructive surgery and regenerative medicine, thanks to the intuition of some pioneers of materials science, chemistry and cell biology[Langer et al, 1993]. They introduced the concept of the autogenic tissue engineering transplant (using patient's own cells), potentially overcoming most limitations of direct transplantation, such as the rejection and pathogen transmission.

In few words, TE is defined as the interdisciplinary field applying the principles and methods of engineering and life sciences to fundamentally understand and develop biological substitutes to restore, maintain or improve tissue functions [Langer et al, 1993].

TEpillars are basically three: cells, signaling factors, and biocompatible support by an artificial ECM named scaffold.

Several of newspaper headlines have captured the scientific and public imagination as to the potential of tissue engineering for tissue regeneration.

In this PhD thesis we will focus on the latter. In the standard scenario, "*the scaffold should allow tissue formation in 3D by good support of cell attachment, proliferation and organization, as well as enabling sufficient nutrient supply to the cells and waste elimination from the cells*" [Badylak SF, 2007; Hollister SI, 2005;Takezawa, 2003]. In our idea, the scaffold assumes a different role. It should also provide the right differentiating signal to mesenchymal stem/stromal cells seeded therein, both guaranteeing this biochemical stimuli and the mechanical support only for the time necessary for cells to rebuild the autologous tissue.

We will focus on the design and optimization of drug-releasing scaffold for the specific application in multilayer tissues, in particular blood vessels and articular cartilage. Multilayer tissues are characterized by peculiarities, which have to be resembled during their engineering process as well. This poses several hurdles to face, so needing a brief overview on the anatomy and histology of both tissues, as well as the current approaches used in clinics, in order to underline the limitations that need to be overcome.

Chapter 1 is just devoted to this; trying to lay the foundations for the following description of the proposed tissue engineered substitutes.

1.1 Vascular tissue

First of all, we need to briefly and roughly discuss the anatomy of the vessels. The blood vessels are the part of the circulatory system that transports blood throughout the body [Elias et al, 1952]. There are three major types of blood vessels: the arteries, which carry the blood away from the heart; the capillaries, which enable the actual exchange of water and chemicals between the blood and the tissues; and the veins, which carry blood from the capillaries back toward the heart (Figure 1).

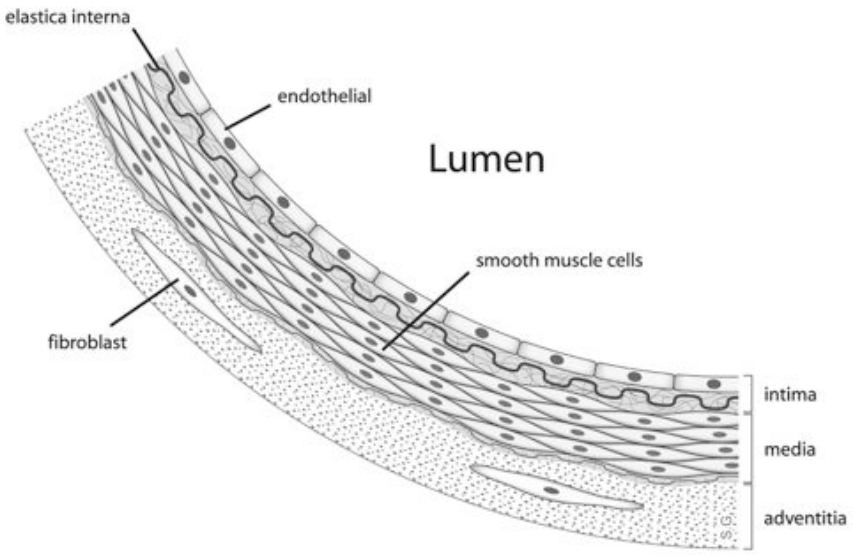

Figure 1. Anatomy of a native blood vessel

The arteries and veins have different structures, veins having two layers and arteries having three:

- *Tunica intima* (the thinnest and inner layer): a single layer of simple squamous endothelial cells glued by a polysaccharide intercellular matrix, surrounded by a thin layer of subendothelial connective tissue interlaced with a number of circularly arranged elastic bands called the internal elastic lamina.
- *Tunica media* (the thickest layer): circularly arranged elastic fiber, connective tissue, polysaccharide substances, the second and third layer are separated by another

thick elastic band called external elastic lamina. The tunica media may (especially in arteries) be rich in vascular smooth muscle, which controls the caliber of the vessel.

- *Tunica adventitia*: entirely made of connective tissue. It also contains nerves that supply the vessel as well as nutrient capillaries (vasa vasorum) in the larger blood vessels.

This peculiar structure grants to blood vessels specific functions. Indeed, arteries have the property of elasticity, meaning that they can expand to accept a volume of blood, then contract and squeeze back to their original size after the pressure is released.
Arteries branch into arterioles as they get smaller. Arterioles eventually become capillaries, which are very thin and branching. Capillaries consist of little more than a layer of endothelium and occasional connective tissue.

1.1.1 Vascular diseases

A vascular disease is a pathological state of large and medium sized arteries and is triggered by endothelial cell dysfunction. Because of factors like pathogens or inflammatory stimuli endothelial cells become activated. This leads to change in their characteristics: endothelial cells start to secrete cytokines and chemokines and express adhesion molecules on their surface [Reape et al, 1999]. This in turn results in recruitment of white blood cells (monocytes and lymphocytes), which can infiltrate the blood vessel wall. Stimulation of smooth muscle cell layer with cytokines produced by endothelial cells and recruited white blood cells causes smooth muscle cells to proliferate and migrate towards the blood vessel lumen. The process causes thickening of the vessel wall, forming a plaque consisting of proliferating smooth muscle cells, macrophages and various types of lymphocytes. This plaque result in obstructed blood flow leading to diminished amounts of oxygen and nutrients that reach the target organ. In the final stages, the plaque may also rupture causing the formation of clots, and as a result strokes.
This phenomenon takes the name of*atherosclerosis*, the build-up of fat and cholesterol deposits on the inside walls [Reape et al, 1999, Elias et al, 1952]. Eventually the narrowed artery causes less blood to flow and a condition called "ischemia" can occur. Ischemia is inadequate blood flow to the body's tissue.

- A blockage in the coronary arteries can cause symptoms of chest pain (angina) or a heart attack;
- A blockage in the carotid arteries can lead to a transient ischemic attack or stroke;

- A blockage in the legs can lead to leg pain or cramps with activity, changes in skin color, sores or ulcers, and feeling tired in the legs. Total loss of circulation can lead to gangrene and loss of a limb;
- A blockage in the renal arteries can cause renal artery disease (stenosis). The symptoms include uncontrolled hypertension (high blood pressure), heart failure, and abnormal kidney function.

1.1.2Current clinical strategies

a. Percutaneous coronary angioplasty (PTCA or PCI) or simply angioplasty, is one therapeutic procedure used to treat the stenotic (narrowed) coronary arteries of the heart found in coronary heart disease.

The angioplasty procedure usually consists of most of the following steps and requires extensive and specialized training. Briefly, once an access into the femoral artery is gainedby means of an "introducer needle", a "sheath introducer" is placed in the opening to keep the artery open and control bleeding.Through this sheath, a long, flexible, soft plastic tube called a "guiding catheter" is pushed. The guiding catheter also allows for radiopaque dyes to be injected into the coronary artery, so that the disease state and location can be readily assessed using real time x-ray visualization.The coronary guidewire is inserted through the guiding catheter and into the coronary artery. While visualizing again by real-time x-ray imaging, the cardiologist guides the wire through the coronary artery to the site of the stenosis or blockage. The tip of the wire is then passed across the blockage. While the guidewire is in place, it now acts as the pathway to the stenosis. The tip of the angioplasty or balloon catheter is hollow and is then inserted at the back of the guidewire, thus the guidewire is now inside of the angioplasty catheter. The angioplasty catheter is gently pushed forward, until the deflated balloon is inside of the blockage.The balloon is then inflated, and it compresses the atheromatous plaque and stretches the artery wall to expand [Meier et al, 2003].

Coronary angioplasty is widely practiced and has a number of risks; however, major procedural complications are uncommon.The most serious risks are death, stroke, myocardial infarction (heart attack) and aortic dissection. A heart attack during or shortly after the procedure occurs in 0.3% of cases. However, PCI has proven to be as effective and less costly than CABG in patients with medically refractory myocardial ischemia [Yang et al, 2005].

b. Coronary artery bypass surgery (CABG) is a surgical procedure performed to relieve angina and reduce the risk of death from coronary artery disease. Arteries or veins from

elsewhere in the patient's body are grafted to the coronary arteries to bypass atherosclerotic narrowings and improve the blood supply to the coronary circulation supplying the myocardium [Haller et al, 2002; Eagle et al, 2004].Grafts can become diseased and may occlude in the months to years after bypass surgery is performed. A graft is considered patent[1] if there is flow through the graft without any significant (>70% diameter) stenosis in the graft.

Graft patency is dependent on a number of factors, including the type of graft used (internal thoracic artery, radial artery, or great saphenous vein), the size or the coronary artery that the graft is anastomosed with, and, of course, the skill of the surgeon(s) performing the procedure.

Generally the best patency rates are achieved with the *in situ* left internal thoracic artery with the distal end being anastomosed with the coronary artery. Saphenous vein grafts have worse patency rates, but are more available, as the patients can have multiple segments of the saphenous vein used to bypass different arteries [Arima et al, 2005].

c. Synthetic grafts have yet to match natural grafts with patency rates ranging from 40% to 50% for lower limb bypass grafts. They are currently used only when autologous grafts are contraindicated. Among the reasons cited are compliance mismatch, thrombogenicity and poor haemodynamics. The difference in radial compliance between the graft and the native vessels at the site of anastomoses accentuated by the inelasticity of sutures has been shown to cause luminal narrowing due intimal hyperplasia. Thrombogenicity also poses a challenge to biomedical researchers as long-term patency rates are not encouraging. These may be overcome by endothelializing these prostheses or making the surface less thrombogenic with the addition of heparin [Kannan et al, 2004].

The ideal vascular graft should be nonthrombogenic, compatible at high blood flow rates, and have similar viscoelasticity to native vessels [How et al, 1985]. When dealing with small diameter (<6mm)vessels in low-flow states, the significance of these factors is amplified. While results with polytetrafluoroethylene (PTFE) and Dacron™ are satisfactory in larger vessels, patency is far lower in small-diameter grafts. In vivo studies have shown a 20% to 25% patency rate with 1 mm diameter PTFE microvessels while all vein grafts in similar settings remained patent. This is because these biomaterials activate thrombus formation on its lumen while the differential compliance at the anastomotic site contributes to the formation of intimal hyperplasia (IH). As such, autologous vein grafts remain the gold standard for microvascular repairs as they are both compliant and

[1]Patency is a term used to describe the chance that a graft remains open.

nonthrombogenic. However donor-site morbidity and the need for an additional surgery limit its potential [Kannan et al, 2004].

*d. Coronary stent*is a metallic meshed tube placed in the coronary arteries that supply the heart, to keep the arteries open in the treatment of coronary heart disease. It is used in the PCI procedure. Stents were shown to improve survivability in the event of an acute myocardial infarction [Armstrong et al, 2006].
However, as the stent is a foreign object, it incites an immune response. This may cause scar tissue to rapidly grow over the stent. In addition, there is a strong tendency for clots to form at the site where the stent damages the arterial wall. Since platelets are involved in the clotting process, patients must take dual antiplatelet therapy afterwards, usually clopidogrel and aspirin for one year and aspirin indefinitely [Serruys et al, 2006]. In order to reduce the treatment, new generation of stent has been developed with biodegradable polymer that release the drugs (Drug Eluting Stents, DES).
However, the dual antiplatelet therapy may be insufficient to fully prevent clots that may result in stent thrombosis; these and the cell proliferation may cause the standard ("bare-metal") stents to become blocked (restenosis). The restenosis, i.e. the development of a thick smooth muscle tissue inside the lumen (neointima), represents one of the main drawbacks of vascular stents. Development of a neointima is variable but can at times be so severe as to re-occlude the vessel lumen, especially in the case of smaller diameter vessels, which often results in reintervention.DES were designed to lessen this problem; by releasing an antiproliferative drug (drugs typically used against cancer or as immunosuppressants), they can help avoid this in-stent restenosis (re-narrowing) [Hannan et al, 2008].

1.1.3 Tissue engineering of blood vessels

The development of autologous tissue engineered vascular grafts (TEVGs), by using cultured autologous vascular wall cells seeded onto a synthetic biodegradable polymeric scaffold,offers a potential improvement over above-mentioned strategies [Naito et al, 2011]. The first TEVG was created by Weinberg and Bell in 1986 [Weinberg et al, 1986]. They generated cultures of bovine endothelial cells (EC), smooth muscle cells (SMCs) and fibroblasts in layers of collagen gel supported by a Dacron mesh. Although physiologic pressures were sustained for only 3–6 weeks, they did demonstrate the feasibility of a TEVG with human cells.
The vascular wall, with its complicated architecture and unique mechanical properties, presents an enormous challenge for tissue engineering. Over the past three decades, much

progress has been made in this pursuit, with several methodologies emerging as key contenders. Among these, here we list any ofthe most used approaches to blood vessel grafting: *EC-seeded synthetic grafts*, *biodegradable synthetic polymer-based constructs*, *cell self-assembly blood vessels*, and *decellularized tissue*[Nerem et al, 2001].

Cell self-assembly model, as it is known, is made with intact layers of human vascular cells grown to overconfluence to form viable sheets of cells and ECM (Figure 2).

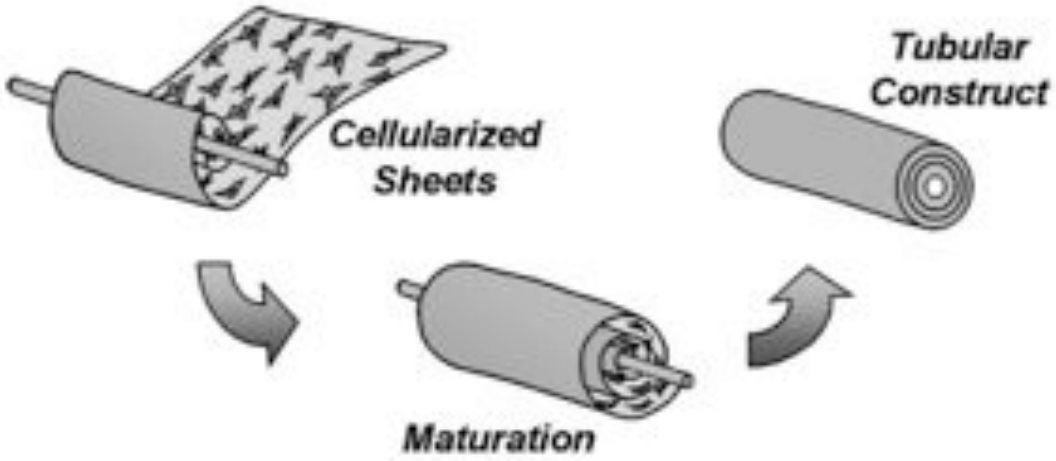

Figure 2. Schematic representation of the cell self-assembly model [Nerem et al, 2001]

To assemble a construct, a SMC sheet is rolled over a permeable mandrel to assume a tubular configuration, forming the medial layer. Similarly, a fibroblast sheet is rolled over the top of the SMC sheet to form an adventitial layer. The tube is cultured to maturity over a time span of 8 weeks. During maturation, the cells assumed a circumferential orientation and produced large amounts of ECM. The fibroblasts in particular produced and organized matrix proteins that enhanced the structural characteristics of the tissue analog. Such constructs were able to withstand more than 2000 mmHg pressure before bursting. Human ECs were then seeded onto the lumen of the matured vessel to form a confluent monolayer.Constructs made using this technique also exhibit adequate mechanical strength for arterial implantation. However, it is not evident from initial reports whether the material exhibits the normal viscoelastic response under physiological loading or whether such a construct would experience compliance mismatch on implantation [L'Heureux et al, 1998].

The *EC-seeded synthetic graft* approach was the first one pursued in vascular tissue engineering [Niklason, 1999]. However, it has several other limitations.Despite the

promise of the surface-modification techniques, the long-term survival and proliferation of ECs on synthetic materials will require an improved model of EC adhesion and coverage. The use of a nonbiodegradable synthetic material would hinder the normal remodeling response of the vascular system. Vascular cells are not equipped to remodel ePTFE or Dacron™ in the same way they remodel collagen and elastin. Thus, the synthetic material becomes a physical barrier to long-term adaptation of the vessel. For this reason *biodegradable polymers*approach has got the upper hand, and is the one pursued by our group. To this extent, poly-L-lactide (PLLA) and poly(lactide-co-glycolide) represent the most attractive avenues for these purposes owing to their adequate mechanicalproperties and biocompatibility. Both of them are bioabsorbable, allowing in vivo vascular cell remodeling to generate a final, functional conduit. During the degradation and remodeling process, the synthetic construct contributes by conferring adequate strength to the conduit, preventing aneurysmal degeneration and rupture.

Although the improvements brought by this approach, there are several issues that must be still addressed. First of all the costly and time consuming in vitro manufacturing process, since 8 weeks of in vitro culturing are required for the construct to exhibit the desired histological and mechanical characteristics [Nerem et al, 2001].

This problem could be overcome by using an alternative but related method,the*acellular approach*. This strategy aims at regenerating a functional vessel by implanting a smart scaffold able to recruitand home progenitors cells from the surrounding host tissue when implanted in vivo.This offers some advantages such as avoiding the isolation and expansion of the autologous cells and the following constructs in vitro manipulation.The one considerable drawback of this approach is that they lack the nonthrombogenic EC lining on the lumen of the graft [Badylak et al, 1989].

Summarizing, a lot of work has been performed in the area of vascular tissue engineering over the past two decades. There are multiple approaches being developed toward this common goal, with new insights constantly emerging in construct development and construct integration, even if no consensus has still been found.There are still several issues that need to be addressed. Among them the major ones seem to be (i) the graft patency, (ii) mechanical properties, and (iii) the balance between the in vivo adaptation and remodeling processes. Moreover, there is also a need to understand the structure-function relationship of engineered blood vessels, with regard to both in vitro development and in vivo integration with the host tissue [Naito et al, 2011; Nerem et al, 2001, Ravi et al, 2010].

1.2 Articular cartilagetissue

As already explained, the second part of my PhD work, so of this thesis, was devoted to the regeneration of osteochondral segment of joints. To this extent, a brief overview regarding the anatomy and the main characteristics of this particular area of the human body is needed.

Articular cartilage, often associated with the osteochondral segment or tissue, is a thick (2.4±0.5 mm in human medial femoral condyles) and specializedconnective tissue covering joint surfaces [Klein et al, 2009], along with an underneath subchondral bone layer. Microscopically, the cartilaginous side is in turn subdivided in adjoining layers, each of them with peculiarities.

In general the articular cartilage is composed of water, collagen, proteoglycans, chondrocytes and other matrix proteins and lipids. It is avascular and also has no nerve supply, therefore not sensitive to early injuries and with little capacity of self-repair, and it lines the ends of long bones. Another characteristics that strengthen this aspect is (i) the relative low number of cells in the tissue, (ii) the low metabolic rate, and (iii) the restricted capacity of chondrocytes to divide and migrate in the articular cartilage because of the matrix fibers [Buckwalter et al, 1983; O' Driscoll et al, 1998].

Articular cartilage is composed by highly specialized cells called chondrocytes. Chondrocytes embryonically originate from the mesenchymeand are responsible for the production of the structural components of articular cartilage including collagen, proteoglycans and other matrix proteins and lipids.They are located in lacunae, usually scattered individually throughout articular cartilage. During growth of the articular cartilage, chondrocytes have a constant, usually roundish shape, but their shape becomes more variable (e.g. spindle-like, fibroblasts-like, etc.), depending on age, pathological state and the cartilaginous layer to which they correspond. Chondrocytes are anaerobic, and receive their nutrition via diffusion of substances within synovial fluid [Buckwalter et al, 1998].

However, extracellular matrix (ECM) is the main protagonist of the articular cartilage. Water contributes up to 80% of the wet weight of articular cartilage, and the interaction of water with the ECM macromolecules significantly influences the mechanical properties of the tissue.The principal articular cartilage ECM component is collagen type II, whichaccounts for 90% to 95% of the cartilage collagen. They are responsible for the tensile strength.Proteoglycans, instead, are responsible for compressive strength and are composed by aggrecan molecules linked to hyaluronic acid (MW ≈ 1.6 MDa). Aggrecan molecules are composed of a protein core with multiple glycosaminoglycans (GAGs)

subunits. GAGs include chondroitin-4-sulphate, chondroitin-6-sulphate and keratin sulphate[Buckwalter et al, 1983].

As previously said, articular cartilage is considered as a multilayer tissue as well, since it could be subdivided into several zones, topographically different in terms of thickness and matrix content, depending on the alignment of collagen fibers so the level of loading (**Errore. L'origine riferimento non è stata trovata.**), which give each zone peculiar characteristics:

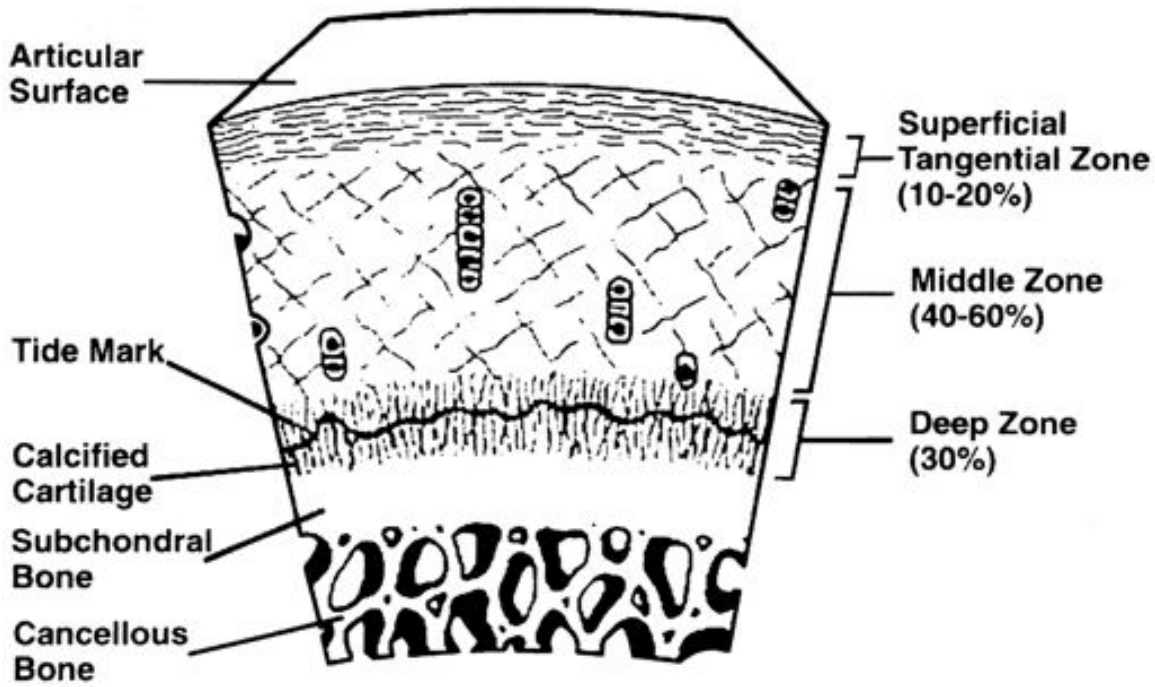

Figure 3. Multilayer architecture of articular cartilage

- **Superficial zone**: collagen fibrils are oriented parallel to the articular surface and impart high tensile strength to withstand the tensile stresses associated with joint loading. This zone is also characterized for the low metabolic activity and hence low healing potential;
- **Transitional (middle) zone** - high concentration of collagen fibers obliquely arranged at right angles to each other to provide a transition to the deep zone;
- **Radial (deep) zone** - the fibers are oriented perpendicular to the subchondral bone. This zone contains the largest-diameter collagen fibrils, the highest concentration of proteoglycans, and the lowest concentration of water;

- **Tidemark** –changes of the tidemark were found to be multiform and metabolically active in the osteoarthritic process. Endochondral ossification depletes the calcified cartilage at the cartilage/bone interface and the tidemark has been thought of as a calcification front advancing in the direction of non-calcified cartilage. Reestablishment of the tidemark is inconsistent in most cartilage repair techniques. In the adult, there is heavy deposition of nano- or micro-crystals of apatites (e.g. hydroxyapatite) in the calcified zone, which prevents diffusion of nutrients across the tidemark;
- **Calcified zone** - acts both as an anchor between articular cartilage and subchondral as an efficient barrier to cellular migration from the underneath bony layer. This layer has the peculiar characteristics to be vascularized, in contrast of the upper cartilaginous layer;
- **Subchondral bone layer** – provides mechanical support to the upper articular cartilage.

In addition to zonal differences in ECM, cells of each of the different zones of articular cartilage are organized distinctly and express zone-specific markers (Figure 4).

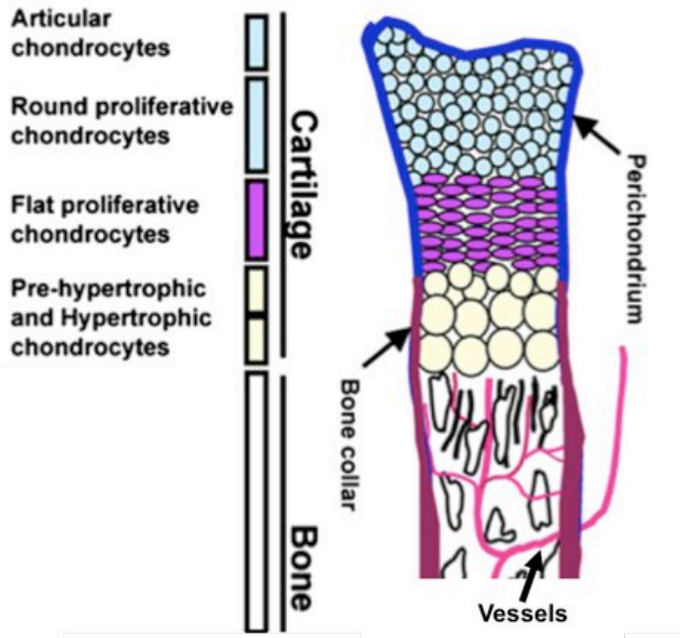

Figure 4. Zonal distribution of chondrocytes in the articular cartilage [adapted from Provot et al, 2005]

In the superficial zone, cells are at a high density, are relatively flattened, and are clustered in a horizontal fashion.Here, the cells secrete proteoglycan 4, a large glycoproteinproduct of the gene *prg4*. This zonalmarker is functionally important as a boundary lubricant,and mutations in the gene are associated with pathologies. Another potential marker for the superficial zone is clusterin, a molecule that is overexpressed in OA. In the middle zone, cells are more spherical and are randomly oriented.Cartilage intermediate layer protein is a potential marker for the middle-deep zones, with apparent autoimmune activity and positive correlation with expression and progression of OA, and other important diseases, such as chondrocalcinosis and lumbar disc disease.In the deep zone, chondrocytes are larger and organized in vertical columns.Interestingly, collagen type X, a marker for chondrocyte hypertrophy and indicator of endochondral ossification during development,is expressed in the deepest layers of articular cartilage [Klein et al, 2009; Reddy et al, 1998].

1.2.1Articular cartilage injuries

The acute and repetitive compressive and torsional joint loading that occurs during normal life activities, with particular intensity in sports, can fatally damage articular surfaces causing pain, joint dysfunction, and effusions. In some instances, this articular surface damage leads to progressive joint degeneration. Three classes of chondral and osteochondral injuries can be identified based on the gravity of tissue damage and the repair response:

- **Damage to the joint surface**, which does not cause visible mechanical disruption of the articular surface, but cause chondral damage and may cause subchondral bone injury;
- **Mechanical disruption of the articular surface limited to articular cartilage**;
- **Mechanical disruption of articular cartilage and subchondral bone**.

Mechanical disruption of articular cartilage stimulates chondrocyte synthetic activity, but it rarely results in repair of the injury, since the above-discussed peculiar characteristics. Disruption of subchondral bone stimulates chondral and bony repair, but it rarely restores an articular surface that duplicates the biologic and mechanical properties of normal articular cartilage. It often results in an unsuitable fibrocartilaginous tissue.
So far, no conclusive surgery treatments have been found to solve this problem. The only possible way seems to be the hyaline cartilage repair, but why?

Repaired fibrocartilage,whichnormally fills osteochondral defects, is less stiff and more permeable than normal articular cartilage, and the orientation and organization of the collagen fibrils in even the most hyaline-like chondral repair tissue do not follow the pattern seen in normal articular cartilage. The decreased stiffness and increased permeability of repair cartilage matrix may increase loading of the macromolecular framework during joint use and result in progressive structural damage, thereby exposing the repair chondrocytes to excessive loads that additionally compromise their ability to restore the matrix. The remaining cells often assume the appearance of fibroblasts as the surrounding matrix comes to consist primarily of densely packed collagen fibrils. This fibrous tissue usually fragments and often disintegrates, thus leaving areas of exposed bone [Buckwalter et al, 2002]. The inferior mechanical properties of chondral repair tissue may be responsible for its frequent deterioration. The worst consequences of these aspects are (i) the osteoarthritis, (ii) the rheumatoid arthritis, and (iii) osteochondritis dissecans.

Osteoarthritis

As we mentioned above, osteoarthritis (OA) is a group of mechanical abnormalities involving degradation of joints, including articular cartilage and subchondral bone.It can be classified into either primary or secondary depending on whether or not there is an identifiable underlying cause [O'Shea et al, 2008].
Primary osteoarthritis is a chronic degenerative disorder related to, but not caused by, aging. As a person ages, the water content of the cartilage decreases as a result of a reduced proteoglycan content, thus causing the cartilage to be less resilient. Without the protective effects of the proteoglycans, the collagen fibers of the cartilage can become susceptible to degradation and thus exacerbate the degeneration. Inflammation of the surrounding joint capsule can also occur, though often mild (compared to that which occurs in rheumatoid arthritis). This can happen as breakdown products from the cartilage are released into the synovial space, and the cells lining the joint attempt to remove them. New bone outgrowths, i.e. osteophytes, can form on the margins of the joints, possibly in an attempt to improve the congruence of the articular cartilage surfaces.
Instead, secondary OA is caused by other factors, such as congenital disorders of joints, diabetes,inflammatory diseases (all chronic forms of arthritis), injury to joints, ligament deterioration, and obesity. However, the resulting pathology is the same as for primary OA [Valdes et al, 2008].

Inflammatory arthritis

Inflammatory cytokines and tissue-damaging proteinases play important roles in joint destruction in rheumatoid arthritis(RA). The pannus is a sheet of inflammatory granulation tissue that spreads from the synovial membrane and invades the joint in rheumatoid arthritis. The incidence of the RA on the population is extremely high, about 1% of the world's population is afflicted, women three times more often than men. Onset is most frequent between the ages of 40 and 50, but people of any age can be affected. It can be a disabling and painful condition, which can lead to substantial loss of functioning and mobility if not adequately treated [Majithia et al, 2007].
A schematic picture depicting the differences between a normal joint with an OA or a RA one is showed in Figure 5.

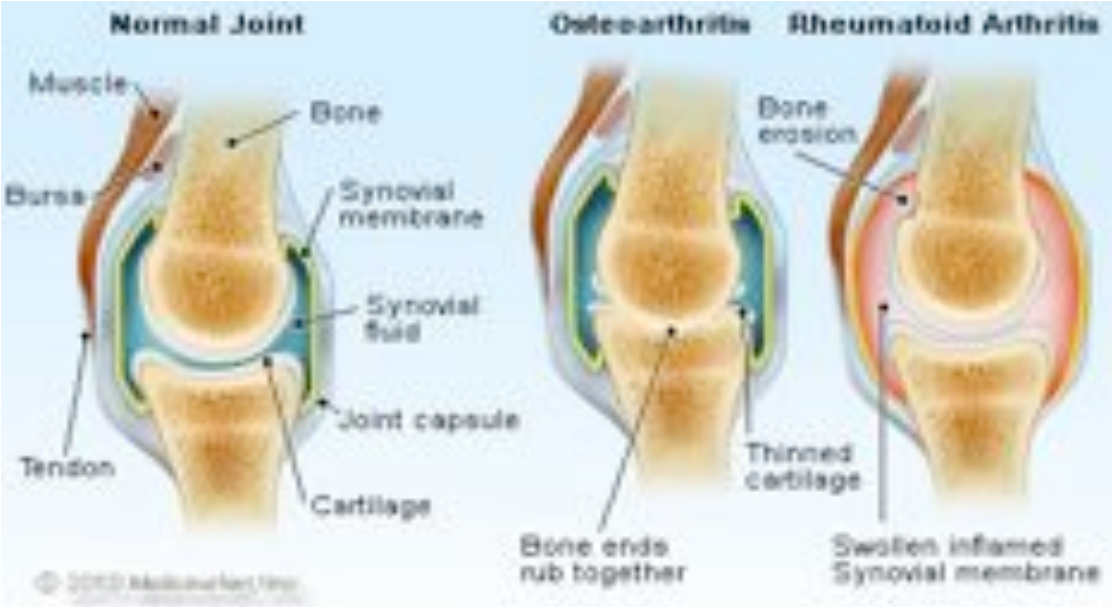

Figure 5. What happens in OA or RA to the normal joint.

Osteochondritis Dissecans and AVN

Osteochondritis dissecans (OCD) is a relatively common condition causing knee pain in children and young adults. It is a condition affecting subchondral bone that manifests as a pathologic spectrum. Initially stages have intact articular surface but softening. This can progress to early articular cartilage separation, partial detachment of an articular lesion, and eventually osteochondral separation with loose bodies. In the knee potential locations are the lateral aspect of the medial femoral condyle (75%), the weight-bearing surface of

the medial (10%) and lateral femoral condyles (10%), and the anterior intercondylar groove or patella (5%).

Although the etiology of these lesions is unclear, it is believed that repetitive microtrauma may interrupt the already tenuous epiphyseal blood supply in the growing child and contribute to the development of osteochondritis dissecans lesions, differences between osteochondrotic and normal cartilage.

There is a decrease in acidic glycosaminoglycans in OCD with thinned subchondral growth plate compared to normal osteochondral samples. Borders to the healthy tissue are clearly visible micro- and macroscopically. Scanning electron microscopy revealed structural differences in the subchondral area. Immunohistochemistry found a general decrease in glycosaminoglycan content and a change in composition. Only faint staining for chondroitin and keratan sulfates was observed in osteochondritic cartilage, whereas increased staining was shown for keratan sulfate in bone. The intraosseous supply to the medial femoral condyle appeared to consist of a single nutrient vessel supplying the subchondral bone with an apparent watershed area of limited supply compared to the lateral femoral condyle [Pappas et al, 1981].

1.2.2Current strategies

The aim of an articular cartilage repair treatment is to restore the surface of an articular joint hyaline cartilage. Over the last decades, surgeons and researchers have been working hard to elaborate surgical cartilage repair interventions. Although these solutions do not perfectly restore articular cartilage, some of the latest technologies start to bring very promising results in repairing cartilage from traumatic injuries or chondropathies.

Broadly taken, there are four major types of articular cartilage repair.

Arthroscopic Lavage / Debridement

Arthroscopic lavage is a "cleaning up" procedure of the knee joint. This short-term solution is not considered an articular cartilage repair procedure but rather a palliative treatment to reduce pain, mechanical restriction and inflammation. Lavage focuses on removing degenerative articular cartilage flaps and fibrous tissue. The main target group is patients with very small defects of the articular cartilage [Jackson et al, 2003].

Marrow Stimulation Techniques

Marrow stimulating techniques attempt to solve articular cartilage damage through an arthroscopic procedure. Firstly, damaged cartilage is drilled or punched until the underlying bone is exposed. By doing this, the subchondral bone is perforated to generate a blood clot within the defect. Studies, however, have shown that marrow stimulation

techniques often have insufficiently filled the chondral defect and the repair material is often fibrocartilage (which is not as good mechanically as hyaline cartilage). However, chances are high that after only 1 or 2 years of the surgery symptoms start to return as the fibrocartilage wears away, forcing the patient to reengage in articular cartilage repair [Steinwachs et al, 2008].

An evolvement of the microfracture technique is the implantation of a collagen membrane onto the site of the microfracture to protect and stabilize the blood clot and to enhance the chondrogenic differentiation of the MSCs. This technique is known as AMIC (Autologous Matrix-Induced Chondrogenesis) and was first published in 2003 [Horas et al, 2003].

Osteochondral Autografts

This technique/repair requires transplant sections of bone and cartilage. First, the damaged section of bone and cartilage is removed from the joint. Then a new healthy dowel of bone with its cartilage covering is punched out of the same joint and replanted into the hole left from removing the old damaged bone and cartilage. The healthy bone and cartilage are taken from areas of low stress in the joint so as to prevent weakening the joint. Depending on the severity and overall size of the damage multiple plugs or dowels may be required to adequately repair the joint, which becomes difficult for Osteochondral Autografts [Bobic et al, 1996].

Cell-based Repairs

Aiming to obtain the best possible results, scientists have striven to replace damaged articular cartilage with healthy articular cartilage. Previous repair procedures, however, always generated fibrocartilage or, at best, a combination of hyaline and fibrocartilage repair tissue. Autologous chondrocyte implantation (ACI) [Peterson et al, 2002]or Matrix-assisted autologous chondrocyte implantation (MACI) [Kon et al, 2009] procedures are cell-based repairs that aim to achieve a repair consisting of healthy articular cartilage.

ACI/MACI procedures take place in three stages. First, cartilage cells are extracted arthroscopically from the patient's healthy articular cartilage that is located in a non load-bearing area of either the intercondylar notch or the superior ridge of the femoral condyles. Then these extracted cells are transferred to an in vitro environment in specialized laboratories where they grow and replicate, for approximately four to six weeks, until their population has increased to a sufficient amount. Finally, the patient undergoes a second surgery where the in vitro chondrocytes are either directly applied to the damaged area (ACI) or seeded into a polymeric porous matrix and then placed underneath the subchondral bone (MACI). These transplanted cells thrive in their new environment,

forming new articular cartilage. So far, these procedures represent the gold standard for the treatment of osteochondral lesions.

1.2.3 Tissue engineering strategies for osteochondral repair

The emergence of tissue engineering strategies for the repair and regeneration of articular cartilage may provide a novel treatment foundation for the treatment of above-mentioned diseases as well as for the prevention of OA. The concept of osteochondral tissue engineering, a hybrid of bone and cartilage regeneration, has attracted considerable attention, particularly as a technique for promoting superior cartilage integration and as a treatment for osteochondral defects.Joint damage that extends the articular cartilage and penetrates the subchondral bone (osteochondral defects) has a uniquely different repair response to that of chondral defects. While the chondral repair mechanism relies solely on the intrinsic healing capabilities of the tissue's single cell source (the chondrocyte), osteochondral defects allow for the recruitment of progenitor cells from the localized bone marrow to assist in the regeneration of the cartilage and underlying bone structures [O'Shea et al, 2008].

According to a classification proposed by Martin and colleagues [Martin et al, 2007], osteochondral tissue-engineered constructs have been generated using: (i) a scaffold for the bone component but a scaffold-free approach for the cartilage component; (ii) different scaffolds for the bone and the cartilage components combined at the time of implantation; (iii) a single but heterogeneous composite scaffold; or (iv) a single homogenous scaffold for both components. These scaffolds have been loaded with a single cell source having chondrogenic capacity, loaded with two cell sources having either chondrogenic or osteogenic capacities, loaded with a single cell source having both chondrogenic and osteogenic differentiation capacity, or used in a cell-free approach.

Another critical aspect is the cell source selection. Articular chondrocytes were the most popular source of cells to engineer cartilage-side grafts. For the clinical implementation of the approaches proposed involving the cellularization of the scaffold cartilage layer, instead, human articular chondrocytes would have to be first expanded in culture, which is associated with cell de-differentiation, leading to a change in the cell morphology and to a downregulation of cartilage-specific genes. This typically leads to an unsuccessful outcome of the study [Martin et al, 2007].

A critical issue associated with the use of this cell source is the harvest of the biopsy from the patient. Indeed, a cartilage biopsy in the joint, even from a non-load bearing site, results in an additional injury, detrimental to the surrounding healthy articular cartilage. To overcome this problem, one exploited alternative was the use of chondrocytes obtained

from non-articular cartilage tissues, such as ear or nose.Several studies have shown that nasal, as well as auricular, chondrocytes have several suitable characteristics, such as (i) ease in harvesting the tissue biopsy with lower site morbidity [Siegel et al, 2000], (ii) expression of collagen types typical of articular cartilage, (iii) retained capacity upon cell expansion to re-differentiate and generate hyaline-like tissue [Tay et al, 2004], (iv) capacity to properly respond to mechanical forces, typically associated with joint loading [Candrian et al, 2008]. However, to finally demonstrate whether the tissue generated by non-articular chondrocytes is adequate for articular cartilage repair, convincing in vivodata from orthotopic experimental studies are still lacking.

To avoid these limitations, several groups have proposed the use of mesenchymal progenitor cells to generate cartilaginous tissues, with particular attention to human, bone marrow-derived mesenchymal stem cells (hBM-MSCs), since they have the capacity to differentiate towards both to the chondrogenic and to the osteogenic lineage.

A key question to be addressed in tissue engineering, and particularly pivotal under the framework of this thesis, is how developing an optimal engineered graft prior to the final implantation, in order to support an optimal repair.A well-developed cartilaginous ECM to one hand could allow for early post-operative rehabilitation and enhance the success rate of the graft survival when subjected to physiologic mechanical loads, to the other hand strongly limits the clinical transfer of tissue-engineered osteochondral grafts.By briefly reviewing the literature, it is clear how a diffused consensus, driven by experimental evidences, is still far to be reached in this key orthopedics field.

1.3 Proposed strategy for a "one-step" approach to engineer multilayer tissues substitutes

The classical tissue engineering approach foresees five consecutive steps, presented in Figure 6. Starting from the tissue harvesting from a biopsy (*point n.1*), autologous cells are extracted and then expanded in plastics using standard cell culture techniques (*point n.2*). After reaching the desired number, cells are seeded in the scaffold (*point n.3*) and cultured in vitro (*point n.4*),usually up to 4 weeks. In this setting, constructs are conditioned with proper stimuli – i.e drug, growth factors, biomolecules – in order to obtain cell proliferation and differentiation and/or ECM production. In few words, in this step a neo-formed engineered tissue will be obtained. Afterwards, the so-obtained tissue is implanted in the donor defect (*point n.5*).

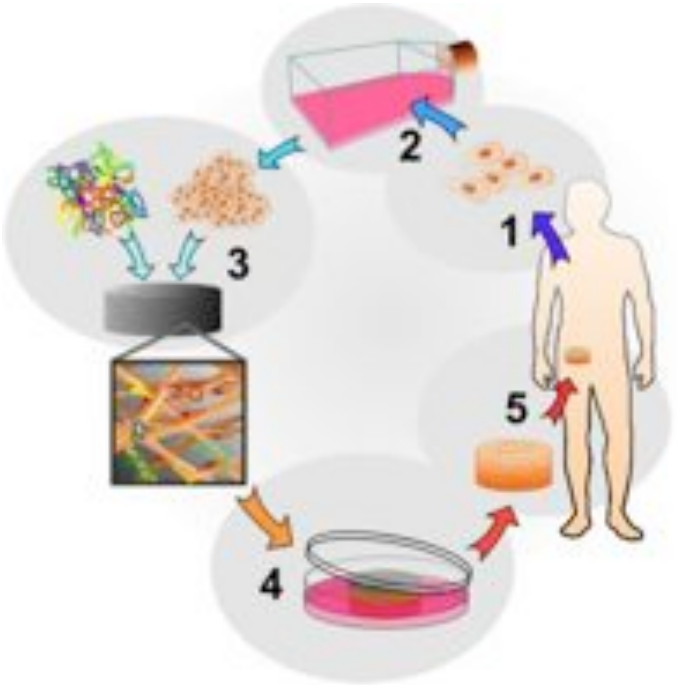

Figure 6. Schematic representation of the classical tissue engineering approach

Nonetheless, this strategy presents some limitations. One major obstacle in delivering tissue engineering products to routine clinical use are the costly, labour-intensive and time-consuming manual processes which are difficult to control and standardize. To be attractive for clinical application, engineered tissues will need to demonstrate (i) cost-effectiveness and cost-benefits over existing therapies, (ii) absolute safety for patients, manufacturers and the environment, and (iii) compliance with the evolving regulatory framework in terms of quality control and good manufacturing practice (GMP). To meet these targets and translate research-scale production into clinically compatible manufacture, the process needs a paradigm change [Pelttari et al, 2009].

Hereby we propose a "one-step" approach, where the in vitro preconditioning of the constructs is not needed since the scaffold itself will provide the proper biochemical stimuli to the cells seeded therein. In particular, in our settings the differentiating factors are released from the scaffold, so driving the differentiation as well as the maturation of freshly-isolated constructs. Matching the neo ECM production time by seeded cells with polymer-based scaffold degradation time, it is possible to regenerate tissues directly in vivo, dramatically shortening times and costs, and also avoiding double-hospitalization.

We hypothesize that this concept could simplify logistical issues surrounding transfer of tissue-engineered constructs into the clinical arena, reduce the need for large and

expensive GMP tissue engineering facilities and minimize operator handling, with the likely final result of reducing the cost of engineered grafts.

Thanks to their plasticity and easy harvesting during surgery human mesenchymal stem/stromal cells (hMSCs) were chosen as the best cell candidate to use for our purposes.

Lastly, in this PhD thesis we applied this strategy to regenerate multilayer tissues, in particular we focused on blood vessels and articular cartilage.

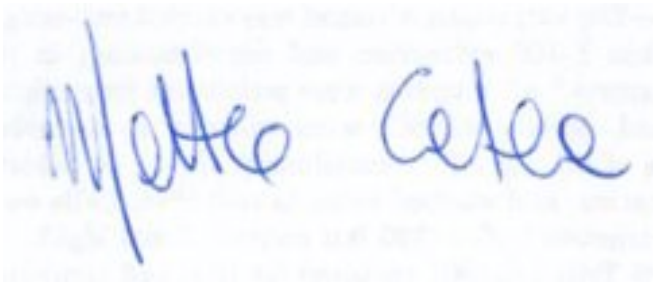

References

Arima, M,Kanoh T, Suzuki T, Kuremoto K, Tanimoto K, et al., "Serial Angiographic Follow-up Beyond 10 Years After Coronary Artery Bypass Grafting", *Circulation Journal* (**2005**), 69: 896-902

Armstrong P, "A comparison of pharmacologic therapy with/without timely coronary intervention vs. primary percutaneous intervention early after ST-elevation myocardial infarction: the WEST (Which Early ST-elevation myocardial infarction Therapy) study". *European Heart Journal* (**2006**), 27: 1530–1538

Badylak SF, "The extracellular matrix as a biologic scaffold material",*Biomaterials*(**2007**), 28:3587-3593

Badylak SF, Lantz GC, Coffey A, Geddes LA,"Small intestinal submucosa as a large diameter vascular graft in the dog", *Journal of Surgical Research* (**1989**), 47:74–80

Bobic V, "Arthroscopic osteochondral autograft transplantation in anterior cruciate ligament reconstruction: A preliminary clinical study", *Knee Surgery, Sports Traumatology, Arthroscopy* (**1996**), 3: 262-264

Buckwalter JA, "Articular cartilage", Intructional Course Lectures (1983), 32: 349-370

Buckwalter JA, "Articular cartilage injuries", *Clinical Orthopaedics & Related Research* (**2002**), 402: 21-37

Buckwalter JA, Mankin HJ, "Articular cartilage: tissue design and chondrocyte-matrix interactions", *Instructional Course Lectures* (**1998**), 47: 477-486

Candrian C, Vonwil D, Barbero A, Bonacina E, Miot S et al., "Engineered Cartilage Generated by Nasal Chondrocytes Is Responsive to Physical Forces Resembling Joint Loading", *Arthrithis and Rheumatism*(**2008**), 58: 197–208

Eagle KA, Guyton RA, Davidoff R, Edwards FH, Ewy GA, et al., "ACC/AHA 2004 guideline update for coronary artery bypass graft surgery: a report of the American College of Cardiology/American Heart Association Task Force on Practice Guidelines (Committee to Update the 1999 Guidelines for Coronary Artery Bypass Graft Surgery)", *Circulation* (**2004**), 110: 340-437

Elias H, Petty D, "Gross anatomy of the blood vessels and ducts within the human liver", *American Journal of Anatomy* (**1952**), 90: 59–111

Haller JD, Olearchyk AS, "Cardiology's 10 greatest discoveries", *Texas Heart Institute Journal* (**2002**), 29: 342-344

Hannan EL, Wu C, Walford G,Walford G, Culliford AT,Gold JP, et al.,"Drug-eluting stents vs. coronary-artery bypass grafting in multivessel coronary disease", *New England Journal of Medicine* (**2008**), 358: 331–341

Hollister SJ,"Porous scaffold design for tissue engineering",*Nature Materials*(**2005**), 4:518-524

Horas U, Pelinkovic D, Herr G, Aigner T, Schnettler R, "", The Journal of Bone and Joint Surgery (2003), 85:185-192

How TV, "Synthetic vascular grafts, and methods of manufacturing such grafts", *United States Patent Application* (**1985**), Patent n. 4,552,707

Jackson RW, Dieterichs C, "The results of arthroscopic lavage and debridement of osteoarthritic knees based on the severity of degeneration", *Arthroscopy: The Journal of Arthroscopic & Related Surgery* (**2003**), 19: 13-20

Kannan RY, Salacinski HJ,Butler PE, Hamilton G,Seifalian AM, "Current Status of Prosthetic Bypass Grafts: A Review", *Journal of Biomedical Material Research Part B: Applied Biomaterials* (**2005**) 74B: 570–581

Klein TJ, Malda J, Sah RL, Hutmacher DW, "Tissue Engineering of Articular Cartilage with Biomimetic Zones", *Tissue Engineering Part B* (**2009**), 15: 143-157

Kon E, Verdonk P, Condello V, Delcogliano M, Dhollander A, et al., "Matrix-Assisted Autologous Chondrocyte Transplantation for the Repair of Cartilage Defects of the KneeSystematic Clinical Data Review and Study Quality Analysis", *The American Journal of Sports Medicine* (**2001**), 37: 156S-166S

L'Heureux N, Paquet S, Labbe R, Germain L, Auger FA,"A completely biological tissue-engineered human blood vessel",*FASEB Journal* (**1998**), 12:47–56

Langer R, Vacanti JP, "Tissue Engineering", *Science* (**1993**), 260: 920-926

Majithia V, Geraci SA, "Rheumatoid arthritis: diagnosis and management", *American Journal of Medicine*(**2007**), 120: 936–939

Meier B, Bachmann D, Luscher TF, "25 years of coronary angioplasty: almost a fairy tale", *The Lancet* (**2003**), 361: 527

Naito Y, Shinoka T, Duncan D, Hibino N, Solomon D, et al., "Vascular tissue engineering: Towards the next generation vascular grafts", *Advanced Drug Delivery Reviews*(**2011**), 63: 312–323

Nerem RM, Seliktar D, "Vascular tissue engineering",*Annual Review of Biomedical Engineering*(**2001**), 3:225-243

Niklason LE, Gao J, Abbott WM, HirschiKK, Houser S, et al., "Functional arteries grown in vitro",*Science* (**1999**), 284:489–93

O'Driscoll SW,"Current concepts review: The healing and regeneration of articular cartilage",*Journal of Bone and Joint Surgery: American Edition* (**1998**), 80:1795-1812

O'Shea TM, Miao X, "Bilayered Scaffolds for Osteochondral Tissue Engineering", *Tissue Engineering Part B* (**2008**), 14: 447-464

Pappas AM, "Osteochondrosis dissecans",*Clinical Orthopaedics and Related Research* (**1981**), 158: 59–69

Pelttari K, Wixmerten A, Martin I, "Do we really need cartilage tissue engineering?", *Swiss Med Wkly* (**2009**), 139:602–609

Peterson L,Brittberg M,Kiviranta I, Akerlund EL, Lindahl A, "Autologous Chondrocyte Transplantation", *The American Journal of Sports Medicine* (**2002**), 30: 2-12

Provot S, Schipani E, "Molecular mechanism of endochondral bone development", *Biochemical and Biophysical Research Communication* (**2005**), 328: 658-665

Ravi S, Chaikof EL, "Biomaterials for vascular tissue engineering", Regenerative Medicine (2008), 5: 107-120

Reape TJ, Groot PH, "Chemokines and atherosclerosis", *Atherosclerosis* (**1999**), 147: 213-225

Reddy AS,"Evaluation of the intraosseous and extraosseous blood supply to the distal femoral condyles",*American Journal of Sports Medicine* (**1998**), 26:415-419

Serruys PW, Kutryk MJB, Ong ATL, "Coronary-Artery Stents", *New England Journal of Medicine* (**2006**), 354:483-495

Siegel NS, Gliklich RE, Taghizadeh F, Chang Y,"Outcomes of septoplasty",*Otolaryngology - Head and Neck Surgery* (**2000**), 122:228–232

Steinwachs MR, Guggi T, Kreuz PC, "Marrow stimulation techniques", *Injury* (**2008**), 39: S26-S31

Takezawa T,"A strategy for the development of tissue engineering scaffolds that regulate cell behavior",*Biomaterials* (**2003**), 24:2267-2275

Tay AG, Farhadi J, Suetterlin R, Pierer G, Heberer M, and et al.,"Cell yield, proliferation, and postexpansion differentiation capacity of human ear, nasal, and rib chondrocytes",*Tissue Engineering*(**2004**), 10:762–770

Valdes AM, Spector TD, "The contribution of genes to osteoarthritis", *Rheumatic Disease Clinics of North America* (**2008**), 34: 581–603

Weinberg CB, Bell E,"A blood vesselmodel constructed from collagen and cultured vascular cells",*Science*(**1986**), 231:397–400

Yang EH, Gumina RJ, Lennon RJ, Holmes DR, Rihal CS, Singh M, "Emergency Coronary Artery Bypass Surgery for Percutaneous Coronary Interventions: Changes in the Incidence, Clinical Characteristics, and Indications From 1979 to 2003", *Journal of the American College of Cardiology* (**2005**), 46: 2004-2009

2. Towards the synthesis of biological prostheses for cardiovascular tissue regeneration

This chapter shows in detail how the research concerning the regeneration of a healthy vessel has been carried on in the labduring my doctoral studies.

First of all, a comparative study was performed in order to find the most suitable sterilization technique on an already developed electrospun biomaterial in terms of overall sterility and affection of the scaffold morphology (**par. 2.1**). Afterwards, a tubular poly-L-lactide (PLLA) scaffold loaded with heparin was developed to act as a differentiating device for mesenchymal stem cells (hMSCs) seeded therein. The hypothesis underneath this work was to drive the differentiation of hMSCs towards vascular endothelial cells in order to obtain a functional synthetic endothelium (**par. 2.2**).This was the first example of *smart scaffold* that represented a leading thread during all my PhD activities. To improve mechanical properties of this construct, the electrospun PLLA scaffold was reinforced with an external armoring poly-ε-caprolactone (PCL) coil. A complete mechanical characterization was performed to test the differences withnative artery properties (**par. 2.3**). Thanks to the encouraging results obtained in vitro, a pilot study on a rabbit model of aorto-aortic bypass was used to test the feasibility of this construct to represent a valid alternative for a future pre-clinical study (**par. 2.4**).

Aiming at creating a tissue-engineered vascular endothelium started from a smart scaffold seeded with mesenchymal stem cells, another approach has been pursued starting from a PCL tubular scaffold. The surface of this biomaterial was properly modifiedto allow a chemical bond with an active and biologically relevant molecule, the nitric oxide (NO). Thanks to this easy as much as innovative biomaterial design, $NO^{\cdot}$molecules are released in a neutral pH environment giving a strong differentiating signal to hMSCs seeded onto the scaffold, as confirmed by our in vitro results (**par. 2.5**).

Finally, having in mind the histoarchitecture of a native vessel, a three-layer compartmented scaffold with oriented drug-delivery capacity for the differentiation,both towards vascular endothelium and smooth muscle phenotype,of a hMSCs single population has been successfully developed (**par. 2.6**).

2.1 Comparative study of different techniques for the sterilization of poly-L-lactide electrospun microfibers: effectiveness vs. material degradation

*adapted from "Rainer A, **Centola M**, Spadaccio C, Gherardi G, Genovese JA, Licoccia S and Trombetta M. Int J Artif Organs. 2010 Feb;33(2):76-85"*

Introduction

In the tissue engineering (TE) fieldseveral studies have demonstrated that the ECM milieu surrounding the cells has physical and structural features in the nanometer scale, and that this arrangement may affect several aspects of cell behavior, such as morphology, adhesion, and cytoskeletal arrangements [Stevens et al, 2005]. Thus, a great deal of effort has been made to fabricate synthetic materials into nanometer scale structures in the attempt to simulate the matrix environment in which seeded cells can be accommodated to proliferate and differentiate toward desired lineages [He et al, 2006]. Electrospinning is one of the approaches that allow the fabrication of several synthetic materials into fibrous and porous structures in the micro- and nano-meter scale, just by controlling a few process parameters [Nair et al, 2004].

Within this scenario, micro- and nano-fibers have become popular candidates for tissue engineering scaffolds in recent years. Such fibers resemble the physical structure of protein fibrils in native ECM and, additionally, the fibrous structure is characterized by a high surface area-to-volume ratio, which provides more substrates for cell attachment. A variety of polymers have been electrospun, and various applications have been proposed, including nerve regeneration [Yang et al, 2006], bone tissue engineering [Woo et al, 2007], vascular engineering [Stitzel et al, 2006], stem cell tissue engineering [Mobasheri et al, 2009], and skin tissue engineering [Venugopal et al, 2005]. Among these materials, poly-L-lactide (PLLA) has been widely investigated because of its good biocompatibility [Simon et al, 2005] and its ability to be modified with inorganic materials in order to improve its biological properties for tissue engineering purposes [Kikuchi et al, 2004]. There is a good degree of evidence suggesting a potential advantage from the use of electrospun polymers in the clinical arena. The need for sterilization required for clinical application demands a careful analysis of the effect that sterilization procedures have on the scaffold, especially given the importance of preserving the previously described fibrillar arrangement to obtain biological effects.

Low polymer melting points and hydrolytic degradation mechanisms result in scaffolds that may be easily damaged by harsh sterilization protocols. Commonly used sterilization

methods like ethylene oxide (EtO) treatment or γ-irradiation have been shown to be inadequate or unsuitable for polymeric scaffolds. The EtO process is highly effective in terms of sterility, but uses a toxic, carcinogenic and allergenic gas, which is potentially harmful to operators, with the additional risk of EtO gas residuals being left inside the devices and later reacting with tissue upon implantation. γ-Irradiation induces ionization reactions in polymeric chain arising in a change of polymer crystallinity and on its average molecular weight [Athanasiou et al, 1996].

Shearer et al investigated four methods for sterilizing flat-sheet and hollow-fiber poly(D,L-lactide-co-glycolide) (PLGA) scaffolds obtained by solvent-exchange technique, to determine and optimize an efficient technique that minimizes structural damage [Shearer et al, 2006]. Recently, the effect of short-wavelength ultraviolet radiation treatment on electrospun PLGA and poly(L-lactide-co-ε-caprolactone) (P(LLA-CL)) has also been investigated [Yixiang et al, 2008]. Our group has recently obtained positive results with a set of electrospun PLLA scaffolds. In the light of these data and their potential application in clinical settings, we sought to evaluate and compare the effect of different sterilization techniques, including autoclave, dry oven, UV irradiation, hydrogen peroxide plasma and ethanol soaking, in the processing of these PLLA scaffolds.

Autoclaving is a very common sterilization technique of proven effectiveness even in the clinical setting, but has been shown to induce modifications in the crystallinity of the polymers. Moreover, because of the temperatures reached during the process (120°C), this method is not suitable for polymers with a low melting point, such as PCL (melting temperature ≈ 60°C).

UV irradiation is commonly used for purification and sterilization of materials in many fields, including industrial settings. UV compromises main structural organization (membrane and nucleic acid) of micro-organisms, leading to impaired reproduction capacity and cell death. The hydrogen peroxide gas plasma (HPGP) process is widely used in operation room settings and exploits low- temperature gas plasma to rapidly sterilize most reusable medical devices and surgical instruments with no toxic residues. Excitation of gaseous hydrogen peroxide with RF allows the generation of highly reactive species interacting with materials and then recombining to form water vapor, oxygen, and other non-toxic by-products, with minimal final moisture formation.

Ethanol soaking treatment is considered a good sterilization method for laboratory use, even if it is unsuitable as a clinical technique.

Materials and methods

Scaffold preparation

Electrospinning of PLLA fibers was performed starting from a 13% w/w solution of PLLA (Sigma, Milwaukee, WI, USA) in dichloromethane (Sigma). The solution was transferred into a glass syringe, which was connected to a high- voltage generator (ES-30, Gamma High Voltage, Ormond Beach, FL, USA). An aluminum earthed plate was used as the collector, placed at a distance of 15 cm. Electrospinning was performed at 15 kV, with a syringe feed rate of 3.5 ml/h. The resulting cloth was divided into several samples of equal size (2 x 2 cm^2), which were sterilized according to different techniques.

Sterilization techniques

Table 1reports the description of the sterilization techniques used and the labeling of the corresponding samples. One sample was not sterilized in order to serve as a reference (sample S0).

Sample name	Technique	Description
S0	Not sterilized	Reference sample
S1	Autoclave	Asco VAPORMATIC 770 autoclave; standard cycle: 120 °C, 20 min
S2	Dry Oven	ISCO ISE 250 oven; 120 °C, 20 min
S3	UV radiation	20W UV lamp (254 nm) for 20 min at a distance of 20 cm
S4	HPGP (Hydrogen peroxide gas plasma)	STERRAD 50 system: standard sterilization cycle at 45 °C for 45 min
S5	Soaking in absolute ethanol (EtOH)	Soaking in 100 mL absolute ethanol (Aldrich) for 3 times, 5 min each, and final rinsing in 500 mL mQ water.

Table 1. Samples nomenclature and description of the corresponding sterilization techniques

Chemical and morphological characterization of samples

Chemical and morphological characterization was per- formed on sterilized samples, using the unsterilized material as a control. Fibers morphology was investigated by means of Field Emission Scanning Electron Microscopy (FE-SEM, Leo Supra 1535, LEO Electron Microscopy, Cambridge, UK). Attenuated Total Reflectance Fourier Transform Infra-Red

spectroscopy (ATR-FTIR) was used to characterize chemical modifications in the polymeric chains of the samples induced by sterilization treatments. ATR-FTIR spectra were collected in the range of 4000-500 cm^{-1}, on a Nicolet Nexus 8700 (Thermo Electron Corporation, Waltham, MA, USA) with a Golden Gate MK2 Diamond (Specac, Orpington, UK) cell. Spectra were recorded positioning the samples on cell platform operating at room temperature (32 scans, 2 cm^{-1} resolution).

Modifications in the crystallinity of the samples were investigated by means of Differential Scanning Calorimetry (DSC, Perkin Elmer DSC7, Waltham, MS). DSC scans were performed in the range -50°C to 250°C at a rate of 20 K/min.

Microbiological sterility assessment

Sterilized samples (from S1 to S5) and an untreated sample (S0) underwent a sterility assay both in solid enriched media and in liquid medium. In the former procedure, samples were streaked onto enriched solid media and incubated for 72 hours. The chosen media were both non-selective (Chocolate Agar and Columbia Agar supplemented with 5% of sheep blood, BD Diagnostic Systems, Spark, MD, USA) and selective (Columbia Colistin-Nalidixic Acid (CNA) Agar with 5% sheep blood and MacConkey Agar; BD Diagnostic Systems). In the latter procedure, samples were cultured in liquid medium (Trypticase Soy Broth, BD Diagnostic Systems), incubated for 6 and 24 hours and subsequently inoculated into the above-mentioned solid media.

After incubation, pure bacterial colonies were identified by means of a clinical grade automated biochemical system (Phoenix Automated Microbiology System, BD Diagnostic Systems) as previously described [Carroll et al, 2006] and manual Analytical Profile Index (API) galleries (BioMerieux, Marcy l'Etoile, France) [Etienne et al, 1984].

Results

ATR-FTIR spectroscopy

ATR-FTIR spectroscopy was used to identify the modifications induced by sterilization techniques on polymeric chains (Figure 7). Spectra were normalized with respect to the most intense signal (1090 cm^{-1}), which could be ascribed to the polymer backbone as described later in this article.

All spectra were dominated by aliphatic polyesters absorptions [Bellamy, 1980]. In particular, reference sample (S0) showed signals characteristic of the ester functional group. In the skeletal stretching and rCH_3rocking region, several absorptions were present. Symmetric and asymmetric stretching modes of C=O and C-O-C groups (νC=O, ν_{sym}C-O-

C and ν_{asym}C-O-C) were present at 1760, 1190 and 1090 cm^{-1}, respectively. The stretching of the C-C bond in the C-CH_3 group (νC-CH_3) could be observed at 1045 cm^{-1}. $r_{as}CH_3$ absorption was positioned at 1130 cm^{-1}. In the CH_3 and CH bending region (1250-1500 cm^{-1}) a signal due to the -CH_3 asymmetric deformation mode ($\delta_{asym}CH_3$) was positioned at 1452 cm^{-1}, while a doublet at 1380-1365 cm^{-1} was assigned to δ_sCH_3 and $\delta_1CH+\delta_sCH_3$ signals, respectively. A broad signal ascribed to the combination δCH+νC-O-C was present at 1270 cm^{-1}.

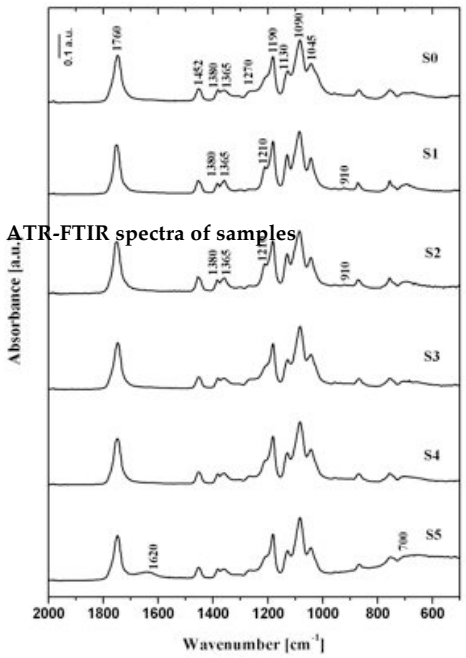

Figure 7. ATR-FTIR spectra of samples

A shoulder at 1210 cm^{-1}, due to the combination of ν_{asym}C-O-C with the rocking mode of -CH_3 group (ν_{asym}C- O-C + $r_{as}CH_3$), was also observed [Kister et al, 1995].

Spectra from autoclave and dry oven treated samples (S1 and S2, respectively) showed the following modifications: an inversion of the intensities of the components of doublet 1380-1365 cm^{-1}, an increase of the signals at 1210 cm^{-1}, and the disappearance of the absorption at 1270 cm^{-1}. In S3, S4 and S5 samples, where scaffolds have been sterilized by UV irradiation, HPGP and EtOH, respectively, these bands showed the same profile of the reference sample S0 without any shift. These data suggest that in samples S1 and S2 the thermal treatment led to a separation of the polymer chains and to an increase in the overall volume.In the spectrum of the EtOH-treated sample (S5), broad signals centered at about 1620 cm^{-1} and 700 cm^{-1} due to physically absorbed water were observed. The presence of water was attributed to the final washing treatment, while no alterations in the polymer structure could be observed.Finally, the spectra of both S3 and S4 samples were found to match the untreated PLLA (S0) spectrum, confirming that these techniques are not harmful to the polymer structure.

DSC analysis of cristallinity

Material crystallinity was assessed by DSC analysis; results are presented in Figure 8.

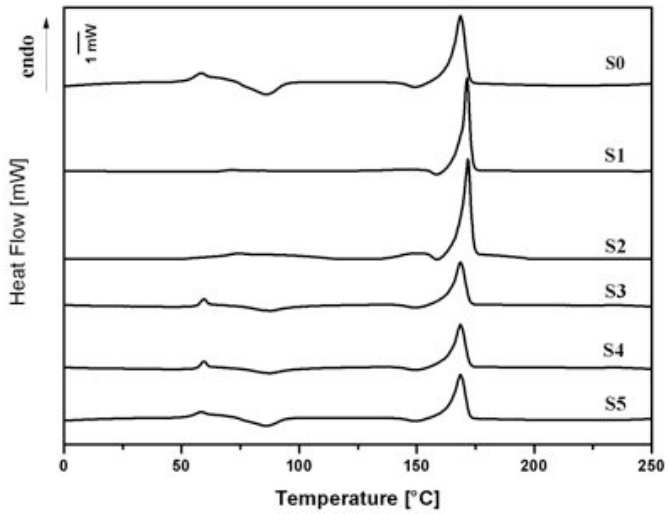

Figure 8. DSC thermograms of samples

Glass transition, crystallinity and melting temperatures, and associated enthalpies were calculated by peak fitting algorithms on the DSC curves, as shown inTable 2.

Sample	Tg [°C]	Tc [°C]	Tm [°C]	Hg [J/g]	Hc [J/g]	Hm [J/g]	% cristallinity
S0	58.40	85.73	168.74	5.0354	-22.0046	55.2619	36%
S1	71.40	N/A	171.40	1.4303	-	58.1007	62%
S2	74.06	N/A	171.73	9.7087	-	52.0490	56%
S3	62.06	91.40	170.07	9.2818	-20.2099	47.9860	30%
S4	59.40	88.07	168.73	6.3129	-13.5209	53.3905	43%
S5	59.05	85.88	168.74	5.1730	-21.8479	53.8951	37%

Table 2. DSC data of S0-S5 samples

The degree of crystallinity was calculated using data from DSC, according to Arnoult et al. [Arnoult et al, 1996]:

$$Xc = (Hf - |Hc|)/H0f$$

where Hf is the enthalpy of fusion obtained from DSC plots, H0f is the enthalpy of fusion of fully crystalline PLLA (H0f = 93 J/g) [Arnoult et al, 1996] and Hc is the cold crystallization enthalpy measured during the DSC runs. Hf represents both the crystalline phase originally present in the samples and the crystalline phase developed during the DSC analysis.

Results reported in Table 2show a significant increase in the Tg/Hg and the melting temperature/enthalpy that paralleled in a more important modification in the % of crystallinity, in the autoclave and dry oven treated scaffold (S1, S2) with respect to the ones UV radiated (S3), or HPGP treated (S4). On the other hand, the sample treated with ethanol (S5) showed no significant differences both in the glass-transition temperature/enthalpy and in the melting temperature/enthalpy with respect to blank sample.

FE-SEM morphostructural analysis

Figure 9shows the FE-SEM micrographs of treated samples together with that of the reference untreated sample (S0).

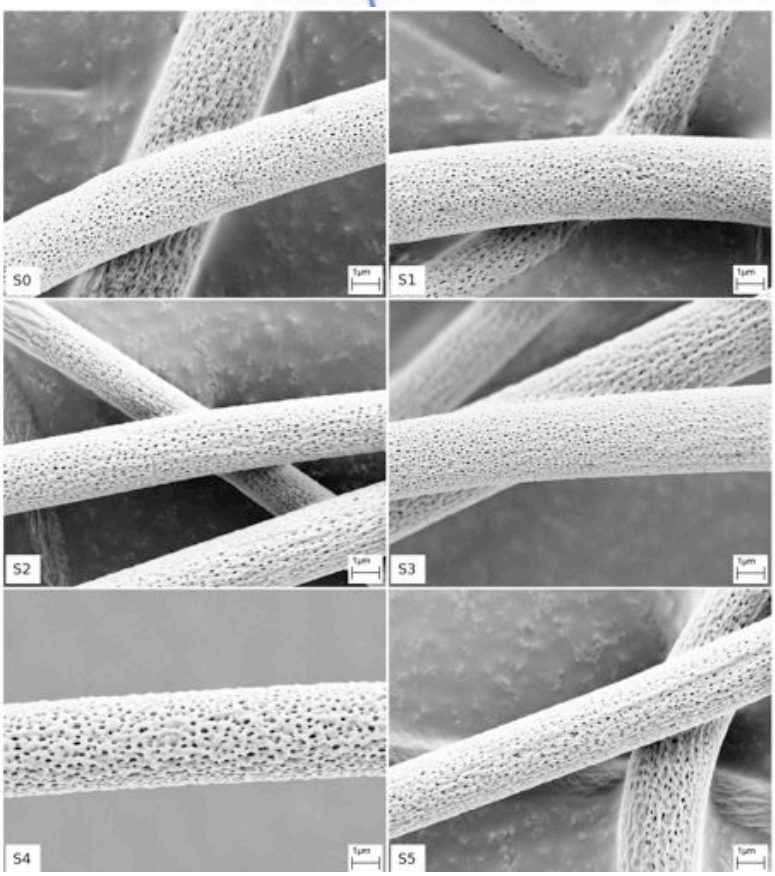

The microstructure of PLLA prior to sterilization consists of micron-sized fibers, with an average diameter of 3.1 microns as calculated using Image-Pro 6.0 (Media Cybernetics, Silver Spring, MD). Fibers of PLLA blank show an intrinsic porosity with an average pore size of ca. 100 nm. The sterilization treatment (S1 to S5) did not affect both the fibers microstructure and the fibers porosity, which

retain the original microstructure.

Microbiological sterility assessment

Microbiological sterility assessment was performed incubating the PLLA patches in suitable culture media, followed by the identification of the isolated colonies.

In the unsterilized sample (S0), the proliferation of three different species of Staphylococci (one of which is S. epidermidis), Bacillus spp and Streptoccus (Gemella spp), was assessed. Samples that underwent ethanol-soaking treatment (S5) showed proliferation of Staphylococcus spp (S. epidermidis) and Rhizobium radiobacter. The presence of a non-fermenting, Gram-negative bacter (Rhizobium radiobacter) in S5, which was not identified in the not sterilized sample (S0), can be probably attributed to a competitive proliferation of several bacterial species in S0, which prevented the identification of Rhizobium.

Sterility was confirmed in the remaining samples (S1, S2, S3 and S4).

Discussions

Several techniques are presently employed for the sterilization of medical devices [Peniston et al, 2007]. Among them, γ-irradiation and EtO are the most common sterilization techniques used in industrial settings. The literature reports that γ-irradiation on PLLA and its copolymers results in an extensive decrease in molecular weight, with further negative impact on thermal and mechanical properties [Henn et al, 1996]. The EtO process uses a toxic, carcinogenic gas, potentially harmful to operators. Recently, it has been shown that EtO is able to alter the topographical properties of electrospun polyurethane scaffolds, resulting in changes in inter-fiber separation, fiber diameter and surface roughness [Andrews et al, 2007]. In particular, this last parameter exerts a fundamental effect on cell cultures, directly affecting cell behavior and regulating cell proliferation and phenotype [Adams et al, 2001; Curtis et al, 1997], especially on cells seeded on biomaterial scaffolds [Meyle et al, 1995; Mainil-Varlet et al, 1997]. Thus, given the biomedical and cellular aims of this work, the authors decided to exclude both γ-irradiation and EtO gas sterilization methods from the analyses. Autoclaving, dry oven, UV irradiation and hydrogen plasma treatments were therefore studied. We sought to evaluate and compare the effect of these different sterilization techniques in the processing of PLLA scaffolds in terms of structural preservation and germicidal effect.

Autoclave cycle, which is a very common sterilization technique of proven effectiveness even in the clinical setting, induces modifications in the crystallinity of the polymer, which may reflect on other properties such as degradation time. Together with autoclaving, dry

oven treatment was also investigated to assess whether lower water vapor content in the sterilization environment could result in different chemical modifications in the polymer structure.

HPGP process was selected for investigation, as it is widely used in the clinical setting to sterilize surgical instruments and other reusable medical devices and is relatively quick, nontoxic, and effective. Moreover, it uses a low temperature with minimal moisture. Recently, Peniston et al. demonstrated that the HPGP sterilization process did not have a significant influence on polymer molecular weight compared to EtO [Peniston et al, 2007].

Ethanol soaking treatment, which is commonly considered a good sterilization method for polymers, showed severe limitations in terms of bacterial contamination.

DSC analysis showed an increase in glass transition temperature (Tg) in all the sterilized samples, which was significantly higher in the autoclave and dry oven groups (S1 and S2) and associated with a significant increase in crystallinity. The increase in Tg could be reliably referred to physical aging, as previously reported [Peniston et al, 2007]. In HPGP (S4) only a slight increase in Tg, not associated with an increase in melting temperature (Tm), was observed. Therefore, the relative slight increase in crystallinity in S4 group could be not totally explained as a direct result of the treatment itself. An increase of crystallinity during in vitro conditioning is frequently documented with PLLA [Iannace et al, 2001], and is thought to be a result of crystal formation by the newly formed short chains generated during the normal degradation process in the amorphous region.

Therefore, UV and HPGP treatments appeared to be the most suitable methods for sterilization in terms of structural preservation and germicidal effect. This result is in partial contrast with the well-known degrading effect of UV radiation on polyesters that is at the basis of photo-ablation techniques [Srinivasan et al, 1986; Cain et al, 1992]. Using conventional sterilization cabinets (with a power of about 0.6 J/h), the thickness of the ablated layer is in the order of the hundreds of nanometers. This phenomenon could be trivial for bulk polymeric materials, but it could have dramatic consequences on nanofibers.

In a recent work, Yixiang and colleagues [Yixiang et al, 2008], showed degradation of PLGA and P(LLA-CL) electrospun scaffolds following 30 minutes treatment with a 254 nm UV germicidal light with an intensity of 285 $\mu W/cm^2$. Polymers exhibited a reduction of the average molecular weight, resulting in faster resorption rate and lower mechanical properties, even if the scaffold morphology remained unaltered. On the other hand, materials retained their biocompatibility, indicating that UV irradiation may not affect the ability of biomaterials to provide a good environment for cell viability. However, since the

electrospun scaffolds that were investigated in the present study exhibit a micron-sized fibrillar structure, they should reasonably be less sensitive to UV-induced degradation with respect to nanosized fibers.

In conclusion, although electrospinning represents one of the most appealing approaches for the fabrication of engineered constructs in the regeneration of diseased tissues and organs, several issues have to be investigated in order to finalize their transfer into common clinical practice. Among these, sterilization issues represent a major concern: the effectiveness and maintenance of sterility, together with the preservation of structural and functional integrity following the sterilization process, are crucial points, especially when the in vivo performance of these biomaterials is considered. This study examined the behavior of a widely used material, electrospun PLLA, when exposed to various common sterilization techniques. Although fibrillar arrangement with nanosized intrafibrillar porosity was almost unaffected by the sterilization processes, when several techniques of analysis were combined, modifications induced by higher temperature treatments were revealed in the material crystalline organization. Further experimental effort will be focused on the evaluation of sterilization treatments in terms of degradation kinetics and mechanical properties.

Conclusions

In light of the exciting promises held by tissue engineering and its potential application in clinical settings, we performed a comparative study of different sterilization techniques applied to an electrospun poly-L-lactide scaffold. The results of this study report that UV irradiation and hydrogen peroxide gas plasma (HPGP) are the most suitable techniques for an effective sterilization of PLLA electrospun scaffolds while preserving chemical and morphological features of the samples.

References

Adams JC, "Cell-matrix contact structures", *Cellular and Molecular Life Sciences*(**2001**), 58: 371-392

Andrews KD, Hunt JA, Black RA,"Effects of sterilization method on surface topography and in-vitro cell behaviour of electrostatically spun scaffolds",*Biomaterials*(**2007**), 28: 1014-1026

Arnoult M, Dargent E, Mano J, "Mobile amorphous phase fragility in semi-crystalline polymers: Comparison of PET and PLLA", *Polymer*(**2007**), 48: 1012-1019

Athanasiou KA, Niederauer GG, Agrawal CM, "Sterilization, toxicity, biocompatibility and clinical applications of poly- lactic acid/polyglycolic acid copolymers",*Biomaterials*(**1996**), 17: 93-102

Bellamy L,"The infrared spectra of complex molecules", London: Chapman and Hall (1980)

Cain S, Burns F, Otis C, Braren B,"Photothermal description of polymer ablation—absorption behavior and degradation time scales", *Journal of Applied Physics* (**1992**), 72: 1572-1578

Carroll KC, Glanz BD, Borek AP, et al., "Evaluation of the BD Phoenix automated microbiology system for identification and antimicrobial susceptibility testing of Enterobacteriaceae",*Journal of Clinical Microbiology*(**2006**), 44: 3506-3509

Curtis A, Wilkinson C, "Topographical control of cells", *Biomaterials* (**1997**), 18: 1573-1583

Etienne J, Reverdy ME, Gruer LD, Delorme V, Fleurette J, "Evaluation of the API 20 STREP system for species identification of streptococci associated with infective endocarditis",*European Heart Journal*(**1984**), 5: 25-27

He W, Yong T, Ma ZW, Inai R, Teo WE, et al., "Biodegradable polymer nanofiber mesh to maintain functions of endothelial cells",*Tissue Engineering*(**2006**), 12: 2457-2466

Henn G, Birkinshaw C, Buggy M, "Comparison of the effects of gamma-irradiation and ethylene oxide sterilization on the properties of compression moulded poly-D,L-lactide", *Journal of Material Science Materials in Medicine*(**1996**), 7: 591-595

Iannace S, Maffezzoli A, Leo G, Nicolais L,"Influence of crystal and amorphous phase morphology on hydrolytic degradation of PLLA subjected to different processing conditions",*Polymer*(**2001**), 42: 3799-3807

Kikuchi M, Koyama Y, Yamada T, et al., "Development of guided bone regeneration membrane composed of beta-tricalcium phosphate and poly(L-lactide-co-glycolide-co-epsilon-caprolactone) composites", *Biomaterials*(**2004**), 25: 5979-5986

Kister G, Cassanas G, Vert M, Pauvert B, Terol A, "Vibrational analysis of Poly(L-lactic) acid",*Journal of Raman Spectroscopy*(**1995**), 26: 307-311

Mainil-Varlet P, Curtis R, Gogolewski S, "Effect of in vivo and in vitro degradation on molecular and mechanical properties of various low-molecular-weight polylactides", *Journal of Biomedical Materials Research* (**1997**), 36: 360-380

Meyle J, Gultig K, Nisch W, "Variation in contact guidance by human cells on a microstructured surface", *Journal of Biomedical Materials Research* (**1995**), 29: 81-8

Mobasheri A, Csaki C, Clutterbuck AL, Rahmanzadeh M, Shakibaei M, "Mesenchymal stem cells in connective tissue engineering and regenerative medicine: applications in cartilage repair and osteoarthritis therapy",*Histology and Histopathology*(**2009**), 24: 347-366

Nair LS, Bhattacharyya S, Laurencin CT, "Development ofnovel tissue engineering scaffolds via electrospinning", *Expert Opinion on Biological Therapy*(**2004**); 4: 659-668

Peniston SJ, Choi SJ, "Effect of sterilization on the physicochemical properties of molded poly(L-lactic acid)", *Journal of Biomedical Material Research B Applied Biomaterials* (**2007**), 80: 67-77

Shearer H, Ellis MJ, Perera SP, Chaudhuri JB,"Effects of common sterilization methods on the structure and proper- ties of poly(D,L lactic-co-glycolic acid) scaffolds",*Tissue Engineering*(**2006**), 12: 2717-2727

Simon CG, Eidelman N, Kennedy SB, Sehgal A, Khatri CA, et al.,"Combinatorial screening of cell proliferation on poly(L-lactic acid)/poly(D,L-lactic acid) blends", *Biomaterials*(**2005**), 26: 6906-6915

Srinivasan R, "Ablation of polymers and biological tissue by ultraviolet lasers",*Science*(**1986**), 234: 559-565

Stevens MM, George JH, "Exploring and engineering the cell surface interface", *Science* (**2005**), 310: 1135-1138

Stitzel J, Liu J, Lee SJ, et al, "Controlled fabrication of a biological vascular substitute",*Biomaterials*(**2006**), 27: 1088-1094

Venugopal J, Ramakrishna S, "Biocompatible nanofiber matrices for the engineering of a dermal substitute for skin re- generation",*Tissue Engineering*(**2005**), 11: 847-854

Woo KM, Jun JH, Chen VJ, et al, "Nano-fibrous scaffolding promotes osteoblast differentiation and biomineralization",*Biomaterials*(**2007**), 28: 335-343

Yang F, Murugan R, Wang S, Ramakrishna S, "Electrospinning of nano/micro scale poly(L-lactic acid) aligned fibers and their potential in neural tissue engineering", *Biomaterials*(**2005**), 26: 2603-2610

Yixiang D, Yong T, Liao S, Chan CK, Ramakrishna S, "Degradation of electrospun nanofiber scaffold by short wave length ultraviolet radiation treatment and its potential applications in tissue engineering",*Tissue Engineering Part A*(**2008**), 14: 1321-1329

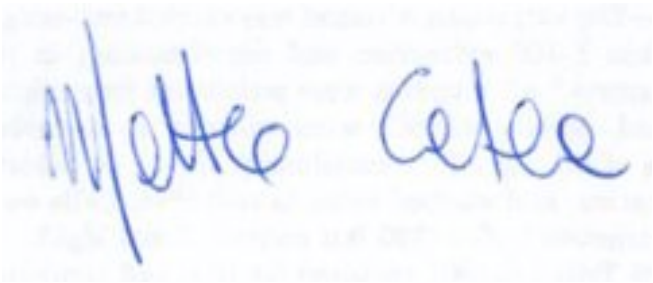

2.2 Heparin-releasing scaffold for stem cells: a differentiating device for vascular aims

*adapted from "Spadaccio C, Rainer A, **Centola M**, Trombetta M, Chello M, Lusini M, Covino E, Toyoda Y, Genovese JA.Regen Med. 2010 Jul;5(4):645-57"*

Introduction

In vascular tissue engineering, the goal is to provide a functional living artery for replacement of diseased small-caliber arteries. As previously discussed, current artificial grafts present significant shortcomings, including thrombosis, infection, limited durability, and inability to grow. To overcome these limitations, Tissue-Engineered Vascular Graft (TEVG) constructs have been developed by using cultured autologous vascular wall cells seeded onto a synthetic biodegradable polymeric scaffold [Shinoka et al, 1998]. The main advantages of autologous TEVGs are increased cell growth, construct durability and resistance to infections, but they are still harnessed by limitations regarding thrombogenicity and donor scarcity. Both preclinical and clinical studies have demonstrated the feasibility of constructing functional vascular grafts from autologous vascular cells seeded onto a biodegradable tubular matrix with large diameter (⌀>6 mm) [Shinoka et al, 2005]. Several types of polymeric biomaterials have been proposed to obtain vascular grafts. Poly-L-lactide (PLLA) and poly(lactide-co-glycolide) (PLGA) represent the most attractive avenues for these purposes, thanks to their adequate mechanical properties and biocompatibility [Sarkar et al, 2006]. Additionally, PLLA and PLGA are bioabsorbable, allowing in vivo vascular cell remodeling to generate a final, functional conduit. During the degradation and remodeling process, the synthetic construct contributes in conferring adequate strength to the conduit, preventing aneurismal degeneration and rupture [Greisler et al, 1992]. Many different techniques have been developed for the fabrication of vascular scaffolds with biopolymers [Spadaccio et al, 2009]. Electrospinning is one of the most effective and functional approaches, with the possibility to be combined to the newest methodologies of cell seeding [Xu et al, 2004]. The small diameter fibers produced by electrospinning exhibit large specific surface area, as well as high permeability, both desirable in a biological setting [Badami et al, 2006].Nano- and micro-fibrous electrospun scaffolds, mimicking the arrangement of connective tissue fibrillar proteins, have been demonstrated to allow the remodeling of vascular grafts in both cellular and extracellular content, thus representing an optimal candidate for TEVGs fabrication [Hashi et al, 2007]. Biopolymers loaded with growth factors, cytokines and drugs have also been developed, generating drug-releasing systems

capable of localized delivery of molecules [Luong-Van et al, 2006; Huang et al, 2003]. However, several issues concerning the clinical applications of TEVGs still need to be answered. The greatest obstacles to the widespread use of TEVGs in clinical practice are the lack of off-the-shelf availability, and the difficulties in harvesting and propagating autologous cells. These problems are especially daunting in vascular surgery, where treatment of an acutely ischemic lower limb is involved. In this context, the use of adult stem cells is an attractive alternative, because of their easy availability in clinical settings (i.e. through bone marrow aspiration) and their notable plasticity that can make them suitable for "bench to bedside" applications. Human mesenchymal stem cells (hMSCs) from bone marrow have been shown to be a suitable candidate for tissue regeneration including vascular, cardiac [Spadaccio et al, 2008] and bone tissues [Spadaccio et al, 2009]. Recently, they have been shown to exhibit antithrombogenic properties, especially in relation to their cell-surface heparan sulfate proteoglycans [Hashi et al, 2007]. In this scenario, we developed an electrospun PLLA tubular scaffold releasing heparin, that was seeded with hMSCs and assayed in terms of cytotoxicity, cell survival, proliferation and differentiation with the aim to develop a device able to both guide the differentiation of stem cells towards endothelium and deliver factors useful in the management of the post-implantation period.

Materials and methods

Scaffold preparation

Heparin-releasing PLLA (PLLA/Hep) scaffold was prepared by electrospinning, starting from a 13% w/w PLLA (Sigma, Milwaukee, WI) solution in dichloromethane (Sigma). Unfractioned heparin (sodium salt, 5000 UI/mL, MSPharma, Gaither, MD) was added to the polymer solution, using methanol (Sigma) as co-solvent, to obtain a final heparin concentration (with respect to PLLA) of 250 UI/g. This concentration was chosen according to both literature and clinical dosage [Lobo et al, 1996], in order to create a device suitable for direct clinical application. Electrospinning equipment was used (DynaSpin, Biomatica, Rome, Italy); the solution was fed through a 28G needle with a feed rate of 1.5 mL/hr and electrospun onto an earthed collector placed at a distance of 15 cm, using a voltage of 15 kV. In order to achieve tubular scaffolds, a rotating cylindrical AISI 316L stainless steel mandrel (4 mm diameter and 6 cm length, rotating at 4500 rpm) was used as the collector target. Additionally, bare PLLA scaffold (PLLA/ctrl) - without heparin addition - was obtained with the same experimental conditions to be used as control only for biological assessments. Microstructure of the obtained materials was evaluated by Field Emission Scanning Electron Microscopy (FE-SEM, Supra 1535, Leo

Electron Microscopy, Cambridge, UK). Image analysis of FE-SEM micrographs was performed by means of the accompanying software. Autofluorescence analysis on the polymer itself was performed in order to assess potential biases or artifacts in further processing for immunostaining. Polymers were excited at different time points within a range spanning between 10 ms and 10 s and autofluorescence was detected under fluorescence microscope (Olympus, Tokyo, Japan).

Drug release study

Heparin release rate was assayed using the Azure A spectrofluorimetric method developed by Jacques et al. [Jacques et al, 1977]. 40 mg of PLLA/Hep scaffold was placed in a 15 mL sealed tube with 800 μL of pre-warmed phosphate buffered saline (PBS) containing 0.03% w/v NaN3, and incubated at 37 °C. 60 μL aliquots of surnatant were timely collected and quantified according to the above-mentioned assay. Activity of heparin was assessed by activated coagulation time (ACT) determination in blood samples exposed to the eluted heparin. 50 mg of PLLA/Hep and PLLA/ctrl samples were separately placed in two sealed vials containing 500 μL of normal saline (NS), and incubated for 24 hours at 37 °C. 100 μL of each surnatant were added to 1 mL of freshly collected blood, and ACT was measured using an automated coagulation analyzer (ACT II, Medtronic, Fridley, MN).

Mechanical properties

Mechanical tests were performed on PLLA/Hep electrospun grafts. Measurements included static compliance, circumferential and longitudinal uniaxial tensile properties and suture retention [Sell et al, 2006; Smith et al, 2008; Stankus et al, 2007].For all the details, please refer to **paragraph 2.3**.

Cell seeding

hMSCs (passage 4, Lonza, Basel, Switzerland) were used for seeding on tubular PLLA/Hep scaffold (4 mm inner diameter, 0.5 mm wall thickness, 5 cm length). Similar experiments were performed on PLLA/ctrl tubular scaffolds as a control for differentiation induction. Scaffolds were seeded with hMSCs under rotating dynamic conditions (12 g) to guarantee uniform cell distribution, at a density of $500 \cdot 10^3$ cells/cm^2 in DMEM supplemented with 10% fetal bovine serum (FBS), 100 units/mL penicillin, 100 μg/mL streptomycin (Lonza) and incubated for 48 hours [Kim et al, 1998]. To standardize culturing protocol and normalize subsequent biological analyses and assessments, seeding

efficiency was calculated as elsewhere described [Soletti et al, 2010]. Briefly, after the seeding of each sample, the medium exuded through the scaffold was collected and used for cell counting with a hematocytometer to calculate seeding efficiency as the percentage of the initial number of cells entrapped within the scaffold over the total amount of seeded cells. To confirm phenotype permanence, additional experiments were performed culturing the constructs up to 1 week.Additionally, control cultures were performed on conventional culture plates, exposing the hMSCs to the elution products of the scaffolds; cells were seeded at the same cellular density of $500 \cdot 10^3$ cells/cm^2 onto transwell inserts, and cultured in the same conditions while exposed to PLLA/Hep and PLLA/ctrl scaffolds.

Cell engraftment

Cell engraftment within the constructs was evaluated by immunohistology and confocal microscopy. Upon culturing, tubular scaffolds were fixed with 4% paraformaldehyde (PFA) for 15 minutes, embedded in O.C.T. cryomatrix, snap frozen and cut in 15 μm slices. To assess cell attachment and engraftment, confocal microscopy was performed, staining cells for F-Actin with rhodamine phalloidin (Molecular Probes, Invitrogen), using TOTO (Invitrogen) as nuclear counterstain. For cell viability assessment, Live/Dead assay (Invitrogen, San Diego, CA), based on cellular membrane intactness, was used. Percentage of viable cells has been calculated counting at least 200 cells in 10 randomly chosen microscopic fields at 10X magnification. Data are presented as the mean value ± standard deviation.

Cell proliferation

Cell proliferation was evaluated by measuring the total cellular DNA content and semiquantitatively by immunostaining for Ki67 by confocal microscopy. Cellular DNA content was obtained as previously described [George et al, 2008]. Constructs were collected and media removed. Constructs were lysed in RIPA buffer added with protease inhibitor cocktail Halt (Thermo Fisher Scientific, Rockford, IL) and cells were sonicated using a pulsed ultrasonic disruptor (Thermo Fisher Scientific) three times for 10 s. DNA content was measured using Quant-iT ds-DNA assay kit (Invitrogen) on a Qubit fluorimeter (Invitrogen).

Cell differentiation

Single immunostaining for CD31 and von Willebrand factor (vWF) (Abcam, Cambridge, UK) and double for Ki67 and CD31 (NeoMarkers, Fremont, CA) were performed as

previously described [Genovese et al, 2007]. Briefly, tissue sections were permeabilized with 0.1% Triton-X 100 (Sigma) in PBS for 10 min. Non-specific binding of antibodies was blocked by incubating the samples for 45 min with 2% bovine serum albumin (Sigma). Samples were incubated 1 hour at 37 °C with mouse monoclonal anti-CD31 (1/100 dilution) and rabbit anti-Ki67 (1/100 dilution) primary antibodies. Samples were then incubated with AlexaFluor488-conjugated secondary anti-mouse IgG and AlexaFluor546-conjugated secondary anti-rabbit IgG (Invitrogen) for 30 min at 37 °C. In negative control experiments, the incubation with primary antibodies was omitted. Nuclei were counter-stained with TOTO. Samples were then mounted in Prolong antifade medium (Invitrogen) and viewed under an Olympus Fluorview F1000 confocal microscope by two independent blinded observers. Flow cytometry for CD31 expression was performed on hMSCs cultured on PLLA/Hep and PLLA/ctrl scaffolds, using CD29 (Neomarkers) as a positive control [Onodera et al, 2006]. Same experiment was also performed on hMSCs cultured in adherence on transwell inserts and exposed to PLLA/Hep and PLLA/ctrl scaffolds, in order to evaluate the biological effectiveness of heparin release. Cells were detached by mild trypsinization and run through a flow cytometer (Accuri Cytometers, Ann Arbor, MI). A minimum of 50.000 events were collected and acquired in list mode with the accompanying software. Acquired data were analyzed using CellQuest software (BD BioSciences, San Jose, CA). Additionally, total protein content was extracted from constructs and evaluated by Western blotting analysis and densitometry analysis [Genovese et al, 2007] using a CD31 monoclonal antibody. Briefly, protein concentration was determined by the bicinchoninic acid (BCA) method and a total protein amount of 25 μg of the lysates were subjected to 8% sodium dodecyl sulfate–polyacrylamide gel electrophoresis (Sigma) and transferred onto 0.20 μm Nitrocellulose P Membranes (Pierce Biotechnology, Rockford, IL). Membranes were blocked in TBS protein-free solution (Tris Buffered Saline pH 7.4 + 0.05% Tween20 + Kathon Antimicrobial agent, Pierce Biotechnology) and were immunoblotted with the primary antibody overnight, followed by horseradish peroxidase–conjugated secondary antibodies anti-mouse IgG (Zymed Laboratories, South San Francisco, CA). Membranes were exposed on radiographic film using an enhanced chemiluminescent substrate SuperSignal West Pico Trial Kit (Pierce Biotechnology). Densitometry analysis was performed using Image-Pro 6.0 (Media Cybernetics, Silver Spring, MD).

Results

Scaffold characterization

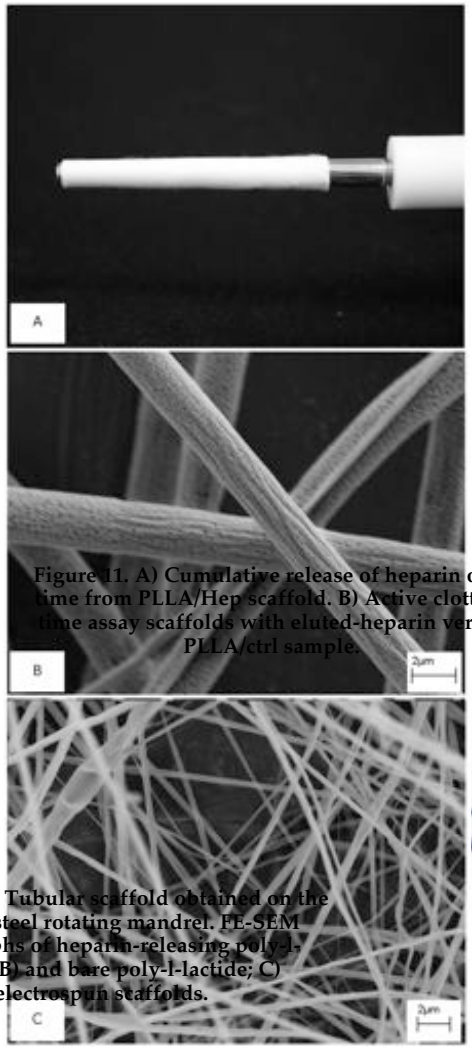

Figure 10. A) Tubular scaffold obtained on the stainless steel rotating mandrel. FE-SEM micrographs of heparin-releasing poly-l-lactide; B) and bare poly-l-lactide; C) electrospun scaffolds.

Figure 10A shows one of the obtained tubular scaffolds on the mandrel. FE-SEM micrographs of PLLA/Hep and PLLA/ctrl electrospun scaffolds are presented in Figure 10B-C, respectively. Both scaffolds consist of a non-woven fibrous mesh, with porosity in the range of 10 μm, but significant differences can be found in fibers morphology. PLLA/ctrl sample shows micron-sized fibers (average diameter 1.5 ± 0.9 μm) and an intrinsic porosity, with elongated pores sized around 100 μm. PLLA/Hep scaffold, instead, shows fibers with smaller diameters (average diameter 450 ± 150 nm) and a non-porous structure. Polymers were investigated in terms of autofluorescence, to prevent potential artifacts in further analyses. Scaffolds showed autofluorescence only after 8.0 ± 0.4 s.

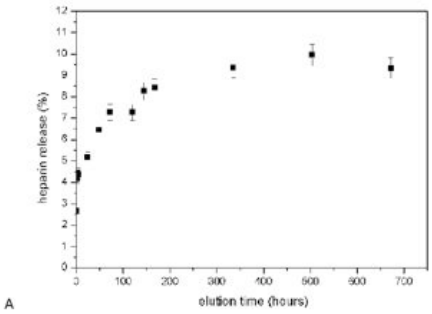

Figure 11. A) Cumulative release of heparin over time from PLLA/Hep scaffold. B) Active clotting time assay scaffolds with eluted-heparin versus PLLA/ctrl sample.

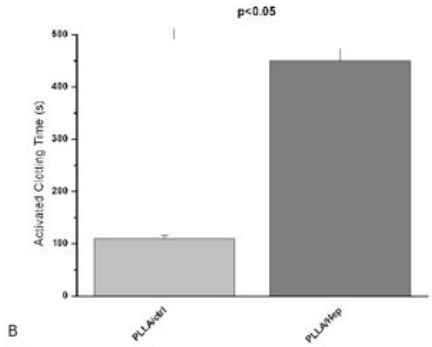

Drug release study

The cumulative release of heparin from the PLLA/Hep scaffold was assessed by a colorimetric assay, originally developed by Jacques et al. [Jacques et al, 1977] and modified by Yang et al. [Yang et al, 1999]. Figure 11A shows heparin release profile. This assay is based on the metachromatic behavior of Azure

A dye, which presents a shift towards shorter wavelengths (from 620 to 520 nm) of the absorption band when reacting with heparin. This reaction is primarily dependent upon the formation of a bond between amino groups of the dye and carboxylic groups of heparin. An initial releasing burst in the first 24 hours could be detected. Subsequently, a progressive decrease in the release rate was noticed up to 4 weeks with a cumulative release of ca. 10% of the total drug load. ACT assay confirmed an increase in coagulation time after exposure to scaffold-eluted heparin (450 s for PLLA/Hep vs 110 s for PLLA/ctrl, $P<0.05$), as reported in Figure 11B.

Mechanical properties

Figure 12shows the typical stress-strain curve obtained by circumferential testing on a PLLA/Hep sample. Table 3reports the results derived from circumferential, longitudinal, compliance and suture retention mechanical testing for PLLA/Hep samples. Some data

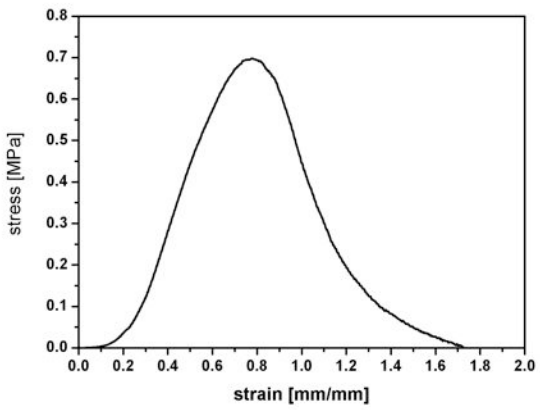

Figure 12. Stress–strain curve for PLLA/Hep sample under circumferential loading

Parameter	**PLLA/Hep**	**Saphenous vein** *[Stankus et al,2007]*
UTS [MPa]	0.72 ± 0.03	
STF [mm/mm]	0.80 ± 0.05	
Pb [MPa]	0.08 ± 0.01	0.22 ± 0.04
PS [MPa]	0.66 ± 0.04	
LSTF [mm/mm]	0.31 ± 0.02	

SRF [N]	0.72 ± 0.04	1.92 ± 0.02
SRT [N/m]	2.67 ± 0.14	
SC [%/100 mHg]	65.9 ± 2.7	26.30 ± 2.75

Table 3. Mechanical properties of PLLA/Hep samples

available from the literature for human saphenous vein are also reported as a comparison.

Cell morphology and differentiation

Experiments were performed in triplicate. Cell seeding was uniform and homogenous and seeding efficacy in the PLLA/ctrl and PLLA/Hep scaffolds were 91.3 ± 1.6 and 93.2 ± 1.7% (P 0.12), respectively. Live/Dead assay demonstrated ≥90% cell viability both in PLLA/Hep and in PLLA/ctrl scaffolds (Figure 13A-C), with the former showing improved survival and an effective cell engrafting after 48 hours of culture.

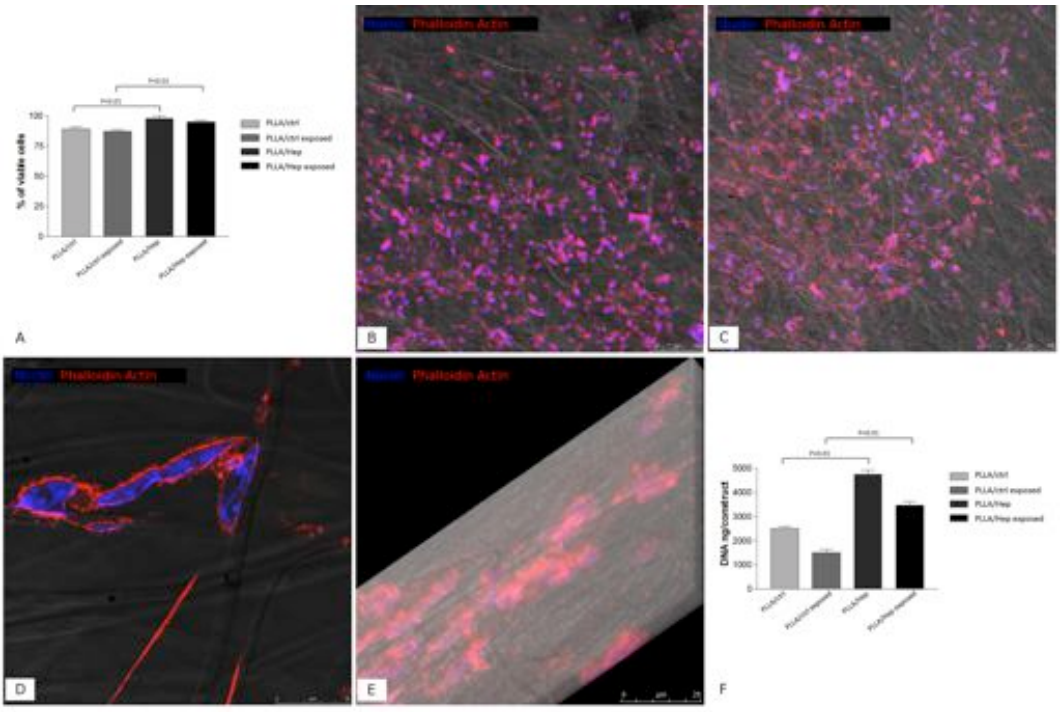

Figure 13. (A) Cells viability analysis in PLLA/Hep and in PLLA/ctrl after 48 h of culture. (B–D) Confocal microscopy: (B) PLLA/Hep seeded with hMSCs after 48 h culturing (100×); scale bar: 100 µm. (C) PLLA/ctrl seeded with hMSCs after 48 h culturing (100×); scale bar: 100 µm. (d) PLLA/Hep seeded with hMSCs for 48 h (400×); scale bar: 25 µm. (e) 3D rendering of the construct showing full thickness engrafting of cells inside the polymer; scale bar: 25 µm. (F) Cell proliferation evaluated by measuring the total DNA content per construct.

In PLLA/Hep scaffold, hMSCs exhibited changes in both cell morphology and protein markers expression, in comparison with PLLA/ctrl. Confocal microscopy for F-Actin with nuclear counterstain showed elongated cells with rare cytoplasm and a high nucleus/cytoplasm ratio (Figure 13D). Nuclei appeared enlarged with loose chromatin and several nucleoli, indicating conditions of non-quiescence. Moreover, membranes showed characteristic indentations and invaginations that resemble caveolae, typical of endothelial cells. The 3D rendering demonstrates full-thickness engraftment and cell migration (Figure 13E). Cell proliferation, as evaluated by measuring the total DNA content per construct, demonstrated a statistical significant increase in the PLLA/Hep scaffold with respect to the PLLA/ctrl sample used as control (Figure 13F). This was also observed for cells cultured on transwell inserts and exposed to PLLA/Hep scaffolds not seeded with cells ($P<0.01$).Immunofluorescence analysis performed on the PLLA/Hep constructs revealed CD31 expression, along with Ki67 positive cells (Figure 14A-C) that were not found in the control one (Figure 14D). In our tubular scaffolds, CD31 positive cells could be detected on the luminal surface of the construct. Flow cytometry confirmed and quantified CD31 positivity, showing a statistically significant higher level of expression in the PLLA/Hep scaffold (Figure 14E).

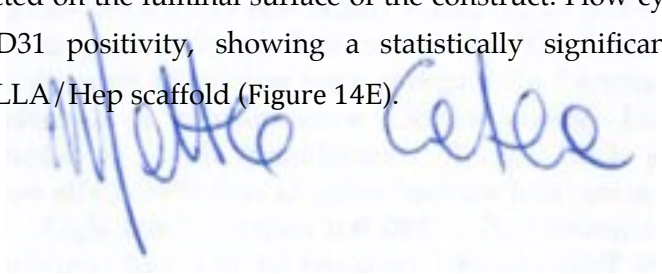

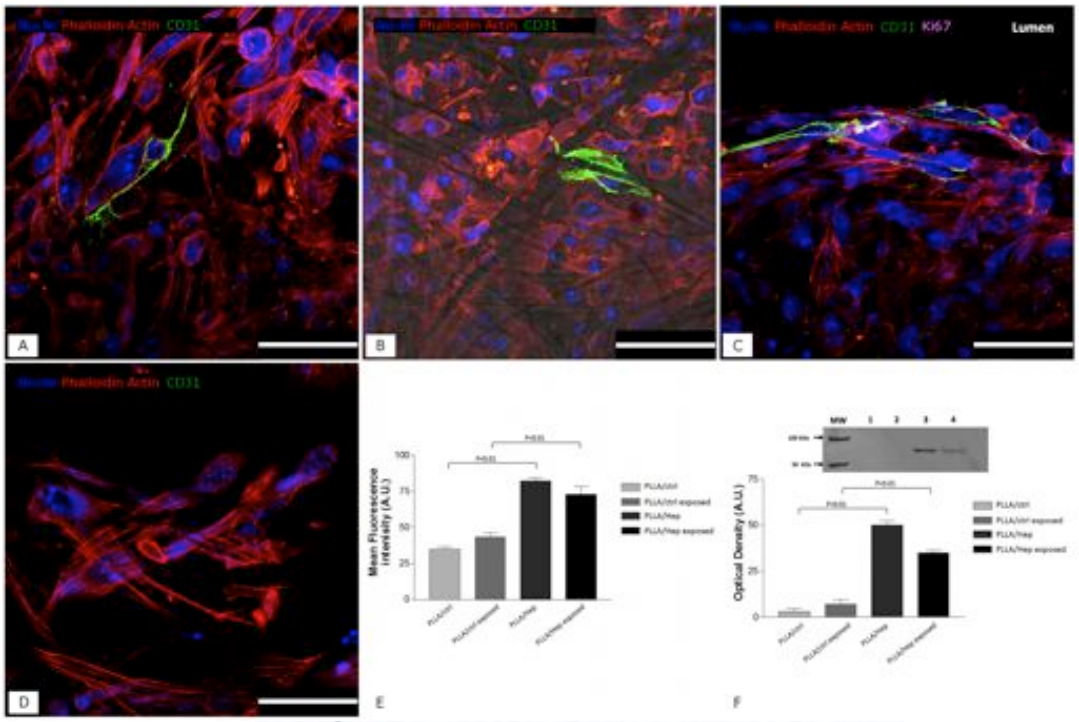

Figure 14. (A–B) PLLA/Hep seeded with hMSCs for 48 h (400×). (B) Phase contrast image has been merged to immunofluorescence image for PLLA/Hep seeded with hMSC for 48 h (400×). (C) Tubular scaffold has been imaged and stained for CD31, F-actin and Ki67. (d) PLLA/ctrl seeded with hMSCs (400×) at same experimental conditions with respect to the PLLA/Hep. Scale bars: 50 µm. (e) Cytofluorometry analysis of CD31 expression. Cells were cultured for 48 h on PLLA/ctrl and PLLA/Hep. (F) Top: western blot for CD31 (83 kDa); lane 1: PLLA/ctrl seeded with hMSC for 48 h; lane 2: hMSCs exposed to PLLA/ctrl; lane 3: PLLA/Hep seeded with hMSCs for 48 h; lane 4: hMSCs exposed to PLLA/Hep. Bottom: densitometry analysis of western blot expressed in optical density.

Interestingly, a significant increase in CD31 positivity could be observed in cells exposed to PLLA/Hep scaffolds in comparison with PLLA/ctrl ones. These findings were confirmed by Western blot analysis, followed by semiquantitative densitometric evaluation (Figure 14F). Extension of culturing time to 1 week confirmed permanence of CD31 positivity. Additionally, cells on the functionalized constructs expressed vWF, a late marker of endothelial phenotype. In these studies, vWF localized both in the membrane and in cell cytoplasm, reliably indicating a still immature form of the protein waiting for its definitive membrane migration and localization (Figure 15).

Discussions

Our aim was to exploit these properties and to develop an *ad hoc* differentiating device for autologous stem cells, able, at the same time, to facilitate and optimize the management of the construct once in the clinical setting. The concept of fabricating a scaffold containing factors, as heparin, able to induce stem cells differentiation and to exert important

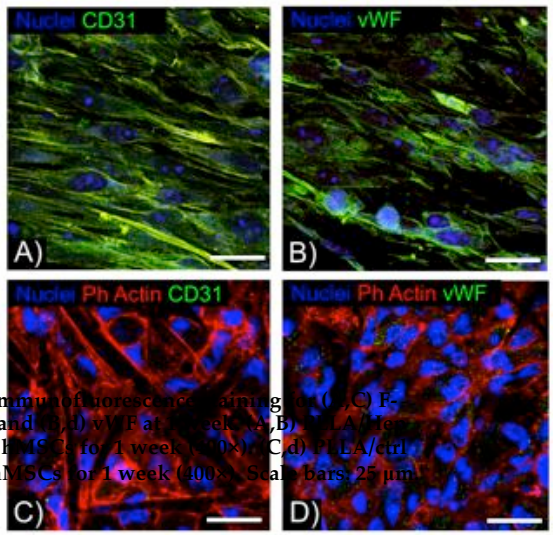

Figure 15. Immunofluorescence staining for (A,C) F-actin, CD31 and (B,D) vWF at 1 week (A,B) PLLA/Hep seeded with hMSCs for 1 week (400×). (C,d) PLLA/ctrl seeded with hMSCs for 1 week (400×). Scale bars, 25 μm.

systemic effects was pursued; this material could represent an alternative to the mostly used TEVGs with mature, fully differentiated autologous endothelial cells, in order to improve their clinical management.In this settings, differentiation would be realized within a three-dimensional ECM-like environment closely mimicking the tissue native architecture and allowing a harmonious ongoing cell growth and differentiation for tissue regeneration.Guided differentiation of an easily recruitable, highly plastic stem cell type, as hMSCs, could overcome the current difficulties related to the low cell yields and quality, mainly due to the patients general conditions, as age, smoke and diabetes [Zilla et al, 1994; Sank et al, 1994]. Scaffolds were developed by means of electrospinning, performing a direct incorporation of the biomolecule in the polymer solution, overcoming the drawbacks of other methods, such as adsorption or microencapsulation [Guan et al, 2007]. Electrospun materials are highly sensitive at small variations in electrostatic and rheological properties of the starting solutions, which may reflect in alterations of the final morphology. FE-SEM characterization, in fact, revealed substantial changes between PLLA/Hep and PLLA/ctrl fibers. In PLLA/Hep samples, addition of the drug and co-solvent caused a decrease in polymer solution viscosity, leading to smoother and thinner fibers. These fibers did not show intrinsic nanosized porosity that characterized fibers in bare PLLA, attributable to a phase separation process during solvent evaporation. Nevertheless, both scaffolds retained adequate porosity between the fibers. This arrangement could provide a favorable environment to cell attachment, growth and differentiation, as closely mimicking the structure of native ECM recapitulating the arrangement of connective tissue fibrillar proteins [Hashi et al, 2007]. As an additional control, to assess whether the above cited differences in fibers morphology may affect differentiation of stem cells cultured within the scaffolds, a set of experiments were also performed on 2D cultures, with cells adhered to conventional plasticware that were exposed to the scaffolds by means of transwell inserts.

Heparin release kinetics was evaluated. The release profile showed an increased steepness following the first 24 hours, indicating an initial releasing burst, reliably associated with drug excess removal immediately after immersion of the scaffold in PBS, and a further sustained release, involving swelling of the polymer network and diffusion of the drug. This kinetics could represent an advantage for eventual clinical applications as providing an immediate high-dose heparin release, potentially able to counteract the well-known initial thrombotic tendency soon after surgical vascular anastomosis, which is at the basis of the early graft failure. Further calculation of the effective amount of heparin released during the first 48 hours following the seeding, revealed a final drug concentration of 12 μg/mL. Noteworthy, this concentration has been used in previous studies that showed endothelial differentiation induced by addition of heparin to culture media [Chabut et al, 2003]. Moreover, released heparin retained its biological functionality, as demonstrated by ACT results.

Tensile behavior of the electrospun material, as assessed from circumferential and longitudinal tensile tests, was compatible with the model of a fibrillar material. According to the model, fibers are progressively recruited by imposed strain, resulting in an increase in the steepness of stress-strain curve. At high stress values, progressive failure of fiber elements is experienced. These phenomena result in a bell-shaped stress-strain curve, as the one provided in Figure 12for the sample under circumferential loading. For further details please see next **paragraph 2.3**.

Results of confocal microscopy of scaffolds seeded with hMSCs were consistent with an adequate cell attachment and viability; in the drug loaded scaffold (PLLA/Hep), morphostructural changes were observed, resulting in cell elongation, reduction in cytoplasm with nuclear enlargement, increase in nucleoli number and appearance of membrane invaginations resembling typical endothelial caveolae.

Proliferation analysis confirmed the generation of a non-hostile microenvironment for cell culturing, with an additional proliferative drive reliably induced by the functionalized scaffold. Along with these findings, in the PLLA/Hep scaffolds a shift towards CD31 positivity could be detected in comparison to PLLA/ctrl, thus indicating a possible endothelial commitment. This finding was confirmed by flow cytometry and is consistent with previous reports describing increased presence of CD31 positive microvessels following subcutaneous application of covalently-bond heparin-modified porous polyurethane scaffold [Bezuidenhout et al, 2008]. An additional marker of endothelial differentiation, vWF, was found to be positively expressed after 1 week culturing, confirming the idea of stem cell differentiation induction.

All these findings support our data concerning the ability of the heparinized scaffold to induce stem cell differentiation towards vascular endothelium.
Moreover, the well reported effect of heparin in the inhibition of smooth muscle proliferation and intimal hyperplasia could allow to speculate on the possible advantage of this heparin functionalized PLLA scaffold in the control of the phenomena recognized to be at the root of graft restenosis [Glagov, 1994; Edelman et al, 2000], and will be the subject of further investigation.
Extended experiments culturing constructs for an additional week demonstrated permanence of the acquired CD31 positive phenotype and the expression of vWF, a late marker of endothelial differentiation. At confocal analysis, the latter showed both a membrane and cytoplasmic and perinuclear localization, reliably suggesting the idea of a still immature form of the protein waiting for its definitive migration at membrane site. Presence of the vWF at 1 week timepoint, together with its subcellullar localization, could be considered as intermediate steps along the differentiation pathway, allowing to speculate on the ongoing maturation of the endothelial phenotype acquired by hMSCs in these settings.
Even if heparin has been previously used in tissue engineering settings, the main concept emerging from this work regards the idea of designing an absorbable scaffold able to define an optimal microenvironment to induce tissue-oriented differentiation of stem lineages, and at the same time to host cells in a structure resembling the natural ECM. In this study we proposed a different approach in tissue engineering, in which the biomaterial is intended as a differentiating system for the stem cell seeded therein, and is capable to guide and orient the differentiation process within a 3D biomimetic structure.

Conclusions

We developed an electrospun PLLA tubular scaffold releasing heparin in which a single and easily recruitable stem cell type or endogenous transmigrated stem cells would encounter an adequate pre-constituted environment, promoting differentiation towards endothelial phenotype. The electrospinning technique, amenable for functionalization, allowed the fabrication of a structure not only mimicking the morphological properties of the native tissue, but even able to assist and guide cell adhesion, growth and differentiation. Moreover, the device can act as a drug releasing system, delivering factors useful both for the management of the immediate post-implantation period and for the maintenance of a milieu that provides the correct signaling to guarantee tissue homeostasis.

References

Badami AS, Kreke MR, Thompson MS, Riffle JS, Goldstein AS,"Effect of fiber diameter on spreading, proliferation, and differentiation of osteoblastic cells on electrospun poly(lactic acid) substrates", *Biomaterials* (**2006**), 27: 596–606

Bezuidenhout D, Davies N, Black M, Schmidt C, Oosthuysen A, Zilla P,"Covalent surface heparinization potentiates porous polyurethane scaffold vascularization", *Journal of Biomaterials Applications* (**2008**), 24: 401–418

Chabut D, Fischer AM, Colliec-Jouault S et al.,"Low molecular weight fucoidan and heparin enhance the basic fibroblast growth factor-induced tube formation of endothelial cells through heparan sulfate-dependent a6 overexpression", *Molecular Pharmacology* (**2003**), 64: 696–702

Edelman ER, Nathan A, Katada M, Gates J, Karnovsky MJ,"Perivascular graft heparin delivery using biodegradable polymer wraps",*Biomaterials* (**2000**), 21: 2279–2286

George J, Onodera J, Miyata T,"Biodegradable honeycomb collagen scaffold for dermal tissue engineering", *Journal of Biomedical Materials Research Part A*(**2008**), 87: 1103–1111

Genovese JA, Spadaccio C, Langer J, Habe J, Jackson J, Patel AN,"Electrostimulation induces cardiomyocyte predifferentiation of fibroblasts", *Biochemical Biophysical Research Communication* (**2008**), 370: 450–455

Glagov S,"Intimal hyperplasia, vascular modeling, and the restenosis problem",*Circulation* (**1994**), 89: 2888–2891

Greisler HP, Cziperle DJ, Kim DU et al.,"Enhanced endothelialization of expanded polytetrafluoroethylene grafts by fibroblast growth factor type 1 pretreatment",*Surgery*(**1992**), 112: 244–254

Hashi CK, Zhu Y, Yang GY et al.,"Antithrombogenic property of bone marrow mesenchymal stem cells in nanofibrous vascular grafts", *PNAS USA* (**2007**), 104: 11915–11920

Huang ZM, Zhang ZY, Kotaki M, Ramakrishna S,"A review on polymer nanofibers by electrospinning and their applications in nanocomposites",*Composites Science and Technology*(**2003**), 63: 2223–2253

Jaques LB, Sue TK, Mcduffie NM, Wice SM,"Heparin and sulfated mucopolysaccharides – a micro system for quantitative differentiation and determination", *Canadian Journal of Physiology and Pharmacology* (**1977**), 55: 1179–1189

Lobo BL, Greene WL,"ACCP consensus conference on antithrombotic therapy. Indicate specific low molecular weight heparin product and dosage",*Chest* (**1996**), 110: 866

Luong-Van E, Grondahl L, Chua KN, Leong KW, Nurcombe V, Cool SM,"Controlled release of heparin from poly(e-caprolactone) electrospun fibers",*Biomaterials*(**2006**), 27: 2042–2050

Onodera N, Tamaki T, Okada Y, Akatsuka A, Aoki D,"Identification of tissue-specific vasculogenic cells originating from murine uterus", *Histochemistry and Cell Biology* (**2006**), 125: 625–635

Sank A, Wei D, Reid J et al.,"Human endothelial cells are defective in diabetic vascular disease", *Journal of Surgical Research* (**1994**), 57: 647–653

Sarkar S, Lee GY, Wong JY, Desai TA,"Development and characterization of a porous micro-patterned scaffold for vascular tissue engineering applications",*Biomaterials*(**2006**), 27: 4775–4782

Sell SA, McClure MJ, Barnes CP et al.,"Electrospun polydioxanone-elastin blends: potential for bioresorbable vascular grafts", *Biomedical Materials* (**2006**), 1: 72–80

Shinoka T, Matsumura G, Hibino N et al., "Midterm clinical result of tissue-engineered vascular autografts seeded with autologous bone marrow cells",*Journal of Thoracic Cardiovascular Surgery* (**2005**), 129: 1330–1338

Shinoka T, Shum-Tim D, Ma PX et al.,"Creation of viable pulmonary artery autografts through tissue engineering", *Journal of Thoracic Cardiovascular Surgery* (**1998**), 115: 536–545

Smith MJ, Mcclure MJ, Sell SA et al.,"Suture-reinforced electrospun polydioxanone-elastin small-diameter tubes for use in vascular tissue engineering: a feasibility study", *Acta Biomaterialia* (**2008**), 4: 58–66

Soletti L, Hong Y, Guan J et al., "A bilayered elastomeric scaffold for tissue engineering of small diameter vascular grafts", *Acta Biomaterialia* (**2010**), 6: 110–122

Spadaccio C, Chello M, Trombetta M, Rainer A, Toyoda Y, Genovese J,"Drug releasing systems in cardiovascular tissue engineering", *Journal of Cellular and Molecular Medicine* (**2009**), 13: 422–439

Spadaccio C, Rainer A, Chello M, Covino E, Trombetta M, Genovese J,"Drug releasing hybrid scaffold: new avenue in cardiovascular tissue engineering", *Tissue Engineering Part A*(**2008**), 14: 691–943

Spadaccio C, Rainer A, Trombetta M et al.,"Poly-l-lactic acid/hydroxyapatite electrospun nanocomposites induce chondrogenic differentiation of human MSC", *Annals of Biomedical Engineering* (**2009**), 37: 1376–1389

Stankus JJ, Soletti L, Fujimoto K, Hong Y, Vorp DA, Wagner WR, "Fabrication of cell microintegrated blood vessel constructs through electrohydrodynamic atomization",*Biomaterials* (**2007**), 28: 2738–2746

Xu C, Inai R, Kotaki M, Ramakrishna S,"Electrospun nanofiber fabrication as synthetic extracellular matrix and its potential for vascular tissue engineering", *Tissue Engineering* (**2004**), 10: 1160–1168

Yang Z, Birkenhauer P, Julmy F et al., "Sustained release of heparin from polymeric particles for inhibition of human vascular smooth muscle cell proliferation", *Journal of Controlled Release* (**1999**), 60: 269–277

Zilla P, Deutsch M, Meinhart J et al., "Clinical in vitro endothelialization of femoropopliteal bypass grafts: an actuarial follow-up over three years", *Journal of Vascular Surgery* (**1994**), 19: 540–548

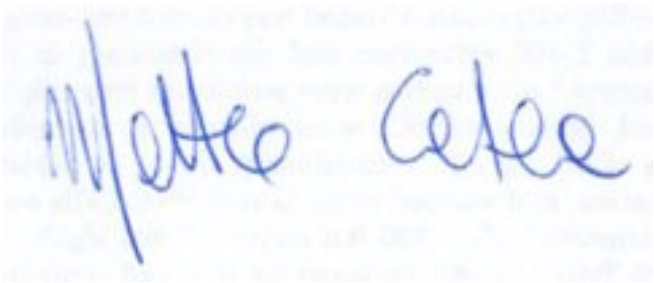

2.3 Combining electrospinning and fused deposition modeling for the fabrication of a hybrid vascular graft

*adapted from "**Centola M**, Rainer A, Spadaccio C, De Porcellinis S, Genovese JA, Trombetta M.Biofabrication. 2010 Mar;2(1):014102. Epub 2010 Mar 10"*

Introduction

It has been previously explained how in the cardiovascular field, tissue engineered vascular graft (TEVG) constructs, developed by using cultured autologous vascular wall cells, seeded onto a synthetic biodegradable polymeric scaffold [Shinoka et al, 1998], represent one of the most encouraging strategies to surmount the shortcomings arising from the surgical replacement with autologous vessels, allografts or xenografts as well as synthetic materials [Xu et al, 2008]. Although the encouraging results obtained with the electrospun PLLA scaffold loaded with heparin introduced in the previous paragraph, the mechanical properties of the proposed TEVG, along with electrospun fibrillar matrices in general, are still poor. The mechanical ability of the scaffold to maintain the structural and functional integrity immediately after implantation and during the remodeling phases still represents an issue [Kim et al, 2008].

With this in mind, we chose to increase the mechanical strength of the scaffold. Fused Deposition Modeling (FDM) was chosen as the candidate technique. FDM creates models out of heating thermoplastic material, extruded through a nozzle, positioned over a computer-controlled table. In the emerging field of the so-called Computer Aided Tissue Engineering (CATE) several groups are reporting the use of FDM for the fabrication of 3D constructs [Sun et al, 2002; Sun et al, 2004].

To improve the performance of biodegradable TEVGs in terms of blood compatibility, researchers have extensively been working on their surface modification using heparin. Addition of heparin is considered a functionalization strategy that enables to capture and concentrate the circulating angiogenic growth factors released during vascular injury. Finally, heparin itself has an important effect on cell differentiation towards vascular endothelium and homeostasis and has been shown to promote endothelial commitment in bone marrow stem cells in our previous work.

Human mesenchymal stem cells (hMSCs) from bone marrow have been shown to be a suitable candidate for tissue regeneration including vascular, cardiac [Spadaccio et al,

2008] and bone tissues [Spadaccio et al, 2009]. Guided differentiation of an easily recruitable and highly plastic stem cell type, as hMSCs, could overcome the current difficulties related to the lack of "off-the-shelf" availability, the low cell yields and quality, and the problems in harvesting and propagating autologous mature fully differentiated endothelial cells.

The aim of this study was to develop a heparin loaded electrospun PLLA tubular scaffold armored on its outer wall with a coil of PCL by FDM technique. The obtained scaffold was seeded with hMSCs and assayed in terms of cell viability, proliferation and differentiation in order to produce a device able both to guide the differentiation of stem cells towards vascular endothelium and to reproduce the histoarchitecture of native blood vessel.

Materials and methods

Tubular scaffold preparation

PLLA loaded with heparin scaffolds (PLLA/Hep) were prepared by electrospinning technique, as described in**paragraph 2.2**.

The following step consisted in the fabrication of the outer poly-ε-caprolactone (PCL, MW 80000, Sigma, Milwaukee, WI) armor. For this purpose, a prototypal FDM apparatus was developed by our group (Figure 16). The apparatus comprises an aluminum heated dispensing head ended with a 21G needle, a X-Y motorized stage (miCos GmbH, Eschbach, Germany) for the positioning of the sample and a Z stage (miCos GmbH) for controlling the distance between the dispensing head and the sample holder. The aluminum dispensing head is supplied of two heating cartridges and a resistance thermometer (Pt100), connected to a programmable temperature controller (model 400, Gefran, Brescia, Italy). Therefore, the pellet-form PCL is charged in the dispensing head and melted at 80 °C. Extrusion process is performed by pressure assisted dispensation, feeding pressurized argon gas by means of a high pressure line (working pressure ca. 8 bar) connected to a control electrovalve.

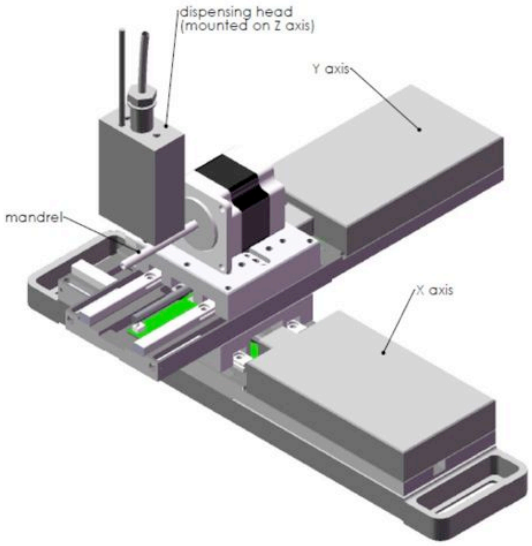

Figure 16. Schematic representation of the FDM apparatus with the dispensing head and the mandrel

Custom developed control software generates the process toolpath and controls the actuation of all the system components (axes movement, dispensing head temperature and electrovalve). The system was tailored to the fabrication of hybrid grafts by the addition of a rotating mandrel, actuated by a stepper motor (Astrosyn model 17PM, Minebea Co, USA) driven by the control software. The PLLA/Hep scaffold was mounted on the mandrel. Combining controlled rotation of the mandrel (10 rpm) with linear motion of the Y-axis stage (150 $\mu m \cdot s^{-1}$), it was possible to accurately wrap the scaffold with an armoring coil of PCL (PLLA/Hep/PCL sample).
Microstructure of these obtained materials was evaluated by Field Emission Scanning Electron Microscopy (FE-SEM, Supra 1535, Leo Electron Microscopy, Cambridge, UK).

Drug release study

Heparin release rate was assayed using the Azure A spectrofluorimetric method, as detailed in the previous **paragraph 2.2**.

Mechanical properties

Mechanical tests were performed both on electrospun grafts and on armored tubes (PLLA/Hep and PLLA/Hep/PCL samples). Great saphenous vein from an adult male patient was also tested as a reference (3 samples for each experimental group). To provide a complete mechanical characterization, measurements included static compliance,

stiffness index, ring and longitudinal uniaxial tensile parameters (including burst pressure), and suture retention [Stankus et al, 2007; Smith et al, 2008; Sell et al, 2006].

In the hybrid structure PLLA/Hep/PCL, the outer helix could not be assumed as a homogeneous layer, undergoing the deformation of the underlying electrospun PLLA layer. Moreover, with the aim to evaluate the strengthening effect provided by this PCL coil with respect to the unarmored sample PLLA/Hep, the author chose to calculate stress and strain values from measured load-displacement data referring to the section of the electrospun layer, that is identical for the two samples. In this assumption, the contribution of the PCL coil reflects in a modification of the mechanical properties of the electrospun layer in the PLLA/Hep/PCL sample.

For what regards circumferential characterization, each construct was cut in rings that were measured by means of a dial caliper. Rings were inserted with two stainless-steel flat hooks that were subsequently fixed to the clamps of a testing device (TH2730, Thumler, Nurnberg, Germany) equipped with a force transducer (Nordisk Transducer Teknik, Hadsund, Denmark), and pulled at 10 mm/min crosshead speed until sample failure. Prior to testing, all samples were preconditioned with cycles at 5% circumferential stretch. Load–displacement data were computed to obtain stress–strain curves starting from specimen geometrical parameters.

According to Nieponice et al. [Nieponice et al, 2008], ultimate tensile stress (UTS) and strain to failure (STF) were considered as the maximum stress value before failure and its corresponding value of strain, respectively. Burst pressure (P_b) was also estimated from UTS using the following law

$$P_b = \frac{2 \cdot UTS \cdot t}{D_0} \quad (1)$$

where D_0 is the initial diameter of the samples and t is the initial thickness of the tested scaffolds. From this stress-strain relationship, the circumferential elastic modulus (CEM) was calculated as the first derivative curve in the linear segment. The maximum elastic modulus (MEM) and the stretch at maximum elastic modulus (SMEM) were, respectively, the maximum value of the derivative curve and its corresponding strain value [Stankus et al, 2007].

Similar approach has been followed for the longitudinal uniaxial tests. Given the peculiar arrangement of the hybrid graft, it was not possible to perform the test using the standard "dog bone" shaped sample, described by Sell et al. [Sell et al, 2006]. Hence, two cylindrical aluminum terminations were inserted at the ends of each construct segment and fixed with epoxy resin. Such terminations were connected to the clamps of the tensile tester.

Test was performed at an extension rate of 10 mm/min. Longitudinal elastic modulus (LEM), peak stress (PS) and longitudinal strain at failure (LSTF) were calculated starting from load-displacement data collected in the tests.

Static compliance tests were performed according to Stankus et al. [Stankus et al, 2007]. Constructs were mounted in a hydraulic circuit and subjected to a pressure ramp (0-250 mmHg) by means of a syringe pump (KD Scientific, Holliston, MA). The circuit was clamped downstream while the pump infused PBS at a constant rate (4 mL/min). Pressure was monitored using a pressure transducer (40PC100G1A, Honeywell, Freeport, IL) connected to the hydraulic circuit, while the outer diameter was measured by using a high-resolution camera and by processing the acquired images with an analysis tool (ImageTool 3.0, UTHSCSA, San Antonio, TX). Samples were preconditioned by clogging the porosities with a high-viscosity freezing medium (OCT Embedding Matrix, CellPath, Newton Pawys, SY). Assuming an incompressible wall, static compliance (SC) was calculated as follows, and reported as % per 100 mmHg as specified in the ANSI 7198 standard [Konig et al, 2009;Sell et al, 2006]:

$$\%C/100mmHg = \frac{D_{110}^{in} - D_{70}^{in}}{D^{in}{}_{70}} \cdot \frac{1}{\Delta P} \cdot 10^4 \quad (2)$$

where the inner diameter was estimated starting from the measured outer diameter and using the assumption of incompressibility of cross-sectional area (A)

$$D^{in} = 2 \cdot \sqrt{\left(\frac{D_{ext}}{2}\right)^2 - \frac{A}{\pi}} \quad (3)$$

Pressure-diameter relationship during static compliance measurements were also used to compute stiffness index, β, via [Stankus et al, 2002]:

$$\beta = \frac{\ln\left(\frac{P_{110}}{P_{70}}\right)}{\frac{D_{110}^{ext} - D_{70}^{ext}}{D_{110}^{ext}}} \quad (4)$$

Finally, suture retention tests were performed on 7 mm long samples by using the previously described tensile testing equipment at an extension rate of 150 mm/min in accordance with ANSI/AAMI VP20:1994 [Sell et al, 2007]. Geometrical characteristics were measured by means of a dial caliper. A single commercial 6.0 prolene loop (Ethicon Inc., Somerville, NJ) was placed 2 mm from the end of the sample, and secured to a hook connected to the upper clamp of the testing device. Suture retention force (SRF) was considered as the maximum force recorded prior to failure, while the suture retention

tension (SRT) was obtained by normalizing the retention force by sample thickness [Stankus et al, 2007].

Cell biology

Please refer to **paragraph 2.2**.

Statistical analysis

Data from biological investigations were processed using SPSS (Statistical Package for Social Sciences) release 13.0 for Windows (SPSS, Chicago, IL). Data are presented as mean ± SD. One-way ANOVA was performed to compare groups with different treatments, followed by multiple pairwise comparison procedure (Tukey test). Significance was at the 0.05/0.01 levels. Student's T test was used for analyzing fibers average diameter, heparin elution profile and mechanical properties, with a significance at 0.05 levels.

Results

Scaffold morphology

Electrospinning on a rotating mandrel was performed to obtain PLLA/ctrl and PLLA/Hep synthetic grafts (Figure 17a, 5 mm diameter, 0.3 mm wall thickness, 6 cm length). Then, these tubular grafts were reinforced with a single-layer helix of PCL coil by means of FDM obtaining a PLLA/Hep/PCL scaffold (Figure 17b). Pictures and FE-SEM micrographs of the obtained tubular PLLA/Hep scaffolds are presented in Figure 17a-c. Electrospun layer was formed by a homogeneous distribution of fibers with average diameter of 450 ± 150 nm (t-Test, P=0.05) as calculated using ImageTool 3.0 (UTHSCSA) starting from electron micrographies.

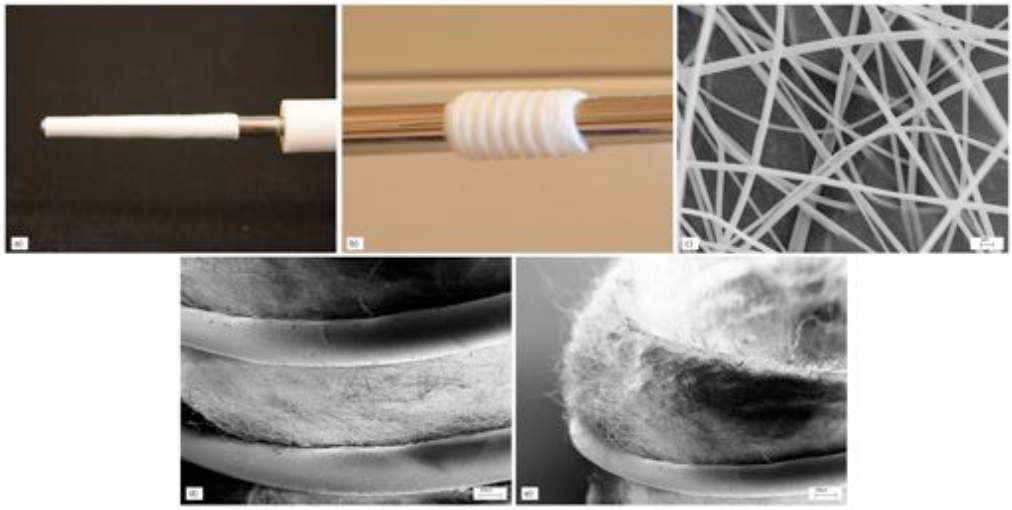

Figure 17. a-b) PLLA/Hep scaffold and PLLA/Hep/PCL obtained on the stainless steel rotating mandrel, respectively. FE-SEM micrographs of: c) PLLA/Hep electrospun scaffolds; d-e) PLLA/Hep/PCL scaffolds with the monolayered helical reinforcement coil

This fibrillar arrangement could represent a suitable environment for cell culturing as it closely mimics the structure of native extracellular matrix, and can potentially provide similar support to cell growth and differentiation.Outer PCL armour was composed of a single filament wrapping the scaffold in a helix arrangement, showing a mean diameter of 0.3 mm, and a pitch of 0.9 mm (Figure 17d-e).

Drug release study

Figure 11A showed heparin release profile, that results much similar to other drug release profiles from a biodegradable polymeric matrix [Yan et al, 2009;Moroni et al, 2006].An initial releasing burst in the first 24 hours, around the 5.75% of the total drug load, could be detected in the PLLA/Hep/PCL sample, followed by a sustained release. A cumulative release of ca. 10% of the total drug load was assessed after 4 weeks (t-Test, P=0.05). An analogous profile was reported for PLLA/Hep sample, showing no influence of PCL coil on drug elution kinetics.

Mechanical properties

Table 4reports the results derived from circumferential, longitudinal, compliance and suture retention mechanical testing for PLLA/Hep, PLLA/Hep/PCL a human saphenous vein sample (SV), together with data for internal mammary artery (IMA) that were taken from the literature [Konig et al, 2009].

Parameter	PLLA/Hep	PLLA/Hep/PCL*	SV	IMA†
UTS [MPa]	0.72 ± 0.03	1.58 ± 0.07	1.15 ± 0.13	
STF [mm/mm]	0.80 ± 0.05	1.78 ± 0.10	1.30 ± 0.04	
P_b [MPa]	0.08 ± 0.01	0.30 ± 0.03	0.16 ± 0.06	0.42 ± 0.17
MEM [MPa]	2.66 ± 0.16	3.37 ± 0.18	3.73 ± 0.17	
SMEM [mm/mm]	0.77 ± 0.08	1.77 ± 0.16	1.30 ± 0.05	
CEM [MPa]	0.54 ± 0.05	0.99 ± 0.08	0.88 ± 0.03	
PS [MPa]	0.66 ± 0.04	2.84 ± 0.15	1.20 ± 0.04	
LSTF [mm/mm]	0.31 ± 0.02	0.92 ± 0.05	0.57 ± 0.03	
LEM [MPa]	2.12 ± 0.13	3.08 ± 0.16	2.11 ± 0.12	
SRF [N]	0.72 ± 0.04	1.31 ± 0.07	4.3 ± 0.23	1.38 ± 0.5
SRT [N/m]	2.67 ± 0.14	4.85 ± 0.26	12.29 ± 0.89	
SC [%/100 mmHg]	65.9 ±2.7	9.72 ± 0.31	25.60 ± 1.13	11.5 ± 3.9
β [adimensional	2.32 ± 0.09	12.93 ± 0.52	5.42 ± 0.25	

Table 4. Mechanical properties of samples calculated from load-displacement data. * Stress/strain values for PLLA/Hep/PCL sample were calculated on the section of the electrospun layer, as previously described. † Data for mechanical properties of IMA have been derived from [Konig et al, 2009].

Stress-strain profiles for PLLA/Hep, PLLA/Hep/PCL and for the reference saphenous vein sample, as recorded during circumferential (Figure 18a-c) and longitudinal (Figure 18d-f) tensile tests are also reported.

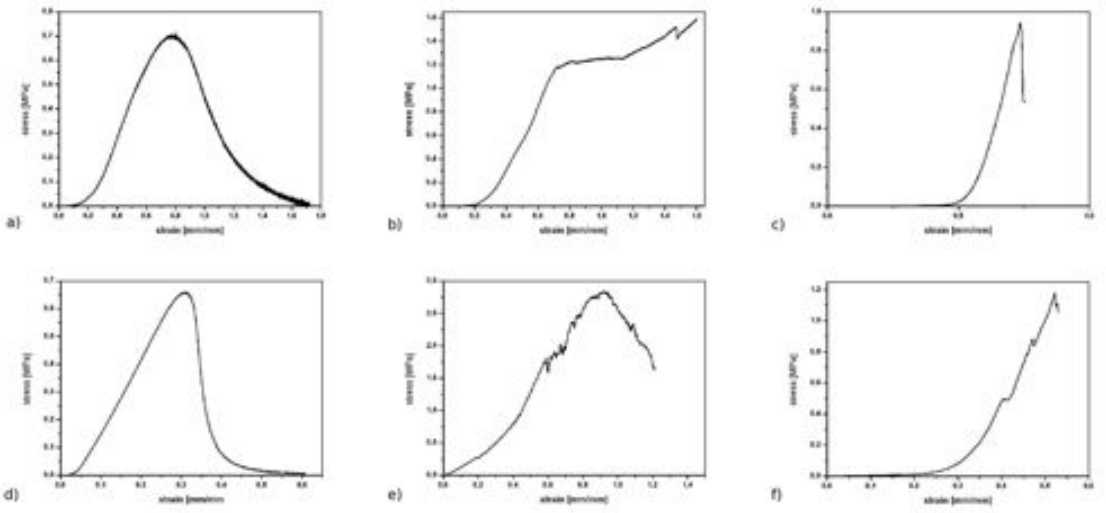

Figure 18. Stress-strain profiles for PLLA/Hep (a-d), PLLA/Hep/PCL (b-e) and for the reference saphenous vein sample (c-f) computed starting from the recorded load-displacement data from circumferential and longitudinal tensile tests, respectively.

Cell morphology and differentiation

Scaffold biocompatibility was assessed in terms of cytotoxicity and proliferation of hMSCs. Live/Dead assay demonstrated ≥90% cell viability both in PLLA/Hep/PCL and in PLLA/ctrl scaffolds (Figure 19a). Initial scaffold population was assayed by measuring the total DNA content per construct on sacrificial samples soon after seeding, showing no significant differences between PLLA/ctrl and PLLA/Hep/PCL. Cell proliferation was also evaluated by total DNA content measurement, showing a statistical significant increase (one-way ANOVA, $P<0.01$) in the PLLA/Hep/PCL scaffold with respect to the control (Figure 19b). In PLLA/Hep/PCL constructs, hMSCs exhibited changes in both cell morphology and protein markers expression, in comparison with controls.

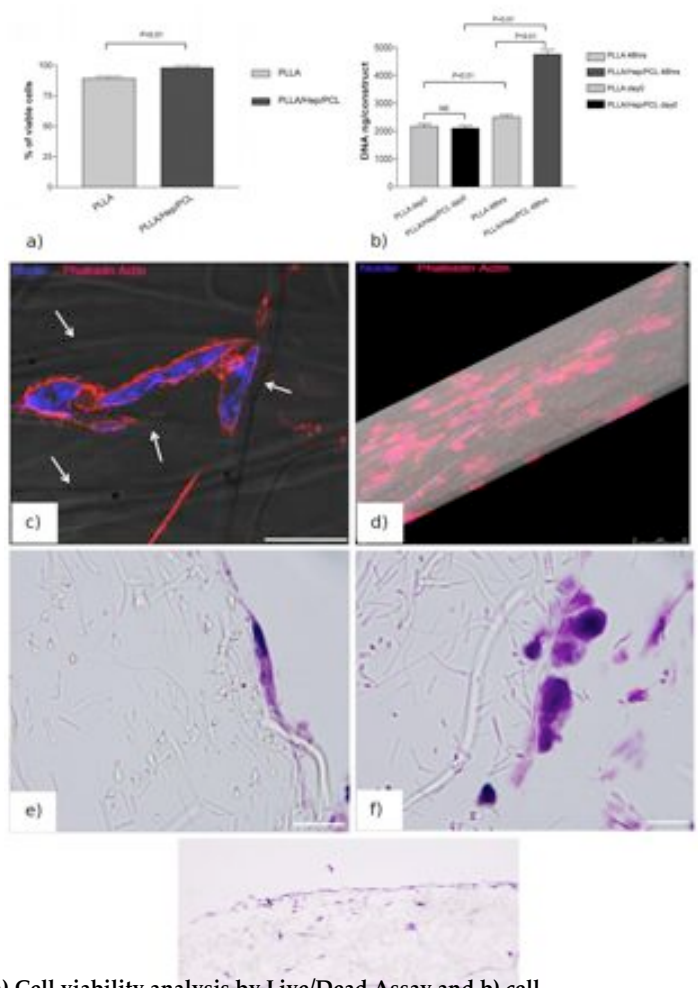

Figure 19. a) Cell viability analysis by Live/Dead Assay and b) cell proliferation evaluated by measuring the total DNA content per nstruct after 48 hours culturing. c) Confocal microscopy of PLLA/ctrl seeded with hMSCs after 48 hrs culturing (100X). Arrows indicate affold fibers. Scale bar: 25 µm. d) 3D rendering of an internal portion of the electrospun ayer in the PLLA/Hep/PCL construct. Hematoxylin/eosin staining of hMSCs attached on PLLA/Hep/PCL fibers: e) 40x. Scale bar: 25 µm; f) 10x. Scale bar: 100 µm. ematoxylin/eosin staining of hMSCs attached on PLLA/ctrl fibers: g) 40x. Scale bar: 25 µm.

Confocal microscopy for F-Actin and nuclear counterstain showed elongated cells with rare cytoplasm and a high nucleus/cytoplasm ratio (Figure 19c). Nuclei appeared enlarged with loose chromatin and several nucleoli, indicating conditions of non-quiescence. Moreover, membranes showed characteristic indentations and invaginations that resemble caveolae, typical of endothelial cells. Confocal microscopy 3D rendering was also performed on a central portion of the constructs (Figure 19d). Standard hematoxylin/eosin staining confirmed engrafting, showing elongated cells attached on PLLA fibers in PLLA/Hep/PCL (Figure 19e-g), and confirming cell migration and engraftment within the scaffold.

Immunofluorescence analysis on the PLLA/Hep/PCL scaffold revealed CD31 expression positive cells, localized on the luminal surface of the construct (Figure 20a).

Flow cytometry confirmed and quantified CD31 positivity, showing a statistically significant higher level of expression (one-way ANOVA, $P<0.01$) in the PLLA/Hep/PCL

scaffolds (Figure 20b). These findings were confirmed by Western blot analysis, followed by a semiquantitative densitometric evaluation (Figure 20c).

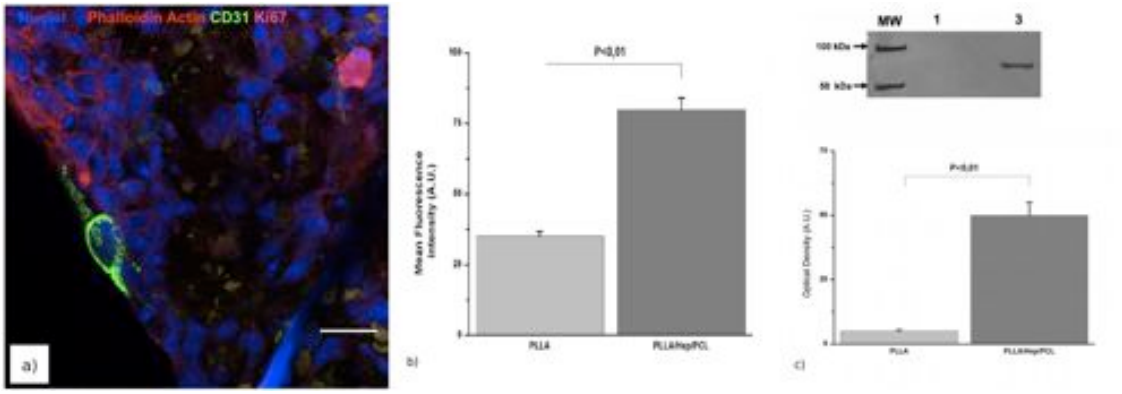

Figure 20. a) Confocal microscopy with immunofluorescence staining for CD31, Ki67 and F-Actin of PLLA/Hep/PCL seeded with hMSCs for 48 hrs (400X). A CD31 positive cell can be detected in an interesting luminal location. Scale bar: 25 µm. b) Cytofluorimetry analysis of CD31 expression of cells on PLLA/ctrl and PLLA/Hep/PCL scaffolds. c) Top: Western Blot for CD31 (83 kDa). MW: molecular weight marker. Lane 1: PLLA/ctrl seeded with hMSC for 48 hrs; Lane 3: PLLA/Heparin armored with PCL coil scaffold seeded with hMSCs for 48 hrs. Bottom: densitometry analysis of Western blot expressed in optical density.

Discussions

With the aim to improve mechanical properties of an already validated electrospun construct, we coupled electrospinning of a tubular scaffold to the deposition of a single, continuous biopolymeric coil performed by fused deposition modeling. Mechanical testing was performed, with the aim to assess the contribution of the outer coil to the overall mechanical properties of the scaffold.

Tensile behavior of bare electrospun material was compatible with the model of a fibrillar material; according to the model, fibers are progressively recruited by imposed strain, resulting in an increase in the steepness of stress-strain curve. At high stress values, progressive failure of fiber elements is experienced. These phenomena result in a bell-shaped curve. Ultimate tensile stress for the electrospun layer was found significantly lower than the saphenous vein tissue chosen as a reference.

In account of the fact that only the PLLA electrospun layer of the hybrid construct is designed to work as a scaffold for tissue regeneration, the authors decided to evaluate mechanical properties for PLLA/Hep/PCL constructs as referred to the geometry of the inner electrospun layer, thus providing a more suitable comparison with the unarmoured PLLA/Hep samples that have similar dimensions. The resulting specific force values do not have a direct mechanical meaning, since these values were not calculated on the real section of the construct, but still provide an 'equivalent stress' value useful for comparison,

and immediately pointing out the strengthening effect of the PCL coil. In particular, static compliance and stiffness index were found to be close to the values reported in the literature for human IMA [Konig et al, 2009]. Burst pressure, as calculated from UTS according to Nieponice et al. [Nieponice et al, 2008], was still significantly lower than IMA, as well as suture retention force. Authors acknowledge that further optimization is still needed to improve mechanical properties to closely match the artery tissue. This could possibly be obtained by tailoring the thickness of the electrospun layer and/or the thickness and pitch of the outer armour coil. Moreover, the evaluation of mechanical properties for on cellularized scaffolds throughout engineered tissue formation has to be performed, and will be the focus of further investigations.

At the same time, however, the obtained hybrid materials succeeded in enhancing the mechanical behavior of bare electrospun materials. The combination of electrospinning for the preparation of nanofibrous scaffolds apt to host cells, with the precise and controlled deposition of a reinforcement layer via fusion deposition modeling resulted in increased mechanical properties, while preserving the optimal fibrillar arrangement for cell attachment and tissue formation.

Our aim was to exploit the heparin above-mentioned properties and to develop an ad hoc differentiating device for autologous stem cells, able - at the same time - to facilitate and optimize the management of the construct once in the clinical setting. The concept of fabricating a scaffold containing factors - as heparin - able to induce stem cells differentiation and to exert important systemic effects, could represent an alternative to the mostly used TEVGs with mature, fully differentiated autologous endothelial cells, in order to improve their clinical management. Regarding the reported two-phases release profile, consisting of an initial burst followed by sustained release, similar behavior is reported in the literature [Bezemer et al, 2000; Moroni et al, 2006]. In the proposed models, release is governed by a combination of diffusion and degradation phenomena. In the earlier stages of the process, the initial burst is driven by Fickian diffusion and sustained by drug gradient concentration. Then, drug release is reliably due to the scaffold degradation, which, in turn, induces a decrease of polymer molecular mass resulting in an increase of permeability and hydrophilicity. The diffusion coefficient increases with the matrix degradation, while, on the other side, the drug concentration in the biopolymer decreases, resulting in an almost constant release rate. This kinetics could represent an advantage for eventual clinical applications as providing an immediate high-dose heparin release, potentially able to counteract the well-known initial thrombotic tendency soon after surgical vascular anastomosis, which is at the basis of the early graft failure.

As described in the previous paragraph, we already produced preliminary data on scaffolds tailored for cardiovascular structures [Spadaccio et al, 2010]. These data represent a proof of principle of the possibility to produce a scaffold suitable for stem cells seeding, containing the appropriate factors to induce a guided differentiation towards the desired phenotype. In these settings, differentiation would be realized within a three-dimensional ECM-like environment closely mimicking the tissue native architecture and allowing a harmonious ongoing cell growth and differentiation for tissue regeneration.

Results of light and confocal microscopy of scaffolds seeded with hMSCs, together with proliferation assay confirmed the generation of a non-hostile microenvironment for cell culturing, with an additional proliferative drive reliably induced by the functionalization with heparin. In functionalized constructs, morphostructural changes were observed, resulting in cell elongation, reduction in cytoplasm with nuclear enlargement, increase in nucleoli number and appearance of membrane invaginations resembling typical endothelial caveolae.

Along with these findings, in the heparin releasing scaffolds a shift towards CD31 positivity could be detected in comparison to bare PLLA, thus indicating a possible endothelial commitment. This finding was confirmed by CD31 expression, flow cytometry and is consistent with previous reports describing increased presence of CD31 positive microvessels following subcutaneous application of covalently-bond heparin-modified porous polyurethane scaffold. All these findings support our data concerning the ability of the heparinized scaffold to induce stem cell differentiation.

Conclusions

In the present work, we show the application of a hybrid technique, combining electrospinning and fused deposition modeling technique to fabricate a biopolymeric scaffold for vascular tissue engineering. We developed a tubular electrospun scaffold reinforced with a single-layer helical PCL coil to ameliorate mechanical properties of the TEVG. Such scaffolds showed better mechanical properties with respect to electrospun grafts, preserving the optimal fibrillar arrangement for initial cell attachment. Biological characterization of such scaffolds after seeding with human mesenchymal stem cells demonstrated the attitude of the scaffold to drive a differentiation process towards vascular endothelium.

References

Bezemer JM, Radersma R, Grijpma DW, Dijkstra DJ, Feijen J and van Blitterswijk CA, "Zero-order release of lysozyme from poly(ethylene glycol)/poly(butylene terephthalate) matrices", *Journal of Controlled Release*(**2000**), 64: 179

Kim GH, Son JG, Park SA and Kim WD, "Hybrid process for fabricating 3D hierarchical scaffolds combining rapid prototyping and electrospinning", *Macromolecular Rapid Communications* (**2008**), 29: 1577

Konig G et al., "Mechanicalpropertiesofcompletely autologous human tissue engineered blood vessels compared to human saphenous vein and mammary artery", *Biomaterials* (**2009**), 30: 1542

Moroni L, Licht R, de Boer J, de Wijn J R and van Blitterswijk C A, "Fiber diameter and texture of electrospun PEOT/PBT scaffolds influence human mesenchymal stem cell proliferation and morphology, and the release of incorporated compounds", *Biomaterials* (**2006**), 27: 4911

Nieponice A, Soletti L, Guan J, Deasy BM, Huard J, Wagner WR and Vorp DA, "Development of a tissue-engineered vascular graft combining a biodegradable scaffold, muscle-derived stem cells and a rotational vacuum seeding technique", *Biomaterials* (**2008**), 29: 825

Sell SA, McClure MJ, Barnes CP et al.,"Electrospun polydioxanone-elastin blends: potential for bioresorbable vascular grafts", *Biomedical Materials* (**2006**), 1: 72–80

Shinoka T etal., "Creationofviablepulmonaryartery autografts through tissue engineering",*Journal of Thoracic Cardiovascular Surgery*(**1998**), 115: 536

Smith MJ, Mcclure MJ, Sell SA et al.,"Suture-reinforced electrospun polydioxanone-elastin small-diameter tubes for use in vascular tissue engineering: a feasibility study", *Acta Biomaterialia* (**2008**), 4: 58–66

Spadaccio C, Rainer A, Chello M, Covino E, Trombetta M and Genovese J,"Drug releasing hybrid scaffold: new avenue in cardiovascular tissue engineering", *Tissue Engineering Part A*(**2008**), 14: 691

SpadaccioCetal, "Poly-L-lacticacid/hydroxyapatite electrospun nanocomposites induce chondrogenic differentiation of human MSC", *Annals of Biomedical Engineering*(**2009**), 37: 1376

Spadaccio C, Rainer A, Centola M, Trombetta M, Lusini M, Chello M, Covino E, Toyoda Y and Genovese JA, "Heparin-releasing scaffold for stem cells: a differentiating device for vascular aims", *Regenerative Medicine* (**2010**), 5: 645-657

Stankus JJ, Soletti L, Fujimoto K, Hong Y, Vorp DA, Wagner WR, "Fabrication of cell microintegrated blood vessel constructs through electrohydrodynamic atomization",*Biomaterials* (**2007**), 28: 2738–2746

Sun W and Lal P, "Recent development on computer aided tissue engineering—a review", *Computer Methods and Programs in Biomedicine* (**2002**), 67: 85

Sun W, Darling A, Starly B and Nam J, "Computer-aided tissue engineering: overview, scope and challenges", *Biotechnology and Applied Biochemestry* (**2004**), 39: 29

XuZC,ZhangWJ,LiH,CuiL,CenL,ZhouGD, et al.,"Engineering of an elastic large muscular vessel wall with pulsatile stimulation in bioreactor",*Biomaterials* (**2008**), 29: 1464

Yan S, Xiaoqiang Y, Shuiping L, Xiumei M and Ramakrishna S, "Controlled release of dual drugs from emulsion electrospun nanofibrous mats", *Colloids Surface Part B* (**2009**), 73: 376

2.4 In vivo evaluation: rabbit model of aorto-aortic bypass

Research objectives

Pilot study to test the in vivo effectiveness of the above-described bioactive tissue engineered vascular conduit fabricated using a combination of electrospinning and fused deposition modeling.

Introduction

As widely discussed in the previous sections, tissue-engineered vessels have been recently proposed as a promising solution to the limitations associated with current therapies for vascular diseases. Previous work in our laboratory has shown that an electrospun poly-L-lactide (PLLA) graft, functionalized with heparin and reinforced with a polycaprolactone (PCL) coil,properly combines the capacity to act as an attractive environment for hosting cells for what regard the electrospun layer, with the tensile properties of the fused deposited PCL. We showed that this composite scaffold is able to withstand physiological vascular conditions as well as to induce the differentiation of the mesenchymal stromal cells seeded within towards vascular endothelium.

The further step was to test the feasibility of this scaffold in an in vivo scenario, with a single-animal pilot study.

We showed that this PLLA/Hep/PCL composite is able to withstand physiological vascular conditions pertaining to high pressure and flow thanks to a complete biomechanical characterization [Centola et al, 2010]. However, it is uncertain whether this composite scaffold would display similar characteristics in the in vivo vascular environment where host tissue response is active. In this study we investigated whether the electrospun composite vascular scaffolds, reinforced with a PCL external coil, are able to maintain vascular cells under physiologic flow conditions. More importantly, we examined the durability and the maintenance of patency of our vascular grafts in situ in a rabbit aorto-aortic bypass model [Tillman et al, 2009].

The only modification performed to the proposed scaffold (**par. 2.3**) was the addition into the electrospun PLLA/heparin mixture of the erythropoietin (EPO). EPOis a potent, physiological stimulus for mobilization, homing and differentiation of the progenitor cells residing in the bone marrow. Thanks to these properties, the proposed scaffold, releasing EPO, will be potentially able to recruit endothelial and mesenchymal progenitors from the blood flow, cellularizing the scaffold.

Thus, the inner layer will act as a drug releasing system delivering factors useful in both the immediate management of the scaffold engraftment and in the maintenance of a milieu providing the correct signaling to guarantee tissue homeostasis and eventual recruitment of endogenous stem cell populations.

Materials and methods

Scaffold synthesis and characterization

A tubular bioactive PLLA electrospun scaffold reinforced with a single-layer helical PCL coil was produced by means of a Computer Aided Tissue Engineering approach, combining electrospinning and fused deposition modeling techniques, as previously described [Centola et al. 2010].

In vivo rabbit model

All procedures were approved by the Institutional Animal Care and Use Committee. A New Zealand White rabbit (Robinson Services, Inc., Mocksville, NC) were treated with aspirin for 1 week during and subsequent to graft implantation. Under general anesthesia, the infrarenal aorta was exposed through a midline abdominal incision. Engineered grafts of 4 cm in length were sutured in an end-to-side fashion to the aorta to realize an aorto-aortic bypass (Figure 21).

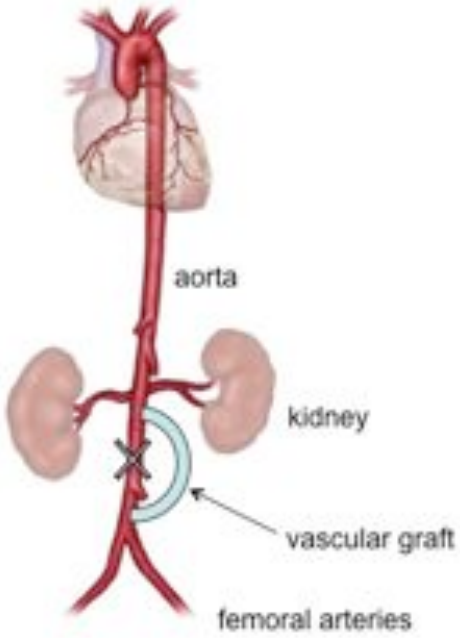

Figure 21. Rabbit aorto-iliac bypass model

The graft was then ligated,using monofilament 8–0 polypropylene sutures, among the two anastomoses to ensure that almost 80% of blood was supplied through the graft. Grafts were explanted 14 days after implantation.

Contrast enhanced vascular imaging

10 days before sacrifice, animals underwent CT scanning with intravenous contrast agent and volume-rendered reconstructions were obtained, in order to examine graft patency and geometry.

Hystology

Scaffolds were explanted and fixed in formalin for histologic analysis. Explanted scaffolds were

Figure 23. A representative contrasted CT scan shows absence of aneurysm along the entire length of the graft.

processed in a tissue processor, embedded in paraffin and sectioned at a thickness of 5 mm. Sections were deparaffinized and stained with hematoxylin and eosin. The stained sections were examined for structural characteristics and evidence of cellular infiltrates.

Results

Structural integrity of grafts in vivo

To determine the feasibility of using electrospun vascular scaffolds for application, baseline structural integrity and host responses to the scaffold material were evaluated in a rabbit aorto-aortic bypass model (Figure 22). At the time of implantation, engineered grafts demonstrated no evidence of transgraft leakage of blood. No bleeding or neurologic complications were encountered throughout the entire duration of this study.

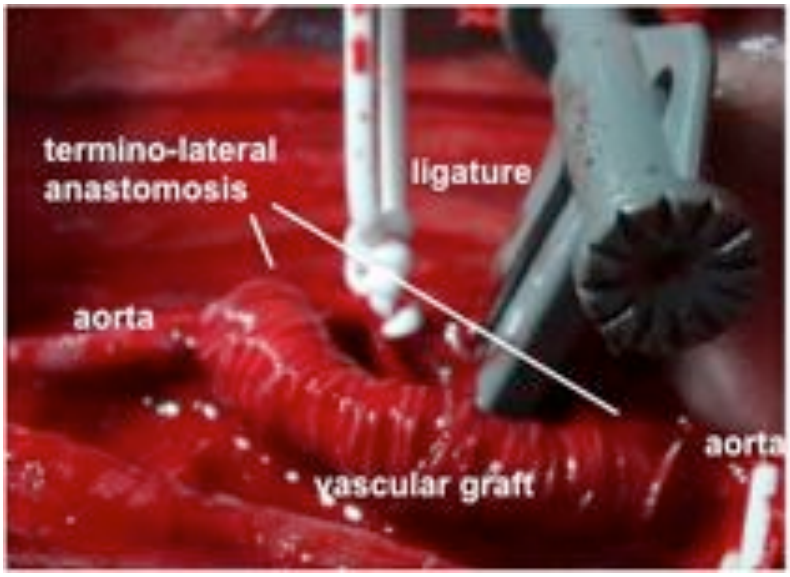

Figure 22. Rabbit aortoiliac bypass procedure: a representative operative image is shown

Graft analyses

Armored scaffolds showed optimal mechanical and suture retention properties and a suitable release profile, as shown in the previous paragraph. Analysis of CT scans and 3D volume rendering demonstrated patency of the graft implanted with adequate distal run off.

To determine whether the implanted electrospun vascular scaffolds maintain structural integrity

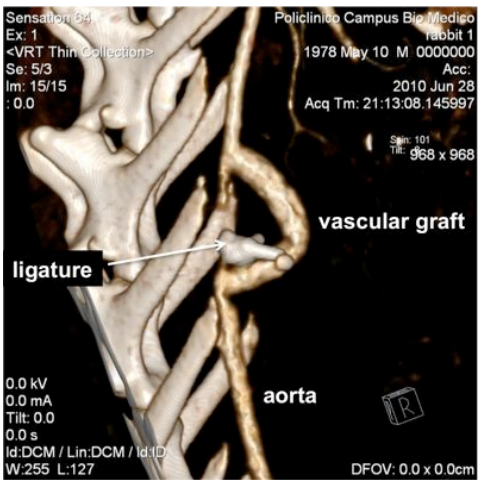

and resist the development of aneurysms, duplex angio-CT was performed at 4 days after implantation (Figure 23), confirming a stable three-dimensional architecture. Throughout the duration of the study, grafts maintained a constant luminal diameter (data not shown). These findings indicate that PCL/PLLAcomposite scaffolds are able to maintain structural integrity under normal hemodynamic conditions. At retrieval, the implanted scaffolds remained intact after serving as a bypass between the aorta and iliac artery.

Histology following explantation showed a perfectly open lumen (Figure 24A-B), an adequate endothelialization with flattened cells lining on the luminal surface of the tubular structure (Figure 24C). No signs of thrombosis could be detected. The outer layer of the prosthesis was populated by elongated cells resembling smooth muscle cells (Figure 24D).

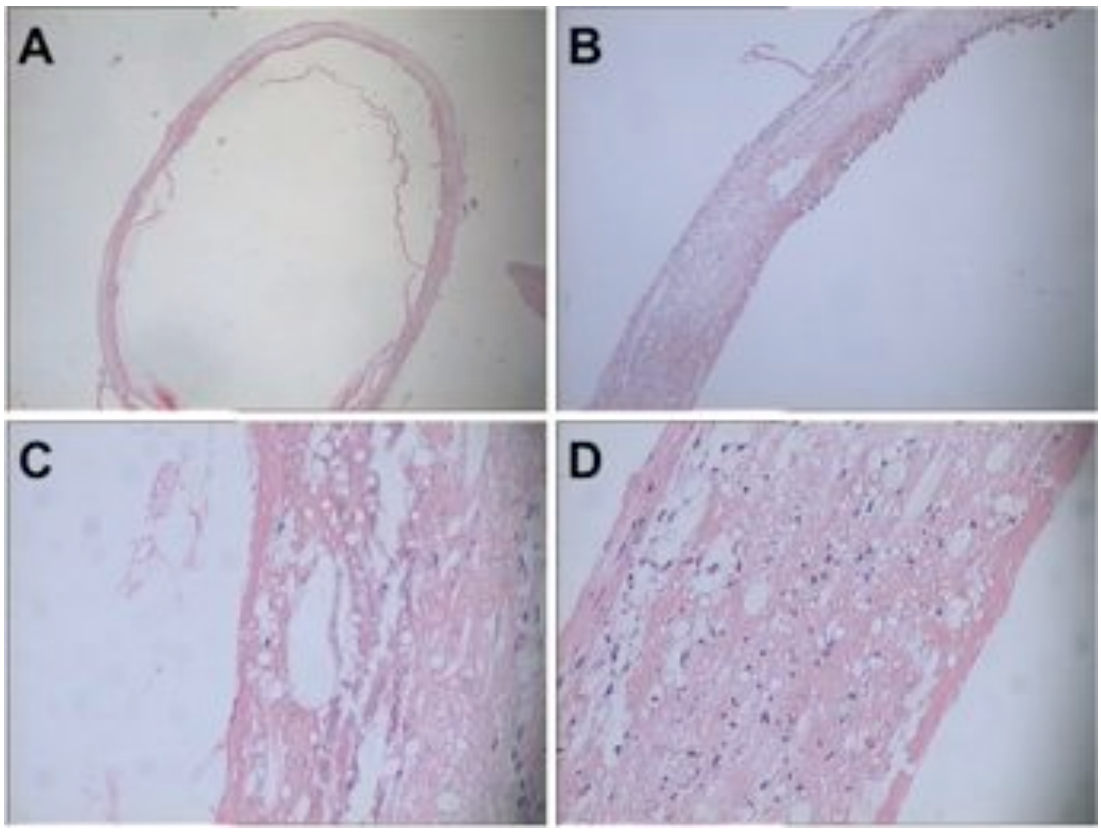

Figure 24. Hematoxylin/eosin staining performed on vascular graft. Radial section 5X (A) and 20X (B), inner (C) and outer (D) side of the graft

Discussionsand Conclusions

In the absence of suitable autologous vein grafts, vascular substitutes must be used to repair diseased vessels. Tissue engineered blood vessels, constructed with cells and support matrices, have become promising vascular substitutes that may improve the outcome of vascular reconstruction procedures. However, finding a biocompatible vascular scaffold, which accommodates vascular cells while maintaining structural integrity under normal hemodynamic conditions, has been difficult.

We developed a tailored engineered device able to overcome the hurdles commonly hampering vascular grafts, thrombogenicity and lack of mechanical strength. Differently from other approaches,we did not pre-seed scaffolds with autologous cells. On the opposite, we focused on the optimization of the biomimetic design of the scaffold and its differentiating abilities. The rationale underlying this study concerned the possibility to exploit the endogenous reparative capabilities of the body and to guide these regenerative resources toward tissue restoration by means of a tailored absorbable material.

This pilot study showed that our PCL/PLLA composite scaffolds are able to recruit cells from the blood flow and maintain structural integrity and patency for at least 2 weeks when implanted in rabbits as an arterial bypass graft.

Future studies will examine whether seeding these scaffolds with vascular cells may improve long-term patency as well as scaffold remodeling. In summary, this study indicates that our smart scaffold may be a clinically applicable alternative to traditional prosthetic vascular graft material.

References

Centola M, Rainer A, Spadaccio C, De Porcellinis S, Genovese JA and Trombetta M, "Combining electrospinning and fused deposition modeling for the fabrication of a hybrid vascular graft", *Biofabrication*(**2010**), 2: 014102

Tillman BW, Yazdania SK, Lee SJ, Geary RL, Atala A, Yoo JJ, "The in vivo stability of electrospun polycaprolactone-collagen scaffolds in vascular reconstruction",*Biomaterials* (**2009**), 30: 583–588

2.5 Surface functionalization of NO-releasing scaffolds for the differentiation of human mesenchymal stem cells

*adapted from "Rainer A, **Centola M**, Spadaccio C, Mozetic P, Petruzziello L, Abbruzzese F, Franchitto G, Chello M, Covino E and Trombetta M, manuscript in preparation"*

Introduction

Nitric oxide (NO) is a diffusible, short-lived free radical, as well as one of the smallest known biologically active messenger molecules and plays a pivotal role in vascular homeostasis modulating the activation and adhesion of leukocytes, limiting platelet aggregation and thrombus formation, and maintaining the vascular smooth muscle in a non-proliferative state, thereby preserving blood vessels from adverse vascular remodeling [Verma et al, 2005]. Biological characteristics of NO could therefore constitute an attractive cue to ameliorate properties of biomaterials for cardiovascular applications.

Noteworthy, one of the reasons considered at the root of the early failure of saphenous vein grafts is the relative paucity of nitric oxide production by these conduits as compared with arterial ones. To this extent, Jun and colleagues developed a diazeniumdiolate-modified polyurethane (DMP) for vascular applications. Diazeniumdiolates are interesting compounds containing the –N(O)=NO– functional group [Loscalzo et al, 2001; Jun et al, 2005]. The anionic portions of these compounds spontaneously decompose in solution to release NO, leaving an amine group as a by-product [Hrabie et al, 2002] with rates of dissociation depending on several factors, such as structure, temperature, and pH of solution [Keefer et al, 1996]. DMP structures demonstrated enhanced rates of proliferation of endothelial cells and increased rates of migration and coverage of the synthetic surface. More recently, incorporation of a diazeniumdiolate NO donor into the backbone of a polyurethane containing both polyethylene glycol (PEG) and the cell-adhesive tyrosine isoleucine glycine serine arginine (YIGSR) peptide sequence has been performed in order to provide a NO local release during the period of graft endothelialization [Lakeshia et al, 2007; Taite et al, 2008]. The laminin-derived cell adhesive peptide sequence YIGSR encourages endothelial cell adhesion and migration [Jun et al, 2005], while the NO release improves endothelial cell proliferation during the period of graft endothelialization. NO-generating, cell-adhesive polyurethane-PEG copolymer showed the ability to reduce platelet adhesion and smooth muscle proliferation, while enhancing endothelial cells

attachment and proliferation. Therefore, the therapeutical potential of NO-generating scaffolds remains high and it may be suitable as a candidate material for small-diameter vascular grafts.

Moreover, accumulating evidence indicates that NO plays an important role in stem cells proliferation and differentiation. Chu et al. showed that NO inhibited the proliferation of bone marrow multipotent progenitor cells (hMSCs) from human, rat and mouse, enhanced Oct-4 expression, and promoted endothelial differentiation of hMSCs through a mechanism independent of cGMP pathway [Chu et al, 2008]. On the other hand, the effect of NO donors and soluble guanylyl cyclase (sGC) activators has been demonstrated in the differentiation of embryonic stem cells (ESCs) into myocardial cells thanks to an increase in Nkx2.5 and myosin light chain mRNA expression on exposure of cells to NO donors. At the same time, a decrease in mRNA expression of both cardiac-specific genes with nonspecific NO inhibitor and a concomitant increase and decrease in the mRNA levels of sGC α1 subunit has been reported [Mujoo et al, 2008]. Since the role of NO in the differentiation of stem cells has not been definitely clarified, one of the purposes of the present study was to determine the effects of NO on a population of bone marrow derived human mesenchymal stem cells (hMSCs).

NO can be generated from several chemical sources, such as S-nitrosothiols, S-nitroso-L-cysteine, organic nitrates, iron-nitrosyl complexes, sydnonimines, C-nitroso compounds and secondary amine-NO complex ions. All of these compounds degrade to form NO, both directly and indirectly. We will concentrate on S-nitrosothiols because it has been shown they are present in vivo as protein adducts (concentration in plasma albumin approx 7 μM [Hall et al, 2009]) and, in recent years, the therapeutic use of these compounds in a variety of clinical conditions has become increasingly apparent. Moreover, it has been generally assumed that naturally occurring S-nitrosothiols act as a depot for NO, which can be released when required. The rates of decomposition of S-nitrosothiols in vitro have been shown to be influenced by a number of factors, such as pH, temperature, and light exposure [Al Sadoni et al, 2000].

Starting from these achievements, we here propose a biomimetic approach where the surface of a poly(ε-caprolactone) (PCL) scaffold was functionalized with S-nitrosothiols in order to produce a NO-releasing construct, in order to assess the role of NO in the differentiation of hMSCs seeded therein toward vascular endothelium.

To enhance the yield of functionalization reaction, and therefore the dose of released NO, we chose electrospinning as the scaffold fabrication technique, as it provides a high surface area-to-volume ratio, besides a suitable environment for hosting cells. Indeed, our

group demonstrated that nano- and micro-fibrous electrospun scaffolds, loaded with suitable bioactive molecules, allow the remodeling of cardiovascular grafts in both cellular and extracellular content, and represent a useful differentiating device for stem cells seeded therein [Spadaccio et al, 2010; Spadaccio et al, 2011].

Materials and methods

Scaffold preparation

A polymer solution containing 15% w/v PCL (MW 80 kDa) in a 7:3 dichloromethane:methanol solvent mixture was prepared. All products were purchased from Sigma (Milwaukee, WI, USA). The solution was transferred into a 5 mL syringe attached to a blunt 23G needle and fed by means of a syringe pump (KD Scientific, Holliston, MA, USA) with a feed rate of 0.5 ml/h and electrospun onto an earthed collector placed at a distance of 10 cm, using a voltage of 8 kV (ES-30, Gamma High Voltage Research, Ormond Beach, FL, USA). PCL scaffolds were then sterilized by UV irradiation (254 nm, 20W) for 20 minutes at a distance of 20 cm.

Microstructure of the obtained membranes was evaluated by Field Emission Scanning Electron Microscopy (FE-SEM, Leo Supra 1535, Cambridge, UK). Average fibers diameter was calculated using ImageJ software (NIH).

Specific surface area (SSA) of the electrospun PCL scaffolds was calculated by BET analysis (Quantasorb, Quantachrome, Boynton Beach, FL, USA). The material was placed in a vacuum chamber and degassed prior to be brought at a constant temperature near to the temperature of liquid nitrogen (ca. -196 °C). Controlled doses of argon were injected and adsorbed on the material's surface. The amounts of gas molecules adsorbed or desorbed was determined by the pressure variations due to the adsorption or desorption of the gas molecules by the material (adsorbate). Knowing the area occupied by one adsorbate molecule, σ [Å^2], and using an appropriate adsorption model, it the number of molecules needed to make a monolayer coverage on the surface of one gram of adsorbent nm was calculated. So, the SSA could be determined by the following:

$$SSA=NAnm\sigma \quad [m^2/g]$$

where NA is the Avogadro's number [i].

Scaffold functionalization

Functionalization reactions were performed under sterility. The PCL scaffold was treated in order to increase the surface concentration of carboxyl groups, slightly modifying the method described by Sun et al. [Sun et al, 2006]. Briefly, the scaffolds underwent alkali-

catalyzed hydrolysis, obtained by soaking for 90 minutes in a heated 0.1 M NaOH solution (T=40 °C) in order to hydrolyze ester groups (leading to free –COO– surface groups), followed by protonation into a 0.01 M HCl solution for 30 minutes at room temperature. These experimental conditions were found to be optimal on the basis of ATR/FTIR characterization.

After extensive washing in PBS, activated PCL scaffolds were immersed in a catalyst solution containing 1-ethyl-3-(3-dimethylaminopropyl) carbodiimide hydrochloride (EDC, Sigma) 0.4 M and N hydroxysuccinimide (NHS, Sigma) 0.1 M, in MES buffer (Sigma, pH=6.20). After reaction for 10 minutes in this mixture, samples were rinsed in PBS and then reacted with a 50 mM L-cysteine (Sigma) solution in MES for 15 minutes (PCL/Cys). Then, PCL/Cys samples were soaked in a 6 mg/mL dithiothreitol (DTT, Sigma) aq. solution for 90 minutes, under nitrogen atmosphere, in order to reduce eventual disulfide bonds among cysteine molecules. Finally, introduction of S-nitrosocysteine groups was obtained by incubating PCL/Cys samples in a sodium nitrite (10 mM) aq. solution (pH 2, HCl) at room temperature for 30 min in the dark (PCL/Cys/NO). Any unreacted thiol groups were then alkylated with N-ethylmaleimide (NEM; 1 mM) at room temperature [m]. PCL/Cys/NO patches were stored in HCl (pH 2) solution at 4 °C up to cell biology phase. A schematic representation of the protocol is shown in Figure 25.

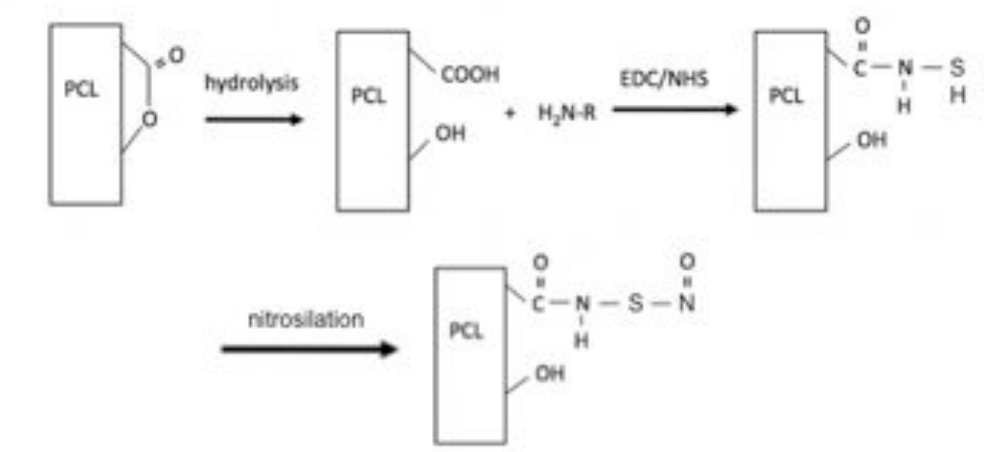

Figure 25. A schematica representation of the protocol used to functionalize electrospun PCL scaffolds

Characterization of modified surfaces

The concentration of surface carboxylic groups on PCL after hydrolysis was determined by indirect titration. Hydrolyzed patches were exposed to a fixed volume of 0.01 M NaOH solution for 10 minutes. Non-hydrolyzed PCL electrospun membranes were used as a

control and exposed to NaOH at the same experimental conditions. Then, 0.01 M HCl solution was used to titrate the NaOH solution to which samples had been exposed. The increase in surface carboxylic concentration could be determined as a difference between the two values. Carboxyl surface concentration was normalized with respect to the polymer average SSA value, calculated from BET analysis. Experiments were performed in triplicate.

Cyteine surface concentration on PCL/Cys scaffolds was assessed by means of Ellman's assay [Ellman, 1959]. The procedure is based on the reaction of the cysteine thiol group with 5,5'-dithiobis(2-nitrobenzoic acid) (DTNB) to give a cysteine/2 nitro 5 thiobenzoic acid (TNB) heterodisulfide group and free TNB, which is quantified by the absorbance of its anion (TNB^{2-}) at 412 nm. Briefly, 100 mg of the reduced PCL/Cys samples were incubated in 1 mL of a 4mM DTNB (Sigma) solution in PBS for 60 minutes under nitrogen atmosphere, then absorbance (412 nm) of the supernatant was read on a UV/Vis Spectrophotometer (Shimadzu, Japan) and TNB^{2-} concentration was calculated against a standard curve, obtained by reacting known amounts of cysteine with DMMB in the 0-100 μM range. Experiments were performed in triplicate.

Nitric oxide release profile

Nitric oxide release profile from PCL/Cys/NO scaffolds was assessed by means of a slightly modified Greiss assay for the colorimetric evaluation of S-Nitrosothiols [Cook et al, 1996]. Briefly, the following colorimetric solutions were prepared: 50 mM sulfanilamide (Sigma) in a 5% w/vol phosphoric acid solution (Component A) and 5 mM N-(1-naphthyl)ethylenediamine dihydrochloride (Sigma) in distilled water (Component B). PCL/Cys/NO samples were immersed in PBS at room temperature in order to start the NO release. 100 μL of supernatant were drawn at selected timepoints up to 120 minutes. 100 μL of components A and B were subsequentially added to the sample and for 10 minutes each in the dark. Finally, the absorbance (at 548 nm) was read by means of UV/Vis Spectrophotometer (Shimadzu). Standard sodium nitrite solutions in PBS in the 0.1-100 μM range were used to perform a calibration curve. These experiments were performed in triplicate.

Cell seeding

Human mesenchymal stem cells (hMSCs) (passage 4, Lonza, Basel, Switzerland) were seeded on PCL/Cys/NO, PCL/Cys and PCL patches, the last two used as a control for biological assessments. Prior to cell culture, PCL, PCL/Cys and PCL/NO patches were

mounted into crown inserts (Scaffdex, Finland) and placed into a 96-well plate. Then, a standard static seeding was performed at the density of $500 \cdot 10^3$ cells/cm^2, as previously described [Kim et al, 1998]. Briefly, 20 μL droplets of hMSC suspension were dispensed on the scaffolds, followed by overnight incubation. To standardize culturing protocol and normalize subsequent biological analysis, seeding efficiency was calculated, as elsewhere described [Soletti et al, 2010]. Briefly, after the seeding of each sample, the medium exuded through the scaffold was collected and used for cell counting with a hematocytometer to calculate seeding efficiency. Then, 200 μL of growth medium was added to each well and constructs were cultured for 7 days in basal medium (Dulbecco's minimum essential medium (DMEM) supplemented with 10% fetal bovine serum (FBS), 100 units/mL penicillin, 100 μg/mL streptomycin).

Cell engraftment and biological assessment

Cell toxicity due to the scaffolds was determined at 4, 8 and 24 hours by using a Vybrant Cytotoxicity Assay Kit (Molecular Probes, Invitrogen) in accordance with the manufacturer's instructions. The Vybrant Cytotoxicity kit monitors the release of the cytosolic enzyme glucose 6- phosphate dehydrogenase (G6PD) from damaged cells into the surrounding medium. Plate was read on a fluorescence microplate reader (Tecan, Männedorf, CH) at 540 nm with correction at 595 nm.

To determine the cell proliferation in contact to produced scaffolds, $5 \cdot 10^3$ hMSCs were separately plated in a 96-well plate (BD, Falcon, San Jose, CA) in growing media and cultured for 24 hours. All the types of scaffolds were added to the wells. Cell proliferation was determined at 1, 3 and 7 days by using a MTT Assay (Molecular Probes, Invitrogen) in accordance with the manufacturer's instructions. Briefly, MTT was added to the cell culture media and incubated at 37° for 3 hours. Cells were then washed three times and DMSO added to each culture and incubated for 10 minutes. Plate was read on a fluorescence microplate reader (Tecan) at 540 nm with correction at 595 nm.

Upon culturing, scaffolds were fixed with PFA, embedded in optimal cutting temperature (O.C.T., Thermo Fisher Scientific), snap frozen, and cut in 15μm slices. Slides were further processed for hematoxilin-eosin staining in order to achieve a morphological analysis. For cell attachment and engraftment assessment was also used confocal microscopy staining cells on the scaffolds for F-Actin with Rhodamine Phalloidin (Molecular Probes) and nuclei using TOTO (Invitrogen) as nuclear counterstain.

Immunostaining

Expression of C31 was evaluated by immunofluorescence. Briefly, frozen tissue sections were permeabilized with 0.1% Triton-X 100 in PBS for 10 minutes. Non-specific binding of antibodies was blocked by incubating the samples for 45 minutes with 2% bovine serum albumin. A mouse monoclonal anti-CD31 (Chemicon, CA) antibody at 1:500 titer was used and subsequently revealed with an Alexa Fluor 488 secondary goat anti-mouse IgG antibody. In negative control experiments, the incubation with primary antibodies were omitted. Cytoplasmic actin was counterstained with Phalloidin Red (Invitrogen) and for nuclear visualization, cells were counter-stained with TOTO. The samples were then mounted in Prolong antifade medium (Invitrogen) and viewed under a confocal microscope (Nikon) by two independent observers.

Realtime reverse transcriptase PCR

Samples at 48 h and 7 days culturing were characterized for expression of vascular endothelium genes. Total cellular RNA was isolated using TRI Reagent (Sigma), performed directly on the cellularized scaffolds. To avoid DNA contamination, RNA was treated with DNase I (Invitrogen, Carlsbad, CA) at 37 °C for 15 min followed by inactivation with 2 mM EDTA at 65 °C for 10 min. Extracted RNA was quantified by spectrophotometric technique (Nanodrop, Invitrogen). 1 μg of total RNA was retrotranscribed using High Capacity cDNA Reverse Transcription Kit (Applied Biosystems) according to the manufacturer's instructions.

Realtime quantitative PCR was performed on 100 ng of cDNA to detect the expression of CD31, VEGF and 18S rRNA as housekeeping gene, using specific primers (TaqMan® Gene Expression Assay, Applied Biosystems) and TaqMan Universal MasterMix II (Applied Biosystems) in a total volume of 20 μL.

Electron Microscopy

Samples were routinely prepared for scanning electron microscopy . Briefly, specimens were fixed by immersion in 2.5% glutaraldehyde solution in a 0.1 M PBS solution at 4 °C for 48 hours. Samples were then postfixed in 1% osmium tetroxide in 0.1 M PBS and water-exchanged with ethanol in graded series.

Specimens for FE-SEM were critical point dried with carbon dioxide (EMITECH K850 CPD, Ashford, UK), mounted on aluminum stubs, metal-coated with 3 nm of platinum (EMITECH K550 Sputter Coater, Ashford, UK), and observed with a S-4500 FE-SEM (Hitachi, Japan), operating at 7-15 kV.

Statistical analysis

Data were processed using SPSS (Statistical Package for Social Sciences) release 13.0 for Windows (SPSS, Chicago, IL, USA). Data are presented as mean ± SD. One-way ANOVA was performed to compare groups with different treatments, followed by multiple pairwise comparison procedure (Tukey test). Assumptions of normality were checked and met. Holm-Sidak method was used to increase the power of the analysis. Pearson's product-moment r coefficient was calculated to evaluate correlations. Significance was set at the .05 level.

Student's t-test was used for analyzing average fiber diameter; characterization of PCL modified surfaces and NO release profile, with significance at 0.05 levels.

Results

Scaffold characterization

FE-SEM micrographs of PCL electrospun scaffolds at different magnifications are showed in Figure 26A-B. Scaffolds consist in a non-woven cloth, with porosity in the range of 10 μm. PCL fibers are non-porous and show an average diameter of 310±90 nm.

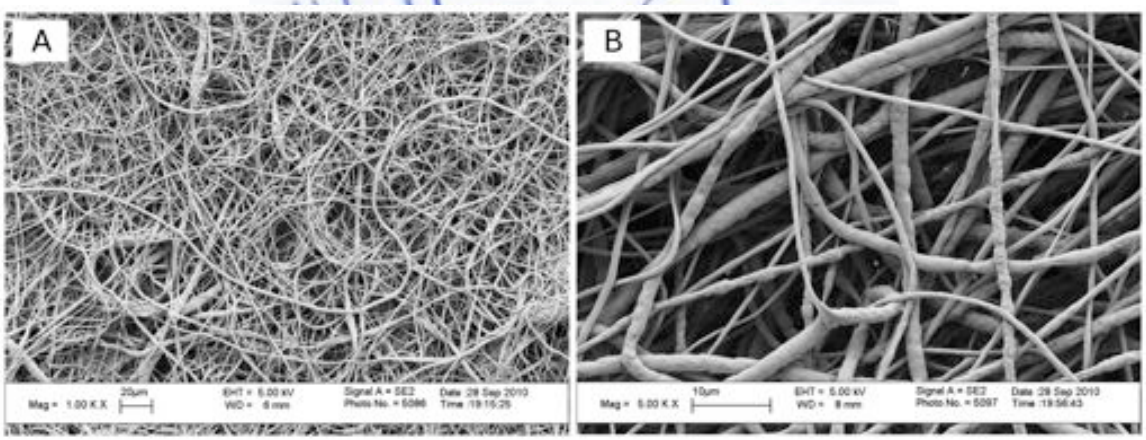

Figure 26. SEM micrographies of electrospun PCL scaffolds at two different magnifications.

This intrinsic fiber porosity could represent a suitable environment for cell culturing as closely mimic the structure of native extracellular matrix, and can potentially provide similar support to cell growth and differentiation.

Results from BET analysis gave an estimated specific surface area of 5.2 ± 0.3 m^2/g.

The surface carboxylic acid group concentration on the PCL surface, as determined by titration, was found to be ca. $1.95 \cdot 10^{-8}$ mol/cm^2. The concentration of L-cysteine grafted on

PCL/Cys surface was $1.18 \cdot 10^{-8}$ mol/cm^2, as calculated by Ellman assay. If compared to the concentration of surface carboxylic groups, this value corresponds to a reaction yield of ca. 60.5%.

The cumulative release of nitric oxide from the PCL/Cys/NO scaffold was assessed by a colorimetric assay, originally developed by Greiss (Figure 27).

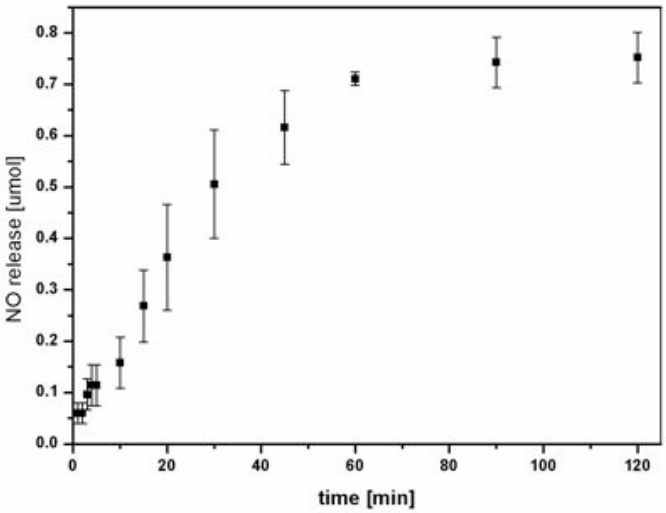

Figure 27. NO sustained release from electrospun PCL scaffold

Nitric oxide release curve showed a sustained release at a much slower rate with increasing time, up to a plateau reached after 90 minutes, where ca. 5% of total NO was released. Additionally, calculating the amount of cells per scaffold we could introduce a new parameter describing the "bioavailability" of NO per each cell. This value ranged around 50 nmol/cell.

Cell morphology and differentiation

Experiments were performed in triplicate. Cell seeding was uniform and homogenous and seeding efficiencies in the PCL/ctrl, PCL/Cys and PCL/NO scaffolds were 91.3 ± 1.6, 92.5 ± 1.3 and 93.2 ± 1.7% ($P<0.12$), respectively. Soon after seeding high cellularity could be detected in the scaffolds by means of nuclear staining and Live/Dead assay performed following 48 hours culture showed a 95 ± 2% viability reliably suggesting an effective cell engraftment.

Both light microscopy by means of regular hematoxylin/eosin staining and confocal microscopy by means of cytoplasmic actin and nuclear counterstain, were used to assess cell engrafting and morphology. In drug loaded polymers hMSCs exhibited changes in both cell morphology and markers expression in comparison with bare PCL scaffolds. Hematoxylin/eosin staining confirmed engrafting showing elongating cells attached on PCL fibers (data not shown).

Cell viability in contact with scaffold degradation productsafter 24 hours of culturing was measured to be around 100% in all the experimental groups (Figure 28A). Cell proliferation, as studied by analysis of total DNA content per construct, demonstrated a statistical significant increase at 7 days respect to T0 in all the scaffolds ($p<0.1$,Figure 28B).

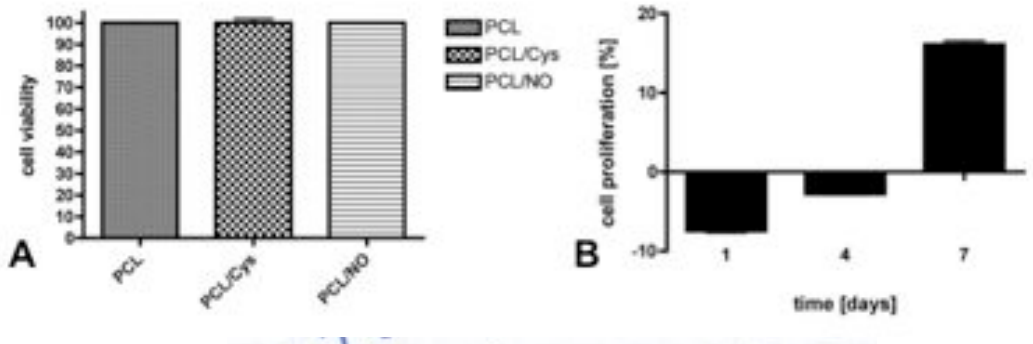

Figure 28. A) hMSCs viability cultured for 24 hours in contact with PCL, PCL/Cys, and PCL/NO scaffolds; B) hMSCs proliferation rate with respect to the DNA content measured soon after cell seeding. Graph shows cell proliferation rate on PCL samples as reference. Other two groups presented similar results (data not shown)

Immunofluorescence analysis revealed no $CD31^+$ cells at 48 hours in all the experimental groups (data not shown). However, after 1 week of in vitro culturing in the PCL/NO scaffolds (Figure 29A) the presence of CD31 positive cells in comparison to the control (Figure 29B) was evident. CD31 nicely stained membranes of cells engrafted among polymeric fibers.

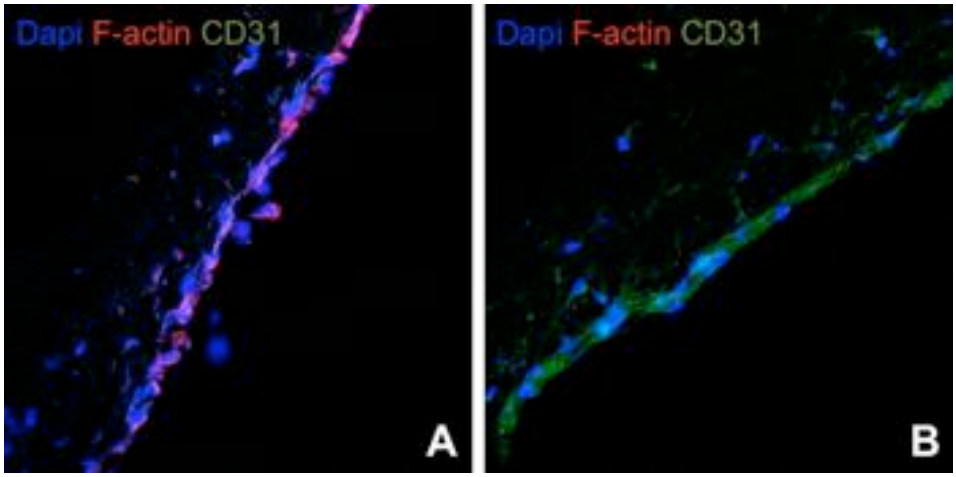

Figure 29. Immunofluorescence for CD31 at 1 week. A) PCL samples ; B) PCL/No samples. Magnification: 40X. Nuclei and F-actin were counterstained with DAPI and rhodamine phalloidine, respectively

SEM analysis confirmed the findings obtained at fluorescence microscopy, clearly showing the differences in terms of morphology between cells cultured in PCL (Figure 30A) and PCL/NO samples (Figure 30B). In particular, in the latter, Figure 30B defines the area of cobblestone-like aggregates of rounded cells organized in buttons adhering to the fibers. At higher magnification, in PCL/NO group, these cells presented a villous surface with numerous membrane indentations and invaginations that resemble caveolae, typical of endothelial cells (Figure 30D).

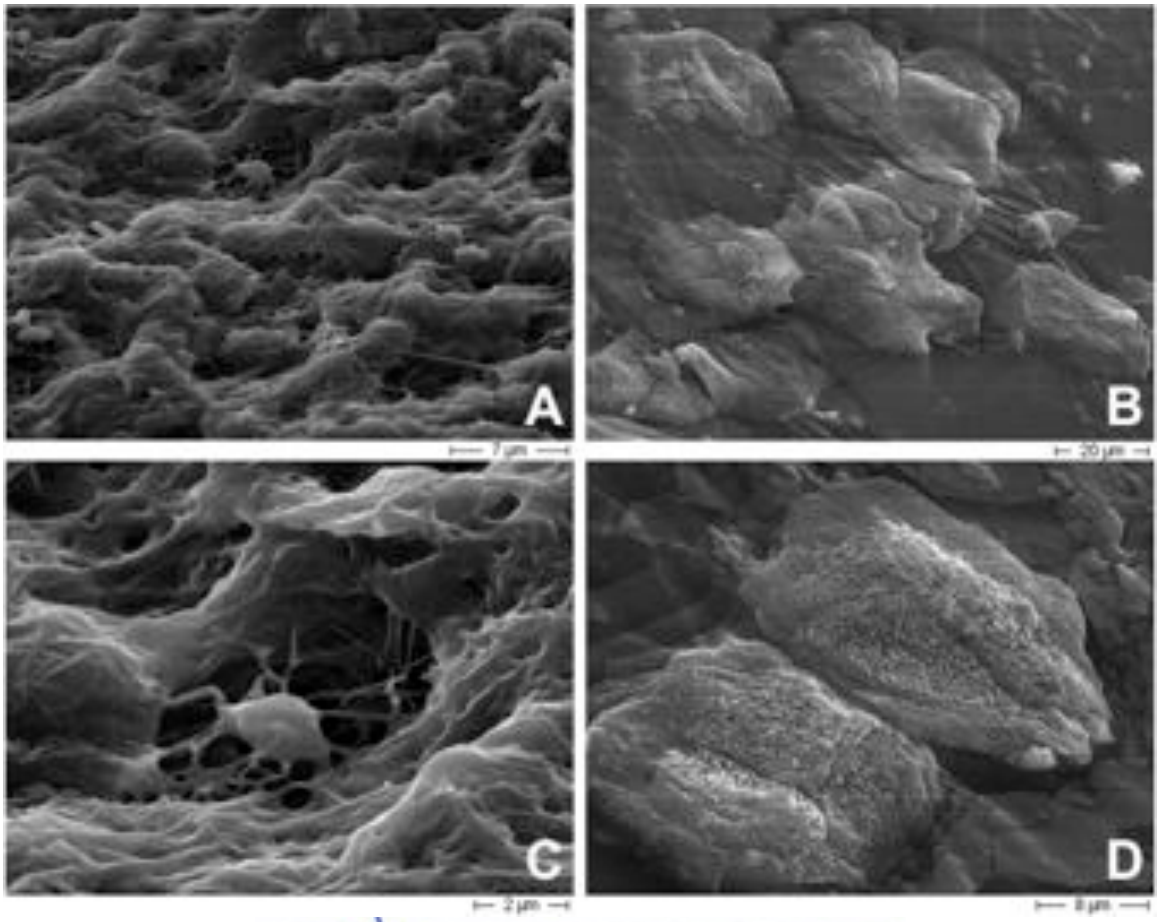

Figure 30. SEM micrographies of PCL (A-C) and PCL/NO (B-D) samples at different magnifications

Gene expression analysis (Figure 31) confirmed the findings of both immunostainings and electron micrographies, showing statistically significant differences in the expression of endothelial cells markers – i.e. CD31 and VEGF – between PCL and PCL/Cys with PCL/NO after 1 week of culturing.

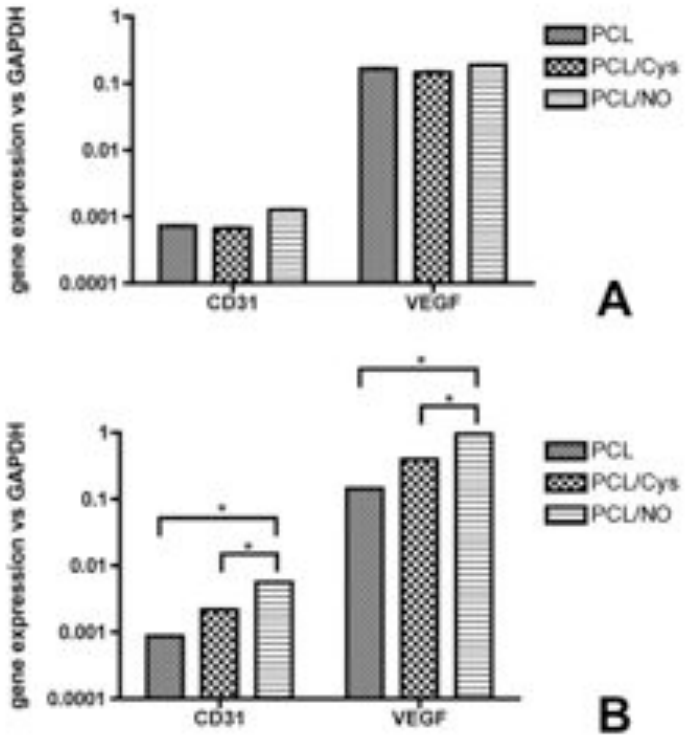

Figure 31. Real-Time analysis performed on samples at 48 hours (A) and 1 week (B)

Discussions and conclusions

Nitric Oxide (NO) is a diffusible short-lived free radical and a signaling molecule with a number of important physiological functions such as smooth muscle relaxation, neurotransmission, and inhibition of platelet aggregation and host defense mechanisms [Murad et al, 2006]. It also plays a role in the pathology of several inflammatory diseases and other pathological conditions such as cancer, diabetes, and neurodegenerative diseases [Davis et al, 2001]. NO also plays an important role in the control of heart rate, contractibility, coronary perfusion, and cardiac development [Sell et al, 2006, Kim et al, 1998]. NO signaling components have been shown to be involved during differentiation of ES cells into cardiac cells. Previous studies by other investigators [Kanno et al, 2004] have shown increased cardiomyogenesis with NO donors and by delivery of the NOS-2 gene in mouse ES cells.

Additionally, NO plays a pivotal role in vascular homeostasis modulating the activation and adhesion of leukocytes, limiting platelet aggregation and thrombus formation [Chello et al, 2008], and maintaining the vascular smooth muscle in a nonproliferative state, thereby preserving blood vessels from adverse vascular remodeling [Verma et al, 2005]. In

this extent, we also demonstrated a role in the modulation of apoptosis phenomena in conditions associated with embalanced cytokine production or impaired immunological control [Cacciapaglia et al, 2009]. Again, it has been speculated that this action could be reliably associated with NO homeostatic effect on cell inflammatory status [Cacciapaglia et al, 2009].

NO signaling is widely known to be associated to endothelial differentiation [Onodera et al, 2006; He et al, 2005].Additionally, it has been recently demonstrated the effect of NO donors and soluble guanylyl cyclase (sGC) activators in differentiation of ES cells into myocardial cells [Mujoo et al, 2008].

Our findings, both morphologically and markers expression, are consistent with the induction of a differentiation pathway towards vascular endothelium.

We could detect the typical in vitro arrangement of endothelial progenitor cells (EPC) reproduced in 3 three dimensions on the PCL/NO functionalized scaffold. Typically, organization in rounded cells aggregates with a peculiar cobblestone arrangement could be observed. This phenomenon is widely seenexperienced in EPC culture from bone marrow and is widely recognized recognized as a crucial phase indicating definitive commitment towards endothelium [Rohde et al, 2007].

We could obtain these findings after 48 h of culturing on functionalizedscaffolds, remarkably suggesting the idea of a powerful differentiating device, able at the same time to release a bioactive molecule particularly important in vascular function and homeostasis.

Additionally, the vascular pre-commitment opens wide and interesting avenues on cardiovascular tissue engineering especially thinking in potential clinical applications.

References

Cacciapaglia F, Spadaccio C, Chello M, Gigante A, Coccia R, Afeltra A, Amoroso A, "Apoptotic molecular mechanisms implicated in autoimmune diseases", *European Review for Medical and Pharmacological Sciences* (**2009**), 13: 23-40

Chello M, Spadaccio C, Patti G, Lusini M, Barbato R, Goffredo C, Di Sciascio G, Covino E, "Simvastatin reduces platelet-endocardium adhesion in atrial fibrillation", *Atherosclerosis* (**2008**), 197: 588-595

Davis KL, Martin E, Turko IV, Murad F, "Novel effects of nitric oxide", *Annual Reviews of Pharmacology and Toxicology* (**2001**), 41: 203-236

He W, Yong T, Teo WE, Ma Z, Ramakrishna S, "Fabrication and endothelialization of collagen-blended biodegradable polymer nanofibers: potential vascular graft for blood vessel tissue engineering", *Tissue Engineering* (**2005**), 11: 1574-1588

Hrabie JA, Keefer LK, "Chemistry of the nitric oxide-releasing diazeniumdiolate ("nitrosohydroxylamine") functional group and its oxygen-substituted derivatives", *Chemical Reviews* (**2002**), 102: 1135-1154

Kanno S, Kim PK, Sallam K, Lei J, Billiar TR, Shears LL, "Nitric oxide facilitates cardiomyogenesis in mouse embryonic stem cells", *Proceedings of National Academic Science U S A* (**2004**), 101: 12277-12281

Keefer LK, Nims RW, Davies KM, Wink DA, "NONOates (1-substituted diazen-1-ium-1,2-diolates) as nitric oxide donors: convenient nitric oxide dosage forms", *Methods in Enzymology* (**1996**), 268: 281-293

Jun HW, Taite LJ, West JL, "Nitric oxide-producing polyurethanes", *Biomacromolecules* (**2005**), 6: 838-844

Lakeshia PY, Taite J, Jun HW, West JL, "Nitric Oxide-Releasing Polyurethane–PEG Copolymer Containing the YIGSR Peptide Promotes Endothelialization With Decreased Platelet Adhesion", *Journal of Biomedical Materials Research Part B* (**2007**), 108-116

Loscalzo J, "Nitric oxide insufficiency, platelet activation, and arterial thrombosis", *Circulation Research* (**2001**), 88: 756-762

Murad F, "Nitric oxide and cyclic GMP in cell signaling and drug development", *New England Journal of Medicine* (**2006**), 355: 2003-2011

Onodera N, Tamaki T, Okada Y, Akatsuka A, Aoki D, "Identification of tissue-specific vasculogenic cells originating from murine uterus", *Histochemistry and Cell Biology* (**2006**), 125: 625-635

Rohde E, Bartmann C, Schallmoser K, Reinisch A, Lanzer G, Linkesch W, Guelly C, Strunk D, "Immune cells mimic the morphology of endothelial progenitor colonies in vitro", *Stem Cells* (**2007**), 25: 1746-1752

Taite LJ, Yang P, Jun HW, West JL, "Nitric oxide-releasing polyurethane-PEG copolymer containing the YIGSR peptide promotes endothelialization with decreased platelet adhesion", *Journal of Biomedical Materials Research Part B: Applied Biomaterials* (**2008**), 84: 108-116

Verma S, Marsden PA, "Nitric oxide-eluting polyurethanes--vascular grafts of the future?", *New England Journal of Medicine* (**2005**), 353: 730-731

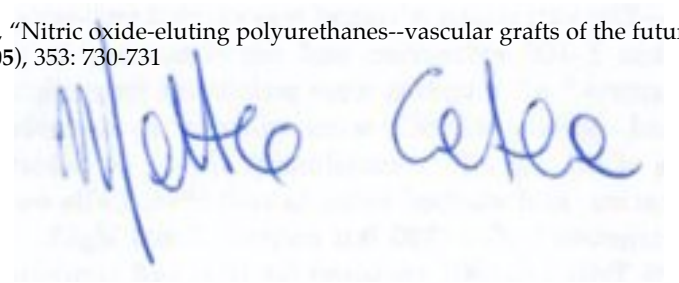

2.6A biomimetic three-layered compartmented scaffold for vascular tissue engineering

*adapted from Rainer A, **Centola M**, Spadaccio C, De Porcellinis S, Abbruzzese F, Genovese JA, Trombetta M.Conf Proc IEEE Eng Med Biol Soc. 2010;2010:839-42*

Introduction

Cardiovascular diseases, including heart attack, myocardial infarction, peripheral artery disorders, coronary arteries occlusion, and atherosclerosis, represent one of the main causes of death worldwide. As we list in the first chapter, current possible treatments are angioplasty, coronary bypass surgery by using autologous vascular grafts or artificial polymeric grafts. However, all these procedures present significant shortcomings, including thrombosis, infection, neointimal proliferation, limited durability, poor mechanical properties, and inability to grow [Avci-Adali et al, 2010]. To overcome these limitations, TEVGs have been developed by using cultured autologous vascular wall cells seeded onto a synthetic biodegradable polymeric scaffold [Shinoka et al, 1998].

After the encouraging results obtained for the endothelial layer regeneration and keeping in mind the native artery histoarchitecture, the natural step forward was to create a cardiovascular device composed by a three-layered hybrid scaffold with oriented drug-delivery capacity for the differentiation of hMSCs seeded therein. The particular scaffold design used is suitable for autologous stem cell seeding and provides a compartmented microenvironment that allows differential cell-commitment and a drug delivery system to induce the required cell differentiation toward the phenotypes characterizing cardiovascular tissues (i.e. vascular endothelium and smooth muscular lineages), improving clinical management immediately following graft implantation.

By means of electrospinning technique and sequential apposition of polymer layers [Srouji et al, 2008], we developed a hybrid construct with a middle pivotal collagen lamina and two PLLA layers on its inner and outer sides. The collagen mesh is designed to improve mechanical stability, tensile resistance and biological support for the attachment, retention and viability of the cells seeded in the polymers around this primary structure. This framework allows compartmenting of two interconnected, but functionally different layers, in which a particular microenvironment, with the capacity to induce simultaneously endothelial and muscular differentiation starting from a single stem cells

population, can be found. The outer layer has been functionalized with TGF-β1 to induce smooth muscle differentiation, while the inner layer will be functionalized with heparin and erythropoietin.

Heparin, beside the well-known and above-mentioned antithrombotic properties, exerts an important trophic effect on endothelium [Spadaccio et al, 2010] and erythropoietin (EPO) is a potent physiological stimulus for mobilization, homing, and differentiation of the endothelial progenitor cells residing in the bone marrow. Moreover, both layers act as a drug releasing system delivering factors useful both in the immediate management of the scaffold engraftment and in the maintenance of a milieu providing the correct signaling to guarantee tissue homeostasis and eventual recruitment of endogenous stem cell populations.

Materials and methods

Scaffolds preparation

PLLA/Heparin-Erythropoietin (PLLA/Hep-EPO) and PLLA/TGF-β1 layers were prepared by electrospinning technique. Briefly, PLLA/Hep-EPO scaffold was prepared by electrospinning starting from a 13% w/w PLLA (Sigma) solution in dichloromethane (DCM, Sigma). Unfractioned heparin (sodium salt, 5000 UI/ml, MSPharma, Gaither, MD) and commercially available EPO solution were added to the polymer solution using methanol (Sigma) as a co solvent, to obtain final growth factor concentrations (with respect to PLLA) of 250 UI/g. Electrospinning equipment was used (DynaSpin, Biomatica srl, Rome, Italy); the solution was fed through a 23 G needle with a feed rate of 1.5 ml/h and electrospun onto an earthed collector placed at a distance of 15 cm, using a voltage of 15 kV. In order to achieve tubular scaffolds, a rotating cylindrical AISI 316L stainless steel mandrel (4 mm diameter and 6 cm length, rotating at 4500 rpm) was used as the collector target. Then, a bovine collagen type-I (BD, Biosciences) was micro-sprayed, by means of an airbrush, on the previous PLLA/Hep-EPO layer in order to obtain a uniform coating. Finally, PLLA/TGF β1 outer layer was electrospun on the so-obtained construct using same process parameters of the tubular scaffold luminal side, starting from a 13% w/w PLLA solution in DCM with TGF- β1 solution (Sigma, 1000 ng/ml) for PLLA/TGF β1. Growth factors concentrations were chosen according to both literature and clinical dosage routinely used in order to create a device as much as suitable for direct clinical application. At the same time, bare PLLA - without growth factors addition - was electrospun at the same experimental conditions to be used as a negative control for differentiation assessment (PLLA/Ctrl).Microstructure of the scaffold was evaluated by

Field Emission Scanning Electron Microscopy (FE-SEM). Starting from electron micrographies, scaffolds intrinsic porosity and fibers mean diameter were calculated by means of the software Image-Pro 6.0 (Media Cybernetics, Silver Spring, MD).

Drug-release study

100 mg of PLLA/Hep-EPO and PLLA/TGF-β1 electrospun layers were separately placed in 15 ml sealed tubes with 3 ml of pre warmed phosphate buffer solution (PBS) containing 0.03% w/v NaN3, and incubated at 37 °C. 200 μl aliquots of surnatant were timely collected and quantified in order to assess the drug release rate of heparin, EPO and TGF-β1 from the polymer matrices. Heparin release was assessed according to an Azure A method as previously described (**par.2.2**). EPO and TGF-β1 release were quantified by means of dedicated ELISA assays (Bender MedSystem, San Diego, CA).

Cell seeding

Human mesenchymal stem cells (hMSCs) (passage 4, Lonza, Basel, Switzerland) were used in the experimental settings for both functionalized scaffold and PLLA/Ctrl tubular composites. Tubular constructs (4 mm diameter, 5 mm long, 0.5 mm thick) were seeded with hMSCs at a density of 106 cells/cm2 under rotating dynamic conditions (12 g) for 48 h in the same basal medium (Dulbecco's Modified Eagle's Medium supplemented with 10% fetal bovine serum, 100 units/ml penicillin, 100 μg/ml streptomycin).

Scaffold biocompatibility

Cell cytotoxicity, attachment and proliferation within the scaffolds were evaluated by means of immunohystology, confocal microscopy and appropriate assays. For cell viability Live/Dead assay (Invitrogen, San Diego, CA) was used. Upon culturing, tubular scaffolds were fixed with paraformaldehyde for 15 minutes, embedded in O.C.T. cryomatrix, snap frozen and cut in 15 μm slices. Slides were further processed for Hematoxilin-Eosin staining in order to achieve a morphological analysis. For cell attachment and engraftment assessment, confocal microscopy was performed, staining cells on the scaffolds for F-Actin with Rhodamine Phalloidin (Molecular Probes, Invitrogen) and nuclei using TOTO (Invitrogen). Cell proliferation was quantitatively evaluated by measuring the total cellular DNA content and semiquantitatively by immunostaining for Ki67 by confocal microscopy. Briefly, constructs were lysed in RIPA buffer added with protease inhibitor cocktail Halt (Thermo Scientific Pierce Protein Research, Waltham, MA) and cells were sonicated using pulses ultrasonic disruptor

(Thermo Fisher Scientific) three times for 10 s. DNA content was measured using Quant-iT ds-DNA assay kit (Invitrogen) on a Qubit fluorimeter (Invitrogen).

Cell differentiation

Single and double immunostaining for CD31, von Willebrand Factor (vWF), smooth muscle actin (SMA) (Abcam Cambridge, United Kingdom) and Ki67 (NeoMarkers. Thermo Fisher Scientific) were performed. Briefly, tissue sections were fixed and permeabilized with 0.1% Triton-X 100 in PBS for 10 minutes. Non-specific binding of antibodies was blocked by incubating the samples for 45 minutes with 2% bovine serum albumin. Samples were then incubated 1 hour at 37 °C with mouse monoclonal anti-CD31, mouse anti-vWF rabbit anti-Ki67, or rabbit anti-SMA primary antibodies (1/100 titer). For triple labeling experiments, samples were incubated with Alexa Fluor 488 conjugated secondary anti-mouse IgG and Alexa Fluor 546 conjugated secondary anti-rabbit IgG (Invitrogen) for 30 minutes at 37 °C, while nuclei were counter stained with TOTO. In negative control experiments, the incubation with primary antibodies was omitted. The samples were then mounted in Prolong antifade medium (Invitrogen) and viewed under an Olympus Fluorview F1000 confocal microscope by two independent blinded observers.

Results

Scaffolds microstructure

FE-SEM micrographs of PLLA/Hep-EPO inner layer and TGF-β1 outer layer are presented in Figure 32A-B, respectively. Scaffolds morphology consists of a non-woven fibrous mesh, with an average diameter of 450 ± 150 nm.

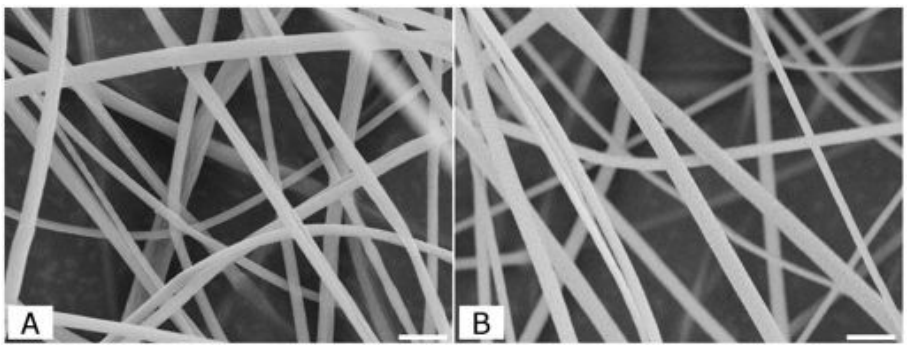

Figure 32. FE-SEM micrographs of PLLA/Hep-EPO (a) and PLLA/TGF-β1 (b) layers. Scale bar: 2 μm.

Drug release study

The release profile of heparin from PLLA fibers is similar to data reported in the literature for other biodegradable polymeric matrices [Yan et al, 2009]. A cumulative release of ca.

10% of the total drug loaded was assessed after 1 week [Spadaccio et al, 2010]. Erythropoietin elution rate showed a similar profile with respect to heparin release. A cumulative release of ca. 300 IU of EPO was assessed after 1 week, which could be a reasonable clinical dosage. TGF-β1 cumulative release was finally assessed. After 1 week, ca. 23.8% of TGF-β1 was released by the biopolymeric matrix, corresponding to ca. 23.8 pg.

Cell morphology and differentiation

Live/Dead assay showed good cell viability (95 ± 2%) and an effective cell engrafting following 48 hours culture. hMSCs exhibited changes in both cell morphology and markers expression when cultured upon functionalized layers (PLLA/Hep-EPO and PLLA/TGF-β1) in comparison with PLLA/Ctrl, where they retained stem phenotype. Hematoxylin/eosin staining confirmed full engrafting in both functionalized and control scaffolds. Immunofluorescence analysis revealed the presence of CD31 expression along with a percentage of Ki67 positive cells in the luminal side (PLLA/Hep-EPO layer) that were not envisaged in the control (data not shown). Moreover, cell membranes showed characteristic indentation and invaginations that resemble caveolae typical of endothelial cells. Interestingly, staining was preferentially localized in the cytoplasm suggesting a still immature state of differentiation (Figure 33A). In the outer region, CD31 and vWF antibodies failed to reveal positivity (Figure 33B), while cells appeared elongated arranged in a monolayer intensively positive for smooth muscle actin (Figure 33C). Additionally, in certain regions of the scaffold, a focal enhancement in cell proliferation could be seen with a multilayered arrangement of rounded vWF positive cells (Figure 33D). Morphological analysis of these cells showed enlarged nuclei with loose chromatin and several nucleoli with rare cytoplasm and a high nucleus/cytoplasm ratio. This might be referred to phenomena of hyperplasia probably related to heparin/EPO trophic stimulus.

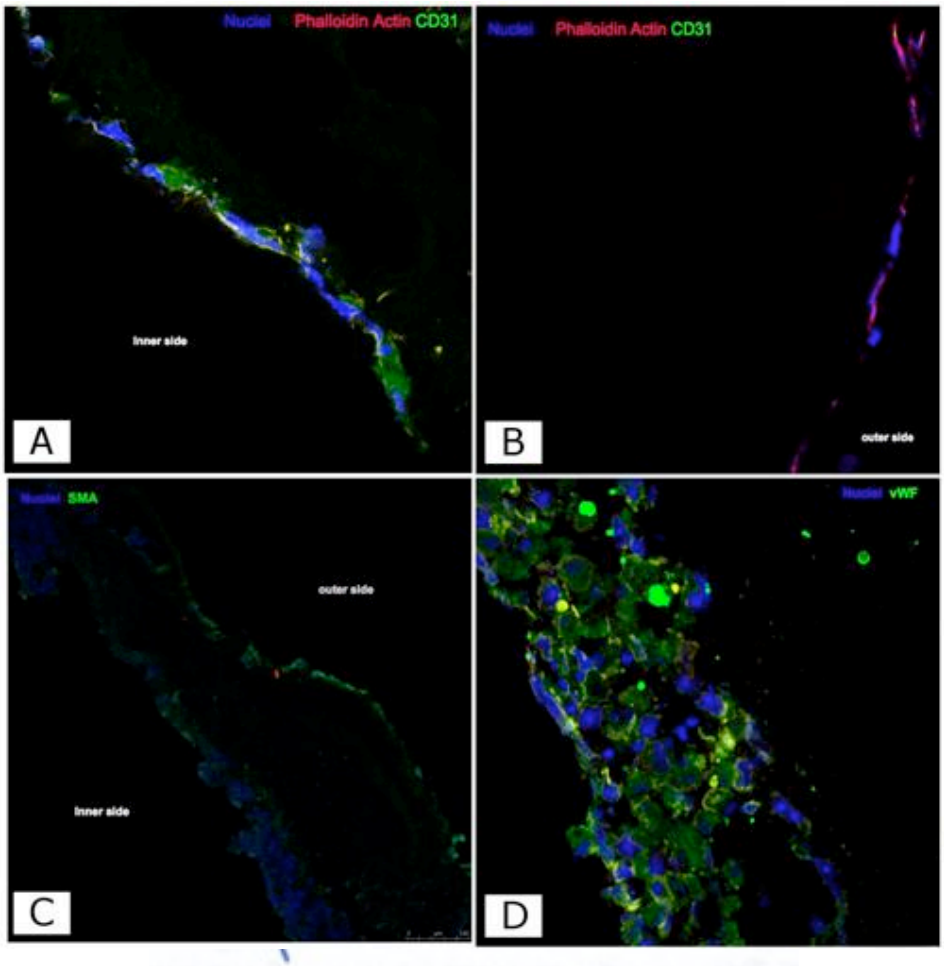

Figure 33. Confocal microscopy with immunofluorescence staining for CD31, SMA and vWF of threelayered graft (400X).

Discussions

The idea at the root of this study was the development of a set of technologies for incorporating polymers and biologically active molecules into 3D scaffolds with appropriate composition, able of mimicking the features of natural cardiovascular tissues. This graded scaffold is able to host hMSCs, eliciting a specific biological response and inducing their differentiation into endothelium/smooth muscle phenotype in order to reproduce the different components of a vascular segment, leading to the complete regeneration of a healthy, autologous tissue. To this extent, we developed a three-layered graft in order to promote the regeneration of vascular tissue by the integration of two synthesis techniques, electrospinning and microspray. This hybrid method allowed the fabrication of functionalized tissue engineered scaffolds, able to recapitulate the native histoarchitecture of vascular tissue, and to promote a regenerative response by stem cells differentiation. In these circumstances, functionalization of the scaffold aimed to both

develop an effective molecule delivery system, and provide an alternative mean capable of releasing localized doses of bioactive molecules over sustained periods of time, minimizing undesired systemic effects, defining a favorable environment for cell engraftment and proliferation and improving the post-implantation management of the grafts. EPO engraftment in the scaffold would provide crucial signaling not only for the differentiation of the seeded mesenchymal lineages but also, in a potential future clinical application, for the recruitment of endogenous populations of stem cells that have been shown to be mobilized during ischemic or inflammatory injuries. At the same time, the presence of heparin would improve cell attachment to the scaffold providing trophic and differentiating signaling for hMSCs towards vascular endothelium [Spadaccio et al, 2010]. Drug release kinetics has also been studied. Both heparin and erythropoietin curve showed an increased steepness following the first 24 hours and a further smoother pattern of release. The initial burst is driven according to Fick's law and sustained by drug gradient concentration. Subsequently, drug concentration locally around the scaffold increases, leading the gradient concentration to zero, and, as a consequence, to an equilibrium described by the plateau in the releasing curve. Then, a further increase in the drug release is reliably due to the scaffold degradation [Yan et al, 2009; Moroni et al, 2006; Bezemer et al, 2000]. Scaffolds have been seeded with hMSCs and evaluated for cell engraftment, viability, proliferation and differentiation. Our findings are consistent with an adequate cell engrafting and a double type of differentiation, related to the compartmented functionalization of the scaffold. Light and confocal microscopy showed an adequate cell attachment and viability with cells exhibiting morphostructural changes resulting in the achievement of an endothelial-like phenotype for cells populating the luminal side of the scaffold and SMA positivity with cell elongation resembling muscular phenotype for cells on the outer layer. The possibility to concentrate and spatially organize in a leading framework biological signals capable of both recruiting and guiding cells for total replacement of all the components of a tissue could have a dramatic impact in the cardiovascular field, as well as in the treatment of many other pathological conditions.

Conclusions

Aiming at surmounting the several limitations of current artificial vascular grafts, we developed a biomimetic multilayered scaffold with a middle, pivotal collagen lamina between two functionalized layers of PLLA fibers by the combination of electrospinning and microspray techniques. The obtained scaffold showed compartmented drug-delivery capacity for the differentiation of hMSCs seeded therein. Applying appropriate cytokines, the inner and the outer layers were able to provide an adequate pre constituted

environment, promoting hMSCs differentiation towards both endothelial and smooth muscle phenotype. The proposed biomimetic vascular bio-prosthesis, recapitulating the microenvironment and the histoarchitecture of native cardiovascular tissues, could be relevant for therapeutic applications in a variety of medical fields.

References

Avci-Adali M, Zieme G, Wendel HP, "Induction of EPC homing on biofunctionalized vascular grafts for rapid in vivo self-endothelialization--a review of current strategies", *Biotech Adv* (**2010**), 28:119-1129

Bezemer J, Radersma R, Grijpma DW, Dijkstra DJ, Feijen J,van Blitterswijk CA, "Zero-order release of lysozyme from poly(ethylene glycol)/ poly(butylene terephthalate) matrices", *J Contr Rel*(**2000**), 64: 179–192

Moroni L, Licht R, de Boer J, de Wijn JR, van Blitterswijk CA, "Fiber diameter and texture of electrospun PEOT/PBT scaffolds influence human mesenchymal stem cell proliferation and morphology, and the release of incorporated compounds", *Biomaterials* (**2006**), 27: 4911–4922

Shinoka T, Shum-Tim D, Ma PX, Tanel RE, Langer R et al., "Creation of viable pulmonary artery autografts through tissue engineering", *J Thorac Cardiovasc Surg* (**1998**), 115: 536-545

Spadaccio C, Rainer A, Centola M, Trombetta M, Lusini M, Chello Met al, "A heparin releasing scaffold for stem cells: a differentiating device for vascular aims", *Regen Med* (**2010**), 5:645-657

Srouji S, Kizhner T, Suss-Tobi E, Livne E, Zussman E, "3-D Nanofibrous electrospun multilayered construct is an alternative ECM mimicking scaffold", *J Mater Sci Mater Med* (**2008**), 19: 1249-1255

Yan Y, Xiaoqiang L, Shuiping M, Xiumei S, Ramakrishna S, "Controlled release of dual drugs from emulsion electrospun nanofibrous mats, *Coll Surf B: Biointerf*(**2009**), 73: 376–381

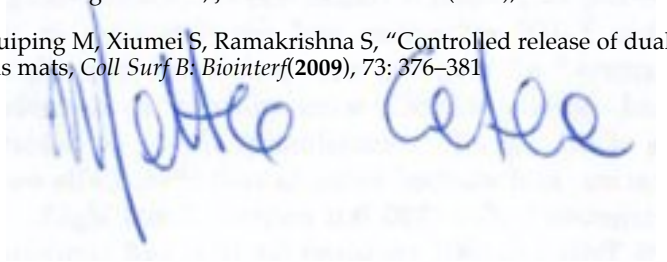

3. Engineering an articular cartilage tissue substitute

Articular cartilage is a smooth, highly specialized tissue characterized by unique biomechanical properties that permit articular movements while minimizing surface friction, to absorb loads in the weight-bearing joints, and to reduce the stress on the subchondral bone. Because of the peculiar features of articular cartilage, such as lack of vascularization in the upper layer and high specialization, this tissue has limited intrinsic healing capacity. When the lesion involves also the underlying bony layer the situation becomes even more complicated.

For this reason, management of osteochondral defectsis challenging and several surgical techniques have been used to repair such lesions. The rationale for reparative approaches, which include all the above-mentioned approaches (**paragraph 1.2**), such as microfractures, subchondral bone drilling, and mosaicplasty, is to stimulate the formation of new fibrocartilage to fill the lesion, although this repair tissue is biomechanically inferior to the original cartilage [Franceschi F et al, 2008].

Tissue engineering (TE) of osteochondral composites has the potential to overcome these limitations, using a combination of scaffold, groth factors and cells (tissue-engineered construct, TEC) [Rose et al, 2002]. In particular, grafting of 3D osteochondral grafts, consisting of a superficial cartilaginous layer and an underlying calcified tissue that can be represents a promising approach to restore the biological and mechanical functionality of the joint [Martin et al, 2007; Mano et al, 2007].

Many TE concepts dealing with osteochondral repair involve the design of bilayered scaffolds [O'Shea et al, 2008] that could regenerate both articular cartilage and subchondral bone, but other strategies have been proposed in literature, such as scaffold for bone component and scaffold-free for cartilage layer, different scaffolds for bone and cartilage components, one homogenous and single layer cell-free scaffold [Martin et al, 2007], as listed in **par. 1.2.3**. However, although scaffolds for repairing osteochondral defects in vivo have improved the quality of the repair tissue compared to untreated controls, the repaired tissues still show both biomechanical properties lower than the native articular cartilage [Kelly et al, 2006] and difficulty in establishing satisfactory integration of new tissue in vivo. Therefore, despite the great efforts that have been done,

more integrated work is needed to seek improved methodologies that could be transposed to clinical practice [Mano et al, 2007].

To this extent, we aim at producing a uniform and well-integrated construct in which cell phenotype, cell to matrix ratio, mechanical properties and permeability are not uniform in space, but follow a biomimetic architecture deriving from computational modeling techniques [Rainer et al, 2011] in order to imitate the zonal regions presented in articular cartilage. The extent to which this can be achieved will be highly dependent on the emergence of novel solid free form fabrication techniques, e.g. 3D printing [O'Shea et al, 2008].For bony layer, biodegradable polymer/bioceramic scaffolds – i.e. polycaprolactione and hydroxyapatite (PCL/Hap) - can be easily processed with rapid prototyping technique, and, at the same time, overcome the limitations of conventional ceramic and polymeric bone and osteochondral substitutes. The main goal of this kind of composite materials (i.e. polymer and ceramic parts) is to take advantage from both organic and inorganic domain in order to improve the final properties, not only by the addition of the properties of the individual components but also from the synergetic effect of the domains [Vallet-Regì et al, 2006].

Moreover, technologies to enhance or prevent angiogenesis in osteochondral TE are mandatory. One of the most urging and unsolved issues seems to be the control of neo angiogenesis at the chondral site and, in particular, the signaling of vascular endothelial growth factor (VEGF) during the chondrogenic differentiation of stem cells. On the basis of recent discoveries in the role of anti-angiogenesis in the chondrogenic pathway [Samaranayake et al, 2010; Matsumoto et al, 2009], our project will be focused on the functionalization of the chondral layer of the scaffold, in order to perform in vivo immunodepletion of circulating VEGF directly at the scaffold site [Takita et al, 2002] and a commercial drug with the VEGF antibody (Avastin®).

The proposed scaffold is composed by the clinically validated hyaluronate-fibrin (HA/FIB) system for the cartilage layer (CL) and a hydroxyapatite-rich polymer-matrix composite for the bone layer (BL). The BL will be fabricated with a trabecular architecture using the FDM head of the rapid prototyping equipment. Several layers of trabecular elements will be deposited one atop the other, by coordinating the relative motion of the dispensing head and the sample holder with the extrusion of the molten PCL/Hap material. Each extruded filament will adhere to the lower layer, therefore obtaining a porous monolith (see Figure 34).

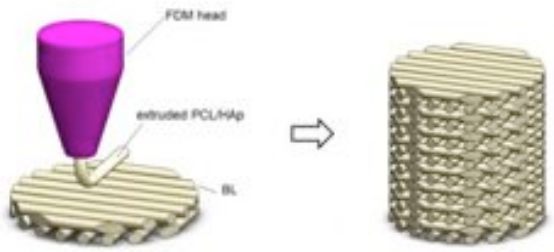

Figure 34. A scheme of the BL production process

Production of the CL will be performed by using the rapid prototyping apparatus[2] as well: HA/FIB solution will be loaded into a 2-cylinder syringe, and mixed directly into the needle upon dispensation. A solid gel block of controlled shape will therefore be created by the subsequent deposition of several layers, again by controlling the relative motion between the dispensing head and the sample holder.

The two layers (BL and CL) will be fabricated one atop the other, creating an overlap between them, in order to infer a good adhesion of the two layers. After the RP process, the obtained two-layer structure will undergo freeze-drying, in order to lyophilize the gel phase of the CL. The lyophilized CL will consist of a 3D sponge, which will remain adhered on top of the BL (Figure 35).

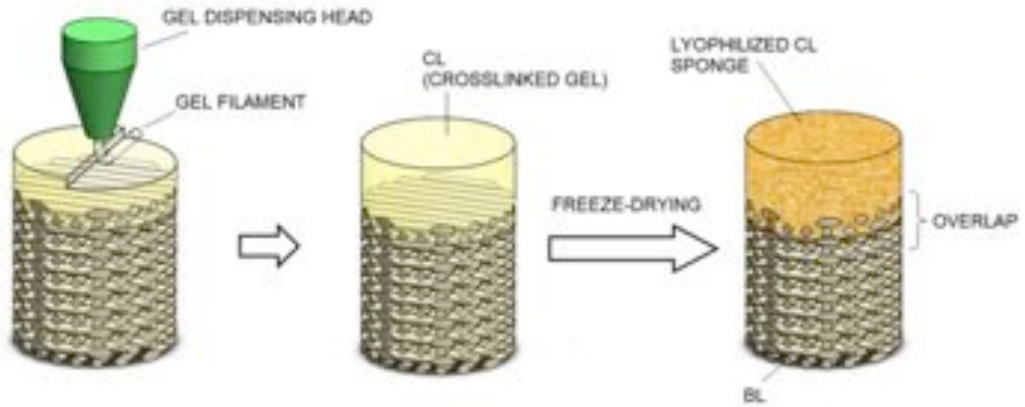

Figure 35. A scheme of the whole production process

[2]Fabrication will take advantage of a rapid prototyping station that our lab has developed in the first two years of my PhD period, and that is capable of fabricating porous 3D systems with fine control over the microstructure and trabecular arrangement of the structural elements of the scaffold. The apparatus has a spatial resolution that exceeds that of the commercially available solutions, is capable of dispensing both molten biopolymers (or polymer-matrix composites) and multi-phase gel systems, using up to 4 different dispensing heads.

In the following two paragraphs scaffolds for bone (**par. 3.1**) and cartilage (**par. 3.2**) layer will be separately discussed in details.

References

Franceschi F et al, *Knee* (**2008**)

Kelly DJ, Prendergast PJ, "Prediction of the Optimal Mechanical Properties for a Scaffold Used in Osteochondral Defect Repair", *Tissue Engineering Part A* (**2006**), 12: 2509

Mano JF, Reis RL,"Osteochondral defects: present situation and tissue engineering approaches", *Journal of Tissue Engineering and Regenerative Medicine* (**2007**), 1: 261

Martin I, Miot S, Barbero A, Jakob M, Wendt D, "Osteochondral tissue engineering",*Journal of Biomechanics*(**2007**), 40: 750

Matsumoto T, Cooper GM, Gharaibeh B, Meszaros LB, Li G, Usas A, Fu FH, Huard J, "Cartilage repair in a rat model of osteoarthritis through intraarticular transplantation of muscle-derived stem cells expressing bone morphogenetic protein 4 and soluble Flt-1", *Arthritis & Rheumatism* (**2009**), 60: 1390

O'Shea TM, Miao X, "Bilayered Scaffolds for Osteochondral Tissue Engineering",*Tissue Engineering Part B*(**2008**), 14: 447

Rainer A, Giannitelli SM, Accoto D, De Porcellinis S, "Bioinspired approach to the design of porous 3D-printed scaffolds",*ABME* (**2011**) in print

Roccaro AM, Russo F, Cirulli T, Di Pietro G, Vacca A, Dammacco F, "Antiangiogenesis for rheumatoid arthritis", *Current drug targets. Inflammation and allergy* (**2005**), 4: 27

Rose FR, Oreffo RO, "Bone tissue engineering: hope vs hype",*BBRC*(**2002**), 22: 292

Samaranayake H, Maäattaä AM, Pikkarainen J, Ylaä-Herttuala S, "Future prospects and challenges of antiangiogenic cancer gene therapy",*Human Gene Therapy*(**2010**), 21: 381

Takita H, Kikuchi M, Sato Y, Kuboki Y, "Inhibition of BMP-Induced Ectopic Bone Formation by an Antiangiogenic Agent (Epigallocatechin 3-Gallate)",*Connective Tissue Research*(**2002**), 43: 520

Vallet-Regiì M, Arcos D, "Nanostructured hybrid materials for bone tissue regeneration", Current Nanoscience (**2006**) 2: 179

3.1 Free-form fabrication of biopolymeric scaffolds for the regeneration of osteochondral bone layer

adapted from ***Centola M****, Giannitelli SM, De Porcellinis S, Accoto D, Vadalà G, Carotti S, Spadaccio C and Rainer A.Tissue Engineering Part A, 2010 Aug; 16(8): A1-A29*

Introduction

In the context of the osteochondral regeneration project above presented, the scaffold plays a pivotal role, since it reproduces a microenvironment not only able to assist and guide cell growth and differentiation, but even to mimick the mechanical properties of the native tissue, receiving, at the same time, important signaling once within the organism. The possibility to concentrate in a leading framework biological signals capable of both recruit and guide cells for tissue loss replacement could have a dramatic impact not only in the osteochondral regeneration area, but also in the treatment of many other pathological conditions.

In vitro fabrication of osteochondral (OC) composites of predefined size and shape starting from appropriate scaffolds, possibly combined with autologous cells, has the potential to overcome the limits showed by currently used clinical approaches. In particular, the use of computer-assisted techniques for the fabrication of scaffolds for tissue engineering is a promising technique for the production of patient-specific biological substitutes. The possibility of producing tissue engineering constructs by means of computer-aided rapid prototyping techniques, starting from patient specific medical imaging data, has raised relevant scientific interest in the last decade. Several works in the literature present the development of experimental setups for the fabrication of 3D constructs, for the so-called Computer Aided Tissue Engineering [Sun et al, 2002]. The concept of customized bony scaffolds for osteochondral repair is extremely interesting, as demonstrating by two works proposed in literature [Woodfield et al, 2004;Yeong et al, 2004; Lee et al, 2010] where computed tomography, coupled with 3D computer aided design and rapid prototyping, could be used to design and engineer customized femoral and tibial cartilaginous implants made of synthetic polymers in defined pore architectures [Martin et al, 2007].

Polymer-based biomaterials are suitable for rapid prototyping technique, and in particular for fused deposition modeling, thanks to their low melting temperature. Nevertheless, in

our "one-step" TE philosophy a scaffold able to withstand physiological mechanical loadings is essential. On the other hand, an osteoinductive material is fundamental to drive osteogenic differentiation of mesenchymal progenitors, and so far, ceramic biomaterials (e.g. hydroxyapatite, tricalcium phosphate) provided the most encouraging results from this point of view. However, those kinds of scaffolds resulted to be fragile, so definitely unadapt to resemble the elasto-plastic mechanical behavior of the native joint. To this extent, biodegradable nano-structured polymer, in combination with bioceramic particles, can overcome the limitations of conventional polymeric ad cercamic bone and osteochondral substitutes [Spadaccio et al, 2009]. In particular, class I hybrid materials, where the ceramic phase is uniformly dispersed in the polymeric matrix, show new and unique properties for several medical and technological applications.

The main goal of hybrid materials is to take advantage from both organic and inorganic domain in order to improve the final properties, not only by the addition of the properties of the individual components but also from the synergetic effect of the domains [Vallet-Regi et al, 2006]. In particular, the inorganic component can provide hardness, strength, and thermal stability, while the organic one provides ductility, hydrophobic character, and chemical reactivity [Arcos et al, 2010; Yury et al, 2010].

We hypothesize that composites-based scaffolds, produced by fused deposition modeling in order to confer them a suitable architecture, might represent a valuable solution when implanting an immature graft for bone repair, since they can recapitulate native biomechanical properties in the first phases upon implantation. Additionally, we aim at producing smart scaffolds, which, exposing biologically active molecules (cytokine, growth factors) on their surface, are able to both promote the synthesis of neo-ECM and then drive osteogenic differentation of human mesenchymal progenitor cells seeded therein, thus inducing a regenerative process by in situ TEC formation.

Materials and methods

Scaffold synthesis

Both polycaprolactone (PCL, Sigma) and PCL/hydroxyapatite (PCL/Hap, Sigma) composite scaffolds were fabricated. In particular, to prepare PCL/Hap composite scaffold with a good degree of homogeneity, a "masterbatch" was prepared by dispersing 20%w/w of Hap into a PCL solution in dichloromethane (DCM, Sigma). The slurry was cast on a glass and solvent evaporated.

At this point, PCL in pelletsor PCL/Hap membranes were loaded in the dispensing head of an in house-developed fused deposition modeling (FDM) apparatus (Figure 36).

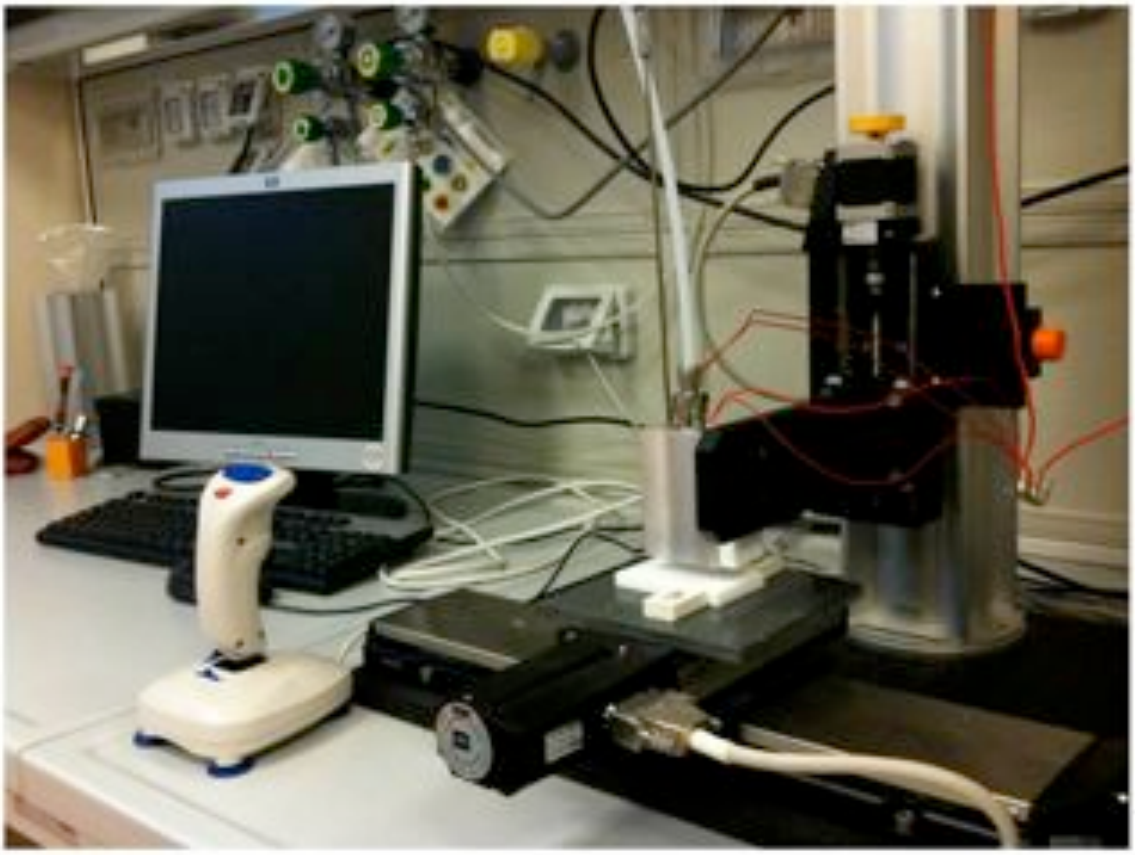

Figure 36. Picture of the FDM apparatus in our lab

The dispenser was heated up to 80°C in order to melt the PCL thanks to two heating cartridges. A resistance thermometer (Pt100), connected to a programmable temperature controller (model 400, Gefran, Brescia, Italy) was used to monitor and control dispensing head temperature. The extrusion process is performed by pressure-assisted dispensation, feeding pressurized argon gas by means of a high-pressure line (working pressure about 8 bar) connected to a control electrovalve. Custom-developed control software generates the process toolpath and controls the actuation of all the system components (axes movement, dispensing head temperature and electrovalve). The system was tailored to the fabrication of orthogonally stratified layers of PCL or PCL/Hapto obtain the scaffolds, by using the following FDM process parameters: needle diameter: 0.8 mm, deposition velocity: 1 mm/s, and working distance between needle and plate: 1.5 mm.Microstructure of the obtained materials was evaluated by Field Emission Scanning Electron Microscopy (FE-SEM, Supra 1535, Leo Electron Microscopy, Cambridge, UK).

Biomaterials functionalization

The so obtained scaffolds were functionalized by grafting bioactive molecules, such as BMP2 (PCL/BMP2 and PCL/Hap/BMP) or VEGF(PCL/VEGF and PCL/Hap/VEGF), on the materials' surface (Figure 37).

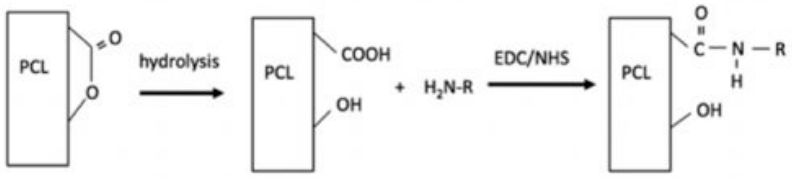

Figure 37. Scheme of the grafting protocol. Letter "R" indicate the generic growth factor (i.e. BMP or VEGF)

Both PCL and PCL/Hap scaffolds were immersed in a 0.1 M sodium hydroxide (NaOH) solution and reacted for 90 min at 40°C. After hydrolysis, scaffolds were protonated with 0.01 mol/L HCl to give polymer surfaces bearing carboxylic groups. Surface carboxylic group density was measured by inverse titration.PCL and PCL/Hap samples bearing carboxylic groups were immersed into an EDC/NHS catalyzing mixture containing 0.4 mol/L EDC and 0.1 mol/L NHS in MES buffer for 10 min. After appropriate washing, the samples were transferred into growth factors solutions in MES buffer (1000 ng/mL) for 1 h in order to obtain a covalent bond between the hydrolyzed polymeric surface and the peptide. Effectiveness of VEGF or BMP-2 grafting was assessed by direct ELISA method performed on the scaffolds (Figure 38).

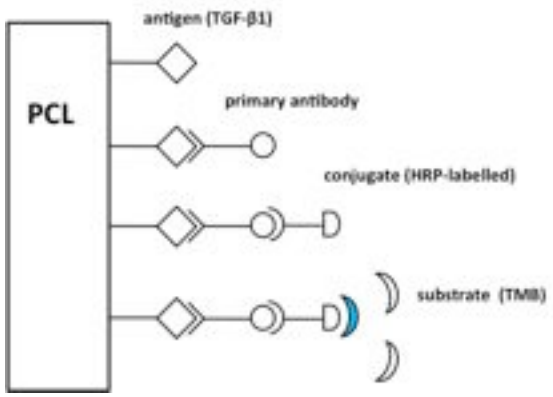

Figure 38. Scheme of the ELISA procedure performed on the functionalized scaffolds

Optimization of the grafting protocol was performed concerning the yield of the hydrolysis reaction and of the peptide binding reaction.

Scaffold biocompatibility

Bioprinted scaffolds were assayed for their biocompatibility with bone marrow-derived human mesenchymal stem cells (hMSCs, Lonza), in terms of cytotoxicity and cell proliferation. To assay the former, $1x10^4$ hMSCs were separately plated in a 96-well plate (BD, Falcon, San Jose, CA) in growing media and cultured for 24 hours. Then, PCL, PCL/Hap, PCL/BMP2, PCL/Hap/BMP2, PCL/VEGF, and PCL/Hap/VEGF scaffolds (6 mm diameter) were added to the wells. Cell toxicity due to the scaffolds was determined at 4, 8 and 24 hours by using a Vybrant Cytotoxicity Assay Kit (Molecular Probes, Invitrogen) in accordance with the manufacturer's instructions. The Vybrant Cytotoxicity kit monitors the release of the cytosolic enzyme glucose 6- phosphate dehydrogenase (G6PD) from damaged cells into the surrounding medium. Plate was read on a fluorescence microplate reader (Tecan, Mänedorf, CH) at 540 nm with correction at 595 nm.

To determine the cell proliferation in contact to produced scaffolds, $5{\cdot}10^3$ hMSCs were separately plated in a 96-well plate (BD, Falcon, San Jose, CA) in growing media and cultured for 24 hours. All the types of scaffolds were added to the wells. Cell proliferation was determined at 1, 3 and 7 days by using a MTT Assay (Molecular Probes, Invitrogen) in accordance with the manufacturer's instructions. Briefly, MTT was added to the cell culture media and incubated at 37° for 3 hours. Cells were then washed three times and DMSO added to each culture and incubated for 10 minutes. Plate was read on a fluorescence microplate reader (Tecan, Mänedorf, CH) at 540 nm with correction at 595 nm.

Cell differentiation

Fourth passage hMSCs (Lonza) were cultured in contact only with the disk-shaped PCL, PCL/Hap, PCL/BMP2, and PCL/Hap/BMP2 scaffolds at a concentration of $1{\cdot}10^4$ cells/cm2. Briefly, $3.6{\cdot}10^3$ cells were added to each of the surfaces in a 96-well plate and cells were cultured in direct contact with the surfaces for 21 days in either basal medium (αMEM + 10% FBS, 1%PS and 1% L-glutamine), or osteogenic medium (Lonza, DMEM+10% FCS, 100mM ascorbate-2-phosphate, and 10mM β-glycerolphosphate and 100nM dexamethasone), at 5% CO2 and 37 °C.

For each experimental condition, a scaffold was fixed with 4% formaldehyde and analyzed by micro-CT, and a scaffold was embedded in Tissue Tek O.C.T. and rapidly frozen in liquid nitrogen. Discs were sectioned with cryotome in transversal direction to make 15 μm thick sections and fixed in acetone. Slides were stained with Rodamine- Phalloidine for F-Actine and nuclei were stained using TOTO (Molecular Probes, invitrogen). Slides were imaged under confocal microscopy.

Samples were also characterized for expression of osteogenic genes. Total cellular RNA was isolated using TRI Reagent (Sigma), performed directly on the cellularized scaffolds. To avoid DNA contamination, RNA was treated with DNase I (Invitrogen, Carlsbad, CA) at 37 °C for 15 min followed by inactivation with 2 mM EDTA at 65 °C for 10 min. Extracted RNA was quantified by spectrophotometric technique (Nanodrop, Invitrogen). 1 μg of total RNA was retrotranscribed using High Capacity cDNA Reverse Transcription Kit (Applied Biosystems) according to the manufacturer's instructions.

Realtime quantitative PCR was performed on 100 ng of cDNA to detect the expression of Sox9, Osterix, Runx2, Alkaline Phosphatase,and 18S rRNA as housekeeping gene, using specific primers (TaqMan® Gene Expression Assay, Applied Biosystems) and TaqMan Universal MasterMix II (Applied Biosystems) in a total volume of 20 μL.

Results and discussions

Scaffold characterization

FE-SEM images confirmed the feasibility of this process to produce suitable scaffolds for tissue engineering aims. Figure 39displaysthe scaffold with best resolution, showingregular trabecular-like fibers with a mean diameter of 150μm and a porosity of 120 μm. These physical properties are adjustable modifying process parameters.

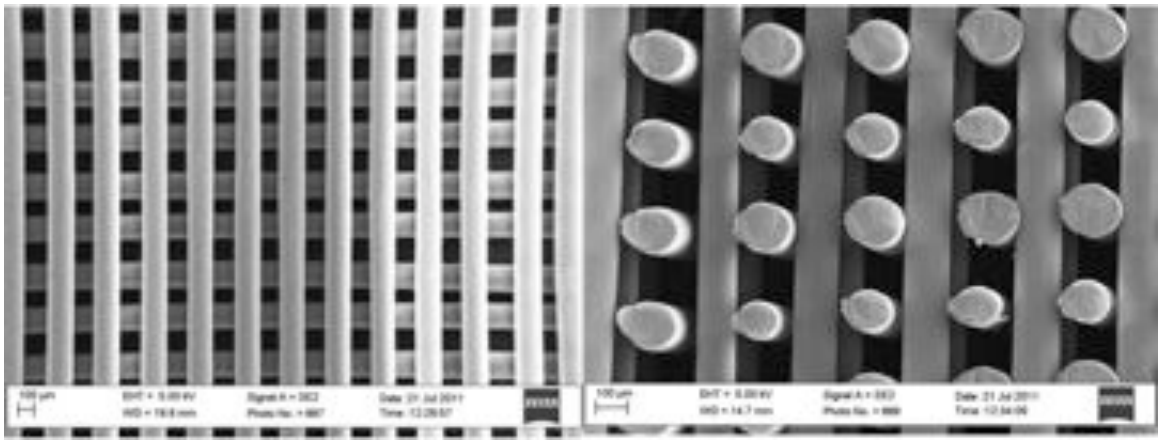

Figure 39. Scanning electron micrographies of PCL bioprinted samples. Top and orthogonal view.

Figure 40, instead, shows a detail of PCL/Hap scaffolds and in particular nanopowders of hydroxyapatite dispersed in the polymeric matrix.

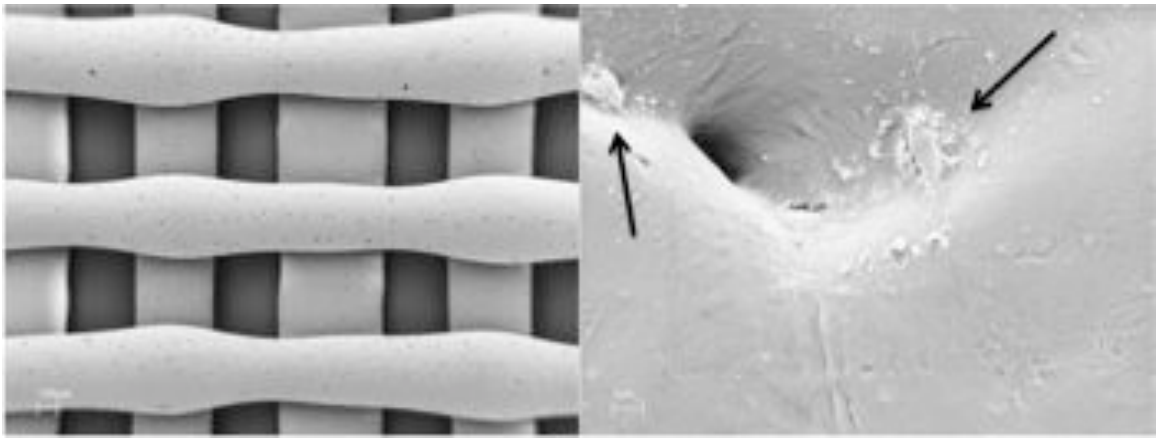

Figure 40. Scanning electron micrographies of PCL/Hap samples. On the right, arrows indicate HAp nanopowders dispersed in PCL matrix

Biomolecules grafting yield

A growth factor surface concentration of 0.3 pmol/cm^2 was assessed on the scaffolds for both VEGF and BMP-2. This value is in the biologically active range to provide correct signaling to cells cultured on the scaffolds.

Scaffold biocompatibility

Adequate cell viability and proliferation confirmed the generation of a non hostile environment. Above-mentioned assays showed a viability upper than 87% (Figure 41A)

and a proliferation rate upper than 45% with respect to negative control (Figure 41B), respectively.

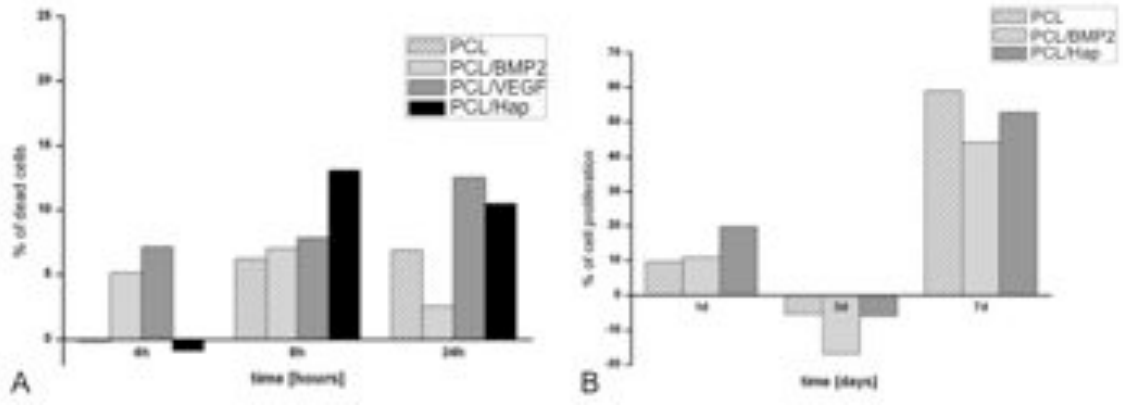

Figure 41. A) Cytotoxicity and B) proliferation assay

Cell adhesion

Cells adhered on the scaffold surfaces and growing in the porosity of the scaffold as shown by microscopic images of the TEC during cell culturing and on the F-Actin and nuclear staining. Figure 42 shows how adherent cells have the tendency to form cellular cords between the porosity between scaffold fibers.

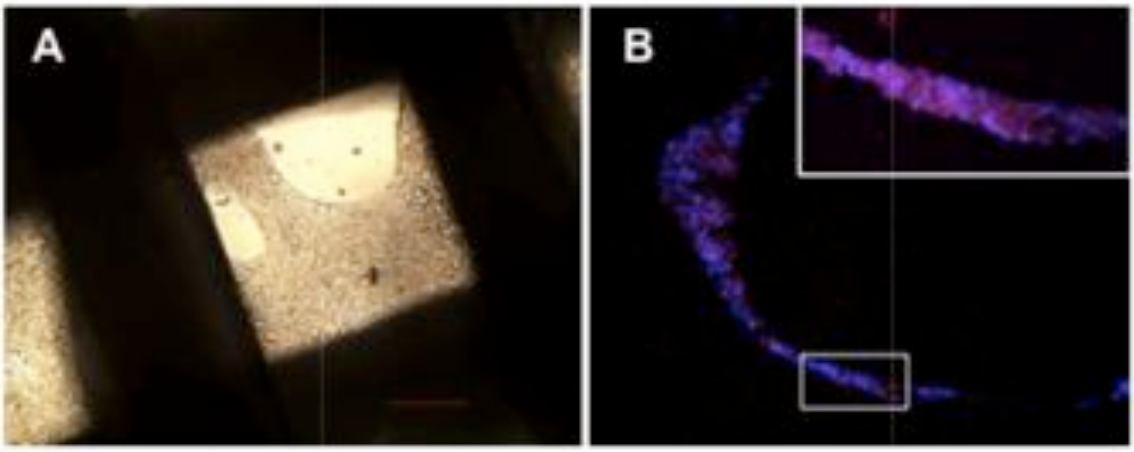

Figure 42. (A) Image showing PCL bioprinted scaffold with adherent hMSC under culture. (B) Section of the TEC after 21 days of culture showing the layer of cells around the surfaces of the scaffold fibers (F-actin: red, Nuclear staining TOTO3: blue)

Cell differentiation

Bioprinted scaffolds were characterized by micro-CT in order to verify the formation of mineralization throughout neo-formed ECM (Figure 43). PCL- and PCL/Hap- based scaffolds functionalized with BMP2 showed mineralization area on the surface of the scaffold indicating an osteogenic MSCs differentiation (arrows in Figure 43C) with respect to the control scaffold (Figure 44).

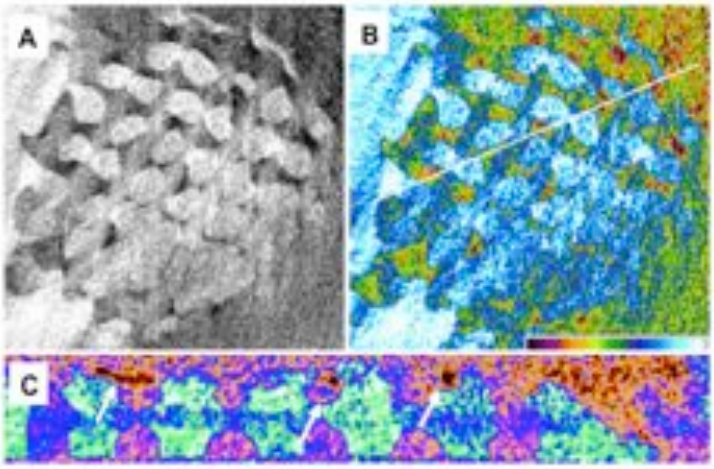

Figure 43. Representative image of the Micro-CT of the TEC cultured under osteogenic conditions showing high radio-dense area on the surface of the scaffold (Arrows in C)

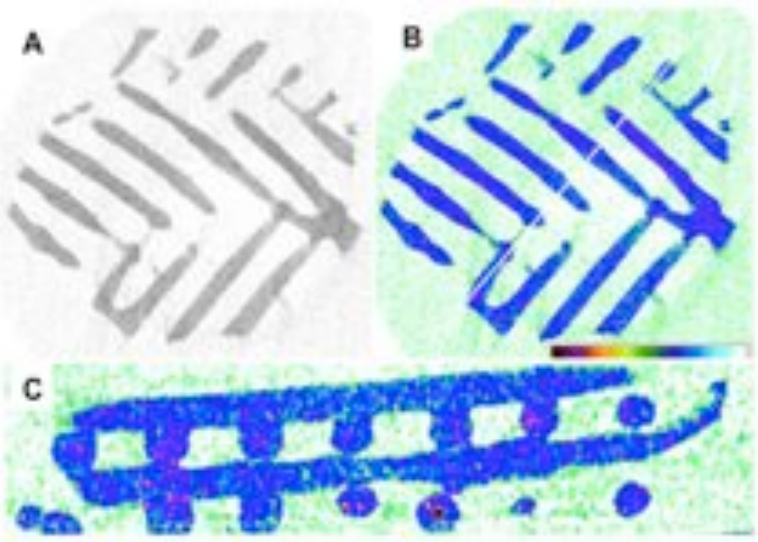

Figure 44. Representative image of the Micro-CT of the control TEC showing homogenous radio-dense scaffold.

Quantitative mRNA expression analysis by Real Time PCR (Figure 45) performed on all the samples show how the BMP2-grafted scaffolds push hMSCs seeded therein towards an osteogenic lineage, as confirmed by the slight upregulation of osterix (Osx) and alkaline phosphatase (AlP) with respect to the control group (PCL alone). Nevertheless, these data need a further confirmation by a proper histological assessment, as well as a longer time point to monitor the evolvment of the gene profile overtime.

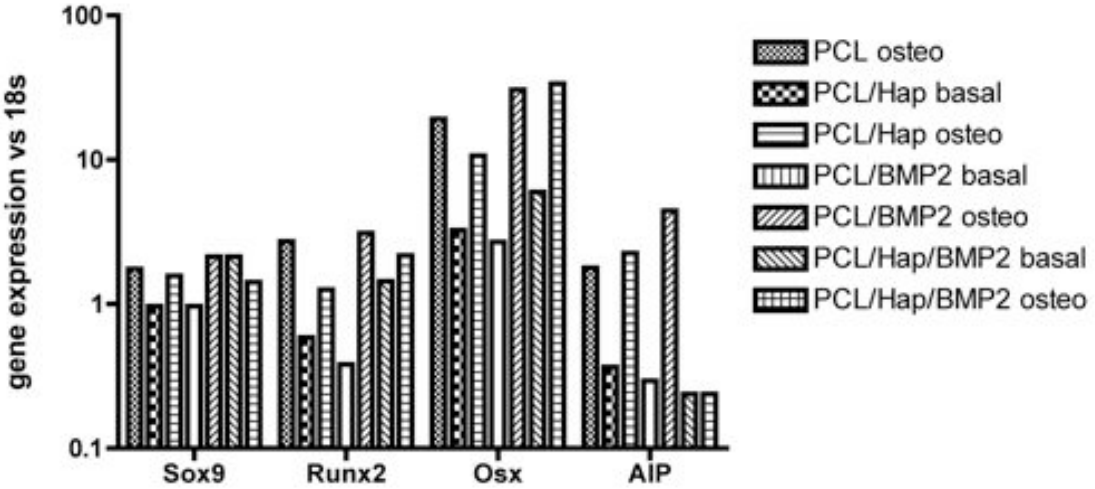

Figure 45. Gene expression of hMSCs cultured in basal or osteogenic medium for 21 days on PCL, PCL/Hap, PCL/BMP2, and PCL/Hap/BMP2 samples

Conclusions

Taken together these experimental data provided the proof of principle of the benefits introduced by (i) the utilization of hybrid materials, which take adavantage from both domains, (ii) the rapid prototyping approach applied to *ad hoc* scaffold fabrication, and (iii) the grafting of bioactive compounds on an already osteoinductive surface in hMSCs osteogenesis in vitro. Full histological characterization is needed to finally prove the feasibility of this approach in bone tissue engineering prior to end up in an in vivo study.

References

Arcos et al, *Acta biomaterialia* (**2010**)

Lee CH, Cook JL, Mendelson A, Maioli EK, Yao H, Mao JJ, "Regeneration of the articular surface of the rabbit synovial joint by cell homing: a proof of concept study", The Lancet (**2010**), 376: 440-448

Martin I, Miot S, Barbero A, Jakob M, Wendt D, "Osteochondral tissue engineering", *Journal of Biomechanics* (**2007**), 40: 750

Spadaccio C, Rainer A, Trombetta M, Vadalà G, Chello M, Covino E, Denaro V, Toyoda Y, Genovese JA, "Poly-L-Lactic Acid/Hydroxyapatite Electrospun Nanocomposites Induce Chondrogenic Differentation of Human MSC", *Annals of Biomedical Engineering* (**2009**), 37: 1376

Sun W, Lal P, "Recent development on computer aided tissue engineering - a review", *Computer Methods and Programs in Biomedicine* (**2002**), 67: 85

Vallet-Regì M, Arcos D, "Nanostructured hybrid materials for bone tissue regeneration", Current Nanoscience (**2006**) 2: 179

Woodfield TB, Malda J, de Wijn J, Peters F, Riesle J, van Blitterswijk CA, "Design of porous scaffolds for cartilage tissue engineering using a three-dimensional fiber-deposition technique",*Biomaterials*(**2004**), 25: 4149

Yeong WY, Chua CK, Leong KF, Chandrasekaran M, "Rapid prototyping in tissue engineering: challenges and potential", *Trends in Biotechnology*(**2004**), 22: 643

Yury A. Shchipunov, "Entrapment of Biopolymers into Sol–Gel-derived Silica Nanonocomposites" in *Bio-inorganic Hybrid Nanomaterials* (**2010**), ed. Wiley-VCH

3.2 Blocking of angiogenesis is required for the successful implantation of an immature graft during neo-cartilage formation

adapted from ***Centola M****, Marsano A, Abbruzzese F, Vadalà G, Scotti C, Barbero A, Martin I, Trombetta M and Rainer A.Biomaterials (2012), insubmission*

Introduction

Damaged articular cartilage has a limited capacity of self-repair due to its avascular nature and low cellular mitotic activity [Wu et al, 2010; Nguyen et al, in press; Ho et al, 2010; Ahmed et al, 2010]. Cell-based repair techniques, such as the current gold-standard matrix-induced (MACI), showed some positive clinical outcome, nevertheless the formation of fibrous repair tissue with inferior mechanical properties and limited durability [Pelttari et al, 2009]. Moreover, as compared to the physiological adult articular cartilage, not mature engineered tissues lack of essential ECM components, like the high molecular weight-hyaluronic acid, and other anti-angiogenic proteins - such as chondromodulin, endostatin, thrombospondin, angiostatin, etc. [Nyberg et al, 2005]. Not completely grown cartilaginous constructs might be therefore exposed to an early blood vessel invasion and host reaction, which might therefore lead to the poor cartilaginous quality [Moretti et al, 2005] and eventually to premature implant degradation. Thus, control of angiogenesis results to be essential for both the development and the physiological maintenance of articular cartilage [Takita et al, 2002]. In particular, it has been demonstrated [Matsumoto et al, 2009] that vascular endothelial growth factor (VEGF), one of the most potent angiogenic factors, plays an essential role in the ossification process at the level of the growth plate, modulating cartilage vascularization and absorpting hypertrophic chondrocytes. Recent data also reveal that chondrocyte-derived VEGF promotes also catabolic pathways in the osteoarthritic cartilage [Matsumoto et al, 2009].

Neo-angiogenesis is also accompanied by the massive infiltration of mononuclear cells, such as monocytes. VEGF acts as a powerful chemoattractant for monocytes [Zentilin et al, 2006], which could potentially lead to a fast macrophage-driven in vivo re-absorption of the implanted engineered cartilage. These aspects strongly underline the importance to control angiogenesis, and in particular the signaling of VEGF. To this extent, cell-based gene anti-angiogenic therapies for cartilage regeneration have been already successfully

investigated by inducing over-expression of either endostatin [Jeng et al, 2010], or chondromodulin [Klinger et al, 2011]. In addition, over-expression of soluble VEGF receptor-1 combined to the release of growth factors form the TGF beta superfamily enhanced cartilage regeneration in a rat osteoarthritic model [Matsumuto et al, 2009] and chondrogenesis of mesenchymal progenitors [Kubo et al, 2009, Matsumuto et al, 2009]. As a valid alternative, we hypothesized that blocking of VEGF could also be reached by releasing an anti-angiogenic molecule from the scaffold, so providing, right upon implantation, the appropriate environment for the full maturation of freshly-seeded engineered constructs. In particular, we developed a hyaluronan/fibrin-based porous scaffold which has been functionalized by the incorporation of a humanized monoclonal anti-VEGF antibody (Bevacizumab, Avastin) [Wang et al, 2004], an FDA approved anti-angiogenic drug. This represents an innovative approach since the inhibition of angiogenesis in engineered cartilage has been achieved for the first time using a FDA-approvable drug eluting scaffold, so overcoming the limitations of gene therapy in terms of a direct clinical translation [Mulligan et al, 1993].

Scaffold biomaterials have been chosen thanks to their biocompatibility, chondro-supportive nature [Ahmed et al, 2010; Wu et al; 2010] and the current quite extensive clinical use of the two single components [Ho et al, 2010; Spiller et al, 2010, Visna et al, 2004, Marcacci et al, 2005]. Among all the promising cell sources, e.g. articular chondrocytes, for cartilage tissue engineering, nasal chondrocytes (NC) represent one of the most interesting for clinical application thanks to the ease and low morbidity harvesting procedure. NC also better retain the chondrocytic re-differentiation capacity upon cell expansion [Tay et al, 2004] as compared to other origin chondrocytes and properly respond to mechanical forces, typically associated with joint loading [Candrian et al, 2008].

Materials and Methods

Scaffold preparation

To prepare fibrin-hyaluronic acid composite gel, a solution containing fibrinogen (Sigma, 20 mg/mL) and HA (Sigma, 10 mg/mL) was prepared in saline (NaCl 0.9%) [Henschen et al, 1983; Zaho et al, 2008; Davis et al, 2010]. This solution was mixed under mild stirring, adding 7.5 (AVA3.75) or 10 (AVA5) μg/mL of Bevacizumab (1 mg/mL, Avastin®, Genentech, San Francisco, CA), and 6000 KUI/mL of aprotinin (Sigma). After complete mixing, thrombin saline solution (Sigma, 0.5 UI per mg of fibrinogen) - 1:1 volume ratio respect to the fibrinogen solution – was added to the fibrinogen-HA solution. Finally, fibrin-stabilizing factor XIIIa (Abnova, Taipei, Taiwan, 1 μL per 20 mg of fibrinogen) was

added in order to crosslink the fibrin polymer chains. Solution was transferred into a 96-multiwell plate and incubated at 37 °C to form a gel [Kim et al, 2010; Park et al, 2009]. Scaffolds were then lyophilized for 3 days at -20 °C in order to obtain a porous sponge. All operations were performed under sterile conditions. Control sponges were generated either without addition of bevacizumab (HA-FIB) or only with fibrin, either supplemented (FIB+AVA) or not (FIB), with 3.75 μg/mL bevacizumab.

Degradation and water uptake assays

Weight loss of the scaffolds was monitored as a function of incubation time in DMEM supplemented with 10% FBS at 37 °C. For three weeks, scaffolds were extracted from incubation medium at selected time points, blot dried and weighed (Wt). Medium was replaced every two days. Weight loss ratio was defined as (W0-Wt)/W0%, where W0 is the initial weight of the scaffold. Experiments were performed in triplicate (n=3) [Zaho et al, 2008; Davidenko et al, 2010; Tan et al, 2009].

To determine water uptake, lyophilized scaffolds were weighed (Wdt) and then incubated in saline at 37°C. Hydrated scaffolds were taken out at selected timepoints within 1 hour, wiped superficially with a filter paper, and weighed (Wwt). The uptake ratio was defined as UR=(Wwt -Wdt)/Wdt. Each experiment was performed in triplicate (n=3) [Davidenko et al, 2010; Tan et al, 2009].

Scanning Electron Microscopy (SEM)

Scaffold morphology was investigated by means of Field Emission Scanning Electron Microscopy (FE-SEM, Leo Supra 1535, LEO Electron Microscopy, Cambridge, UK) after being sputtered with gold.

Mercury intrusion porosimetry

Pore size distribution was determined by mercury intrusion porosimetry (Carlo Erba Instruments) according to the Washburn equation:

$$p \cdot r = -2 \cdot \gamma \cdot \cos\theta$$

Where p is the applied pressure, r is the pore radius, γ is the surface tension of mercury and θ is the contact angle of mercury. In particular, a mercury surface tension of 480 mN/m and a contact angle of 141.3° were imposed. Pressure was applied between 13 and 101 kPa, corresponding to pores in the range 10-220 μm.

Compressive mechanical test

Cylindrical hydrated HA-Fib scaffold samples (6 mm diameter, 8 mm height) were tested under compressive loading using a mechanical testing system equipped with a 10 N load

cell (model 3365, Instron, Norwood, MA) at a strain rate of 0.05 min-1. The compressive modulus (E*) was extrapolated from raw data. Hydrated samples were measured following incubation in saline solution at 37 °C for 30 min. Experiments were performed in triplicate (n = 3) [Davidenko et al, 2010; Tan et al, 2009].

ELISA quantification of the released Avastin®

To quantify the bevacizumab release from the scaffold, bevacizumab-loaded constructs were incubated in DMEM at 37°C and 5% CO2 and surnatants were withdrawn at fixed time points, up to three weeks. 96-well plates were incubated overnight at 4°C with 50 μL of bevacizumab-containing surnatants, and solutions with different concentrations of bevacizumab in order to obtain the calibration curve. After a washing step with PBS containing 0.05% Tween 20 (washing buffer) the remaining protein-binding sites were blocked by 2 hours incubation at room temperature with 200 μL blocking buffer (PBS+0.05% Tween 20 containing 1% BSA). Plates were washed twice with washing buffer and then, 50 μL of HRP-conjugated, anti-mouse IgG H+L antibody (Southern Biotech, Birmingham, AL), diluted 1:3000 in blocking buffer, were added to each well. After 90 minutes at room temperature followed by washing, 90 μL OPD (prepared by dissolving tablet sets in 20 mL distilled water, Sigma) was added and the reaction was allowed to develop at room temperature in the dark for 30 minutes. The color reaction was stopped by adding 50 μL of 10% sulfuric acid per well. Reading was performed at 492 nm using an ELISA plate reader (Tecan).

Cell isolation and expansion

Specimens of healthy nasal cartilage tissue were harvested postmortem from biopsy specimens of the nasal septum of 4 individuals (mean age 51 years [range 31-84 years]), in accordance with the local ethics committee of University Hospital Basel, Switzerland. Nasal chondrocytes (NC) were isolated following 22 hours of incubation at 37°C in 0.15% type II collagenase and resuspended in DMEM containing 10% FBS, 4.5 mg/ml D-glucose, 0.1 mM nonessential amino acids, 1 mM sodium pyruvate, 100 mM HEPES buffer, 100 UI/ml penicillin, 100 μg/ml streptomycin, and 0.29 mg/ml L-glutamate (complete medium) [Candrian et al, 2008]. All products were purchased from Gibco.

NC were plated in culture dishes at a density of 104 cells/cm2 and expanded in complete medium supplemented with 1 ng/mL of transforming growth factor-β1 (TGF-β1, R&D Systems, Minneapolis, MN, USA) and 5 ng/mL of fibroblast growth factor-2 (FGF-2, R&D Systems). When subconfluent, cells were detached by treatment with 0.05% trypsin/0.53

mM EDTA, and either replated at 5x103 cells/cm2, or used in the next experiments at passages P2 or P3.

Cytotoxicity test

HA-Fib, AVA3.75 and AVA5 sponges for a total weight of ca. 80 mg were separately placed in a 15 mL tube containing 2 mL of DMEM overnight in the incubator. 5*103 NC were separately plated in a 96-well plate in DMEM-based complete medium and cultured for 24 hours. Then, complete medium was supplemented with scaffold elution products. Cell toxicity due to the scaffolds was determined at 4, 8 and 24 hours by Vybrant Cytotoxicity Assay Kit® (Molecular Probes, Invitrogen) in accordance with the manufacturer's instructions. Plate was read on a fluorescence microplate reader (Tecan) at 540 nm with correction at 595 nm.

HUVEC proliferation assay

Human umbilical vein endothelial cells (HUVEC) were cultured in gelatin-coated tissue culture plates using a growing medium (GM, M199 supplemented with 20% FBS, 100 μg/mL endothelial cells growth supplement, 50 UI/mL heparin, 100 UI/mL penicillin, and 100 μg/mL streptomycin). All products were purchased from Sigma (Sigma, Milwaukee, WI, USA), except for M199 medium (Gibco, Invitrogen, Carlsbad, CA, USA). Cells were cultured at 37°C in a humidified, 5% CO2 atmoshpere. When at confluence, HUVEC were detached, plated in a 96-wells plate at a density of 5000 cells/well and cultured overnight with the same medium. The following day, medium was changed into one containing low FBS amount in order to starve the cells (named Assay Medium, AM, consisting of M199 supplemented with 5% FBS, 10 UI/mL heparin, 1% penicillin/streptomycin). A different amount of human recombinant Vascular Endothelial Growth Factor (VEGF, R&D, range investigated: 0-10 ng/mL), in order to obtain a titration curve of HUVEC VEGF-induced proliferation. Two different doses of Avastin® and surnatants with scaffold degradation products were tested. Avastin® at the concentration of 200 and 500 μg/mL and surnatants (ratio 1:1) were preincubated with AM containing different amounts of VEGF at 4°C for 2 hours before adding them to the cells. After two days, the HUVEC metabolic activity has been measured by MTS assay (Cell Titer 96®, Promega, Madison, WI, USA), according to the manufacturer's protocol.

Degradation products for this assay were obtained by constructs generated by NC loaded on either HA-FIB alone or functionalized with Avastin® (AVA3.75), or FIB alone or functionalized (FIB+AVA), without adding the aprotinin in order to accelerate the

degradation of the biomaterials. The constructs were generated by using NC seeded at a density of 1.25*104 cells/cm3 and cultured on 1% agarose coated petri dishes for 1 week in complete medium. Surnatants were collected at fixed time points (1, 4 and 7 days). High molecular weight hyaluronic acid (500 μg/mL) was used as a control for the scaffold degradation products to assess its single anti-angiogenic potential [Pardue et al, 2008].

Monocytes migration assay

To see whether Avastin® capacity to block VEGF is also effective in inhibiting the monocytes invasion of the constructs, and also whether scaffold degradation products might also play a role in attracting monocytes, a specific migration assay was developed and used. PBMC (Peripheral Blood Mononuclear Cells) were isolated from peripheral blood of healthy donors (n=2) by gradient centrifugation. Monocytes were purified by using the MACS CD14 isolation kit (Miltenyi Biotec, Bergisch Gladbach, Germany), according to the manufacturer's protocol.

$12.5*10^3$/well freshly isolated CD14+ monocytes were plated in the upper chamber HTS-Transwell-24 well microplate (Corning, Lowell, MA, USA) by using 50 μL of serum-free DMEM (SFM). 200 μL of different types of surnatants were added in the lower chamber to act as chemoattractants: SFM, SFM supplemented with 10 ng/mL of VEGF as a positive control [Zentilin et al, 2006], SFM+VEGF containing bevacizumab, added using the optimal stoichiometric ratio with VEGF – i.e 2.6:1 [Wang et al, 2004], and collected surnatants containing the scaffold degradation products. The plate was incubated for 20 hours at 37 °C in a 5% CO2 atmosphere. Afterwards the plate was washed with PBS in order to remove any traces of phenol red that may interfere with the following analysis and then put at -70 °C to lyse the cells. The quantification of the migrated monocytes was performed by means of the CYQuant® cell proliferation assay Kit (Molecular Probes), according to the manufacturer's protocol.

To obtain scaffold degradation products for this assay, HA-FIB and FIB scaffolds, without the addition of aprotinin in order to accelerate the scaffold degradation, were cultured for 1 week in serum-free medium (DMEM supplemented with 1 mM sodium pyruvate, 100 mM HEPES buffer, 100 UI/ml penicillin, 100 μg/ml and surnatants were collected at fixed time points (1, 4 and 7 days).

In vitro pellet culture model

To assess the effect of bevacizumab on the chondrogenic potential of NC, de-differentiated NC (n=2) were induced to re-differentiate in pellet cultures, as previously described [Francioli et al, 2007]. Briefly, NC were suspended in srum-free DMEM supplemented

with 1% liquid media supplement (ITS+1, Sigma, 10 mg/mL), 1.25 mg/mL human serum albumin (Sigma), 0.1 mM ascorbic acid 2-phosphate (Sigma), 10-7 M dexamethasone (Sigma) and 10 ng/mL TGF-β1, with or without the addition of 3.75 μg/mL bevacizumab. Aliquots of 5*105 cells/0.5 mL were centrifuged at 1100 g for 3 min in 1.5 mL polypropylene conical tubes (Sarstedt, Numbrecht, Germany) to form pellets. Pellets were cultured for 2 weeks.

In vitro 3D culture

HA-FIB, AVA3.75, AVA5 and FIB cylinder-shaped scaffolds (6 mm diameter and 4 mm height) were placed on dishes coated with a thin film of 1% agarose and statically seeded with NC (P2-P3, n=2) from the top using a density of 1.2*104 cells/cm3. Constructs were statically cultured for 2 weeks in complete medium supplemented with 10 mg/mL insulin (ACTRAPID HM), 0.1 mM ascorbic acid 2-phosphate (Sigma), 10 ng/mL TGF-β3 (Novartis, Basel, CH), and 3000 KUI/mL aprotinin. These supplements were previously shown to enhance chondrogenesis of dedifferentiated human chondrocytes during in vitro culture [Miot et al, 2010].

In vivo ectopic mouse model

In parallel, NC (n=3) were statically seeded on the same types of scaffolds using the same cell density and cultured overnight in complete medium. Constructs were then implanted in the back of nude mice (CD1 nu/nu, athymic, 5-weeks-old females) in pockets between excised muscle fascia and subcutaneous tissue. All animals in this study were treated according to institutional guidelines. Constructs were harvested after 1, 3 and 6 weeks and processed for histological analyses.

Histological analysis

Pellets and/or constructs, after washing in PBS, were fixed in 4% formalin overnight, embedded in paraffin and cross-sectioned (5 μm thick sections). The sections were stained with Safranin O, Alizarin red and Masson's trichrome (Reactifs RAL, Martillac Cedex, France). The sections were also processed for immunohistochemistry to visualize mouse anti-human types II, I and X collagen, MMP-13 and BSP (all antibodies were purchased by MPBiomedicals, Solon, OH, USA), as described by Grogan et al [Grogan et al, 2003]. In order to distinguish from the endogenous mouse immunoglobulins in the tissue the mouse primary antibody, a M.O.M.™ kit (Vector Laboratories, Burlingame, CA, USA) was used according to the manufacturer's instructions. Images were acquired using an Olympus BX-61 microscope. The immunobinding was detected with biotinylated secondary antibodies and using the appropriate Vectastatin ABC kits (Vector

Laboratories). The red signal was developed with the Fast Red kit (Dako Cytomation) and sections counterstained by Haematoxylin.

Immunofluorescence was performed on in vivo generated constructs which were embedded in optimal cutting temperature (O.C.T.) (Sakura Finetek, Torrance, CA) matrix, and freshly frozen in isopentane cooled-liquid nitrogen. Cryosections (10 μm thick) were incubated with the primary antibodies rat anti mouse CD31 (BD, Franklin Lakes, NJ, USA) and F4/80 (BD). DAPI was used to counterstain the nuclei. Alexa Fluor 546 secondary antibodies (BD) were used. Fluorescence images were acquired using a confocal microscope (Nikon).

The ingrowth of host vessels, as well as murine macrophages, was quantified by digital image processing by means of Image J software (NIH, Bethesda, MD, USA), starting from CD31- and F4/80- stained sections, respectively, as elsewhere described [paper Ludovic?]. Briefly, different images per group (n=5) were acquired with 10x magnification object in order to have an overview of the whole section, by using an Olympus BX61 microscope (Munster, Germany). The percentage area positive for CD31 or F4/80 was calculated by normalizing the values to the area of the whole section, excluding the outer fibrotic capsule.

Histological scoring system

The quality of the in vivo tissue-engineered cartilage (n≥3 per each experimental group and time point) was assessed by a scoring system, which combines the validated Bern [Grogan et al, 2006] and ICRS II [Mainil-Varlet, 2010] scores. The here used scoring system was optimized for cartilage tissue engineering in an ectopic model. In particular, the engineered cartilaginous tissues were evaluated by the quality (Safranin O staining), the presence of calcification (Alizarin Red staining) and the ingrowth of host vessels (IF for CD31). Table 5details the criteria used in the evaluation process, each with equal weight on the final score. All samples were evaluated in a blinded way by 5 different experienced observers.

Scoring categories	*Score*
1. Intensity of Safranin O-fast green stain[1]	
No stain	0
Weak staining of poorly formed matrix	1
Moderately even staining	2
Even dark stain	3
2. Distance between cells/amount of matrix accumulated[1]	

High cell density with no matrix in between (no spacing between cells)	0
High cell density with little matrix in between (cells <1 cell-size apart)	1
Moderate cell density with matrix (cells approx. 1 cell-size apart)	2
Low cell density (cells >1 cell-size apart) with an extensive matrix	3
3. Cell morphologies represented[1]	
Condensed / necrotic / pycnotic bodies	0
Spindle / fibrous	1
Mixed spindle / fibrous with rounded chondrogenic morphology	2
Majority of rounded / chondrogenic	3
4. Uniformity of Safranin O staining[2]	
Complete disorganization of stained areas	0
Less than 50% of Safranin O stained areas respect to the total volume	1
50-80% of Safranin O stained areas respect to the total volume of the section	2
Overall homogeneity of the staining	3
5. Abnormal calcifications within the cartilage newly formed[2]	
Strong presence of abnormal calcifications inside the neo-formed cartilage	0
Presence of some calcification spots inside the newly-formed cartilage	1
Presence of very few calcification spots inside the repaired cartilage	2
Complete absence of calcifications throughout the newly-formed cartilage	3
6. Vessels ingrowth (within the newly formed tissue)[2]	
Vessels ingrowth inside the core of the repaired cartilage	0
Vessels ingrowth until the inner rim of the neo-formed cartilage (ca. two thirds of newly-formed cartilage's total volume)	1
Vessels ingrowth until the outer rim of the neo-formed cartilage (ca. one third of newly-formed cartilage's total volume)	2
No presence of vessels or vessels confined in the external fibrotic capsule	3

7. Final score	
Not-formed cartilage. Basically, just fibrotic tissue	0-6
Inhomogeneous and fibrocartilagineous tissue, having just few and not-connected areas of a good newly formed cartilage	6.1-11
Moderately good tissue, having less than 60% - respect to the total volume - of a good newly formed cartilage	
Very good quality of homogeneity of newly formed cartilage	11.1-15

15.1-18

Table 5. Histological scoring system (1 Grogan et al, 2006; 2 Mainil-Varlet, et al, 2010) * 5 um-thick paraffin-embedded sections

Finally, to test the accuracy and the reliability, and for the validation of the proposed score, the maximum (σ_{max}) and overall variability (σ_{ov}) of the scores among the observers were calculated. The variability (σ) was defined as:

$$\sigma = \frac{s}{\bar{x}} * 100[\%]$$

where s is the variance and $\bar{x}$ the average calculated from the marks given by the five different observers for a single scoring category.

Biochemical analysis

Pellets and/or constructs were digested with protease K (0.25 mL of 1 mg/mL protease K in 50 mM Tris with 1mM EDTA, 1 mM iodoacetamide, and 10 mg/mL pepstatin-A) for 15 h at 56 °C, as previously described [Miot et al, 2010]. GAG amount was measured spectrophotometrically using 1,9-dimethylmethylene blue chloride (DMMB) dye [Farndale et al, 1986], with chondroitin sulfate as a standard, and normalized to the deoxyribonucleic acid (DNA) amount, measured spectrofluorometrically using the CyQuant® cell proliferation assay Kit (Molecular Probes) and with bovine DNA as a standard.

Real time- quantitative reverse transcriptase polymerase chain reaction (RT-rtPCR)

Total RNA of pellets and in vitro constructs was extracted using TRIzol® (Life Technologies, Basel, Switzerland). RNA was treated with DNaseI using the DNA-free™ Kit (Ambion, Austin, Texas) and quantified spectrophotometrically. cDNA was generated from 3 µg of RNA by using 500 µg/ml random hexamers (Promega AG Dübendorf, Switzerland) and 1 µl of 50 UI/ml Stratascript™ reverse transcriptase (Stratagene, Amsterdam, NL), in the presence of dNTPs. cDNA was used in the qPCR reaction performed and monitored on an ABI Prism 7700 Sequence Detection System (Perkin-Elmer/Applied Biosystems, Rotkreuz, Switzerland). TaqMan® Gene Expression Assays (Applied Biosystems) were used for gene expression measurements. Cycle temperatures and times as well as primers and probes used for the housekeeping gene (GAPDH) and the genes of interest (collagen type I and type II) were as previously described [Strobel et

al, 2010]. Assays on-Demand (Applied Biosystem) were used to measure the expression of Sox-9 (Hs00165814_m1), VEGF (Hs00900055_m1), and chondromodulin-I (Lect-1, Hs0017087_m1). Gene expression was assessed at least in quadruplicate.

Statistical analysis

Data are presented as means ± SD (n≥3). Statistical analysis was performed using the unpaired or non-parametric t-test, taking into account the normal distribution of the collected data by means of Prism® software (GraphPad Software, LaJolla, CA, USA). P values lower than 0.05 were considered statistically significant.

Results

Characterization of HA-Fibrin scaffold

Under our fabrication conditions, HA-fibrin-based scaffolds resulted to have a reproducible geometry (cylinder of 6 mm diameter and 8 mm height) with similar microstructure. SEM showed that Avastin® incorporation did not affect the final microstructure and pore size and distribution of the sponge-like scaffolds (Figure 46A-B). The pore size was found to be in the range of 220 μm. Both scaffolds functionalized or not with Avastin® resulted to have similar porosity (71±3% and 69±5%, respectively).

HA-fibrin scaffolds lost about 50% just in the first 48 hours and only 45% of their total weight in the following three weeks in culture.

Water uptake ratio was estimated to be 7.6-fold higher than the weight of the dry ones.

The compressive mechanical behavior of our scaffolds resembled that of the elastomeric, low-density, and open-cell spongy materials [Gibson and Ashby, 1997].

The compressive modulus (E*) was similar for the hyaluronic acid (HA)-fibrin (FIB) scaffolds functionalized (8.35±0.04 kPa) or not (8.39±0.08 kPa) with bevacizumab.

Scaffold cytotoxicity test showed that NC viability was higher than 99.2 % in all the experimental groups.

Bevacizumab (Avastin®) release was consistent with the degradation timing of the HA-FIB scaffold (Figure 46C). Within the first 48 hours the bevacizumab release was about one third of the total dose initially loaded. From day 7 to 10 its release reached a plateau until to completely being eluted during the third week of culture.

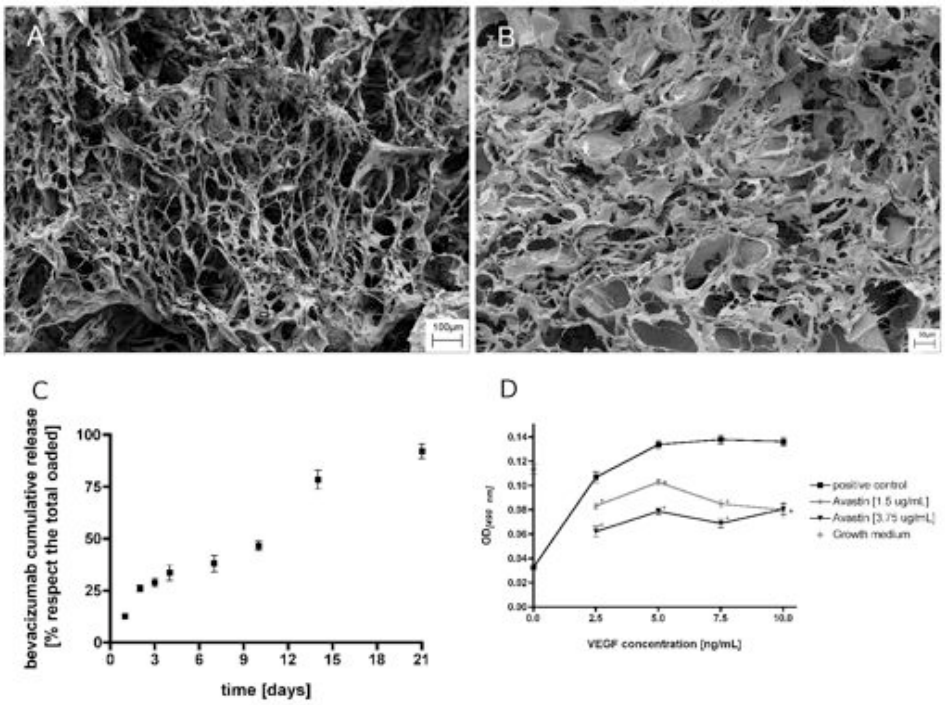

Figure 46. Scaffold characterization. a-b) SEM micrographies of scaffolds a) without and b) Avastin; c) Bevacizumab release curve; d) Bevacizumab activity and dosage;e) Role of each scaffold component on HUVEC proliferation; f) Monocytes migration assay

Avastin® activity and dosage

Avastin® activity and the appropriate amount to efficiently block different VEGF concentration were assessed by performing a HUVEC proliferation assay. HUVEC showed a VEGF dose-dependent proliferation rate reaching a plateau at a concentration of 10 ng/mL (Figure 46D- positive control curve). The supplementation of both 1.5 and 3.75 μg/mL of Avastin® in the culture medium reduced the HUVEC metabolic activity, stimulated by VEGF (Figure 46D). The HUVEC metabolic activity was statistical significantly different when cultured in presence of Avastin® for all the VEGF concentrations used. The higher concentration of Avastin® tested was more effective in blocking the VEGF-induced HUVEC proliferation, and therefore selected for the in vitro and in vivo experiments.

In vitro 3D pellet culture

Avastin® resulted not to affect the in vitro intrinsic chondrogenic potential of NC. Safranin O staining showed no major differences, in terms of staining intensity and uniformity, chondrocytes morphology between the group treated with Avastin and the not treated one (Figure 47A-B). Biochemical analysis confirmed the histological one, no

statistically significant difference was found indeed in the glycosaminoglycans content of experimental groups treated or not with Avastin® (Figure 47C). Avastin® supplementation in the culture medium resulted also to not affect the expression at mRNA level of hyaline- (Sox9 and type II collagen) and bone/fibro- (type I collagen) chondrocytic markers and VEGF (Figure 47D). No statistically significant differences were indeed found in the two groups ($p<0.01$).

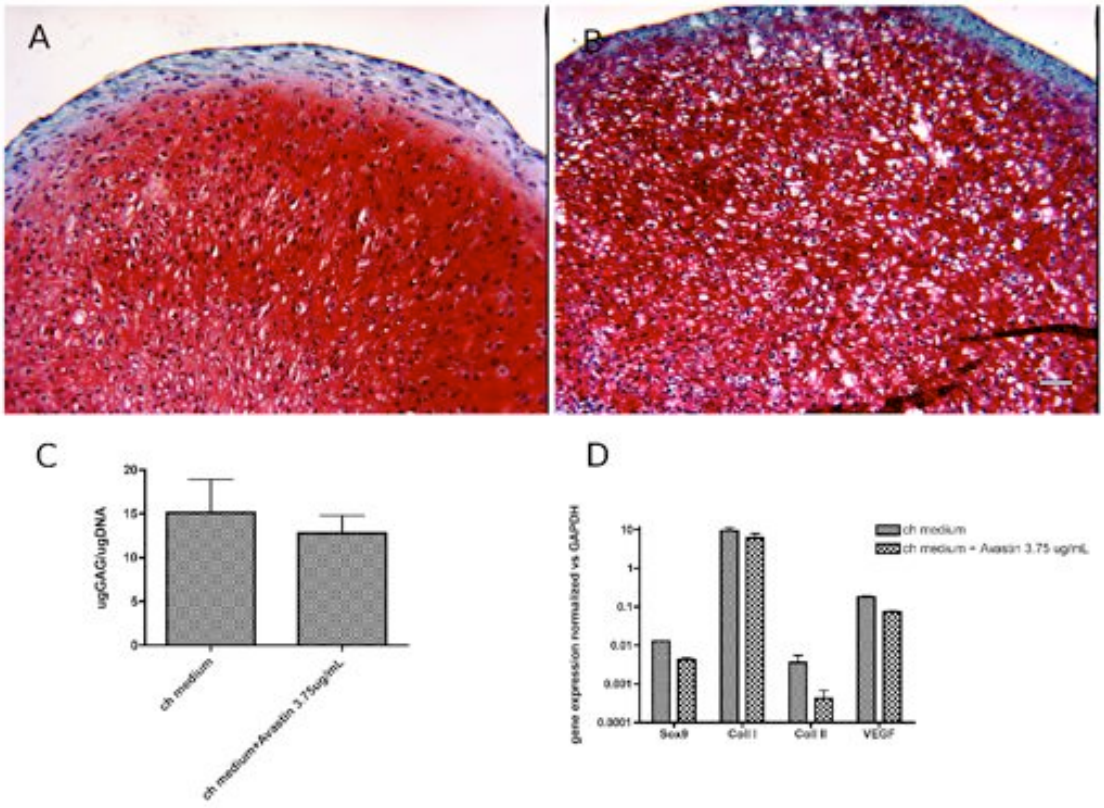

Figure 47. 3D pellet culture system. Histological staining for Safranin O of pellets cultured in chondrogenic medium (ch medium) supplemented (B) or not (A) with 3.75μg/mL Avastin for 2 weeks. Quantification of GAG /DNA ratio for NC generated pellets (C). Analysis at mRNA level of Sox9, types I (Coll I), II (Coll II) and VEGF genes

In vitro scaffold-based 3D culture

Only in presence of HA in the scaffold composition cartilaginous matrix was formed by NC in vitro. FIB alone scaffold indeed did not result to be chondro-supportive. As compared to the engineered tissues generated with fibrin alone (FIB), the constructs engineered with scaffolds containing also HA (HA-FIB) deposited a statistically significant higher amount of GAG (Figure 48C), confirming therefore the intense staining for Safranin O staining and the typical chondrocytic like cell morphology (Figure 48A-B).

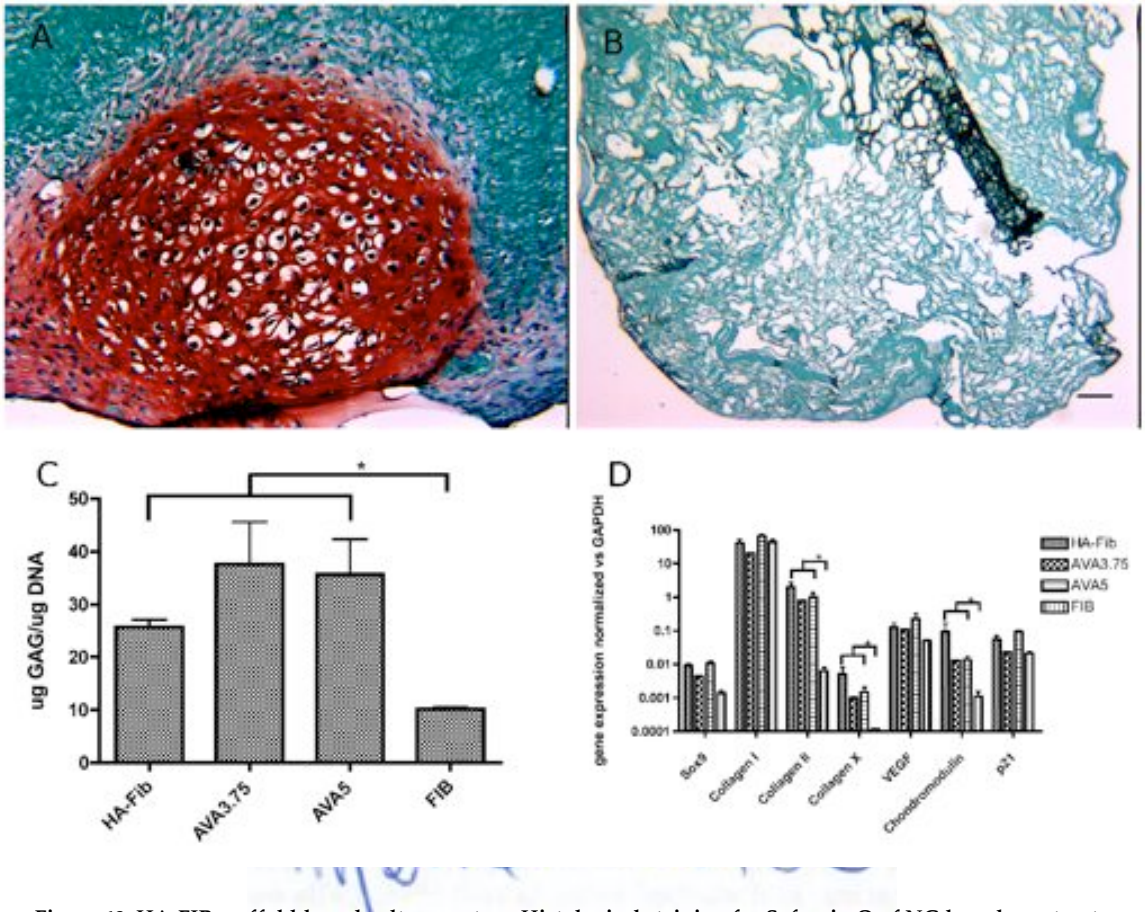

Figure 48. HA-FIB scaffold-based culture system. Histological staining for Safranin O of NC-based constructs generated by using either HA-FIB (A) or FIB (B) scaffolds cultured in chondrogenic medium up to 2 weeks. Quantification of the GAG/DNA ratio (C) of cartilaginous constructs generated by NC loaded either on either FIB alone as control or HA-FIB alone or functionalized by the supplementation of 3.75 (AVA3.75) or 5 (AVA5) μg/mL of Avastin. Analysis at mRNA level of the same experimental conditions

The presence of HA in the FIB-based scaffold resulted to statistically increase also the expression of some chondrocytic genes, such as collagen type II and chondromodulin (Figure 48D). Type X collagen expression at mRNA level was also upregulated in the presence of HA in the scaffolds. Avastin® did not affect both the GAG deposition and the gene expressions of the analyzed markers. Taken together, these evidences strongly point out the importance of HA in our system in order to obtain a good tissue-engineered cartilage.

In vivo ectopic mouse model

Following subcutaneous implantation, a strong quantitative difference between the scaffolds with and without Avastin® was given by the percentage of constructs not resorbed at different time points, as reported inFigure 49.

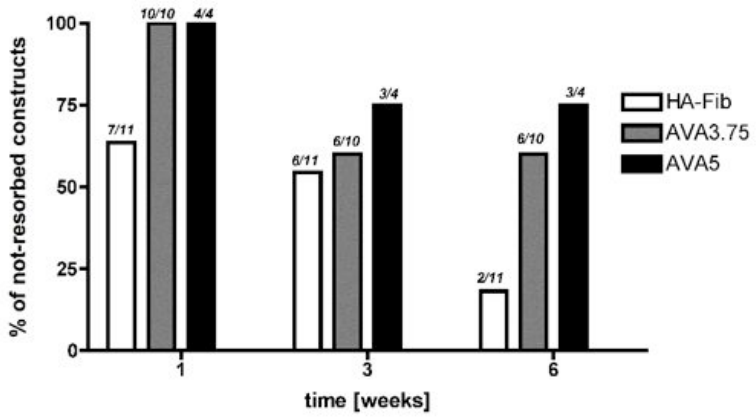

Figure 49. In vivo constructs degradation - % of not resorbed constructs respect to the implanted

Only the 18.2% of HA-Fib constructs was found after 6 weeks, compared with the 60% and 75% for what regard the AVA3.75 and AVA5 constructs, respectively. Interestingly, no differences in terms of percentage of degraded constructs were found between 3 and 6 weeks time-points, for the scaffolds loaded with Avastin®, so indicating the 3 weeks time-point as the most critical one for the final success of the implantation. These data impressively underline the role of the blocking of angiogenesis for the successful implantation of an immature graft in vivo.

However, no major differences were observed in terms of the quality of cartilage formed in the not resorbed constructs between the experimental groups with or without Avastin® (Figure 50), demonstrating (i) the high chondrogenic potential of NC even in absence of an in vitro chondrocytic pre-commitment and (ii) the self-sustaining capacity of the neo-formed engineered cartilage. Since no remarkable differences were also found between the two different concentrations of Avastin® (3.75 or 5 μg/mL), histological results from the condition with 3.75 μg/mL of Avastin® (AVA3.75) were only shown.

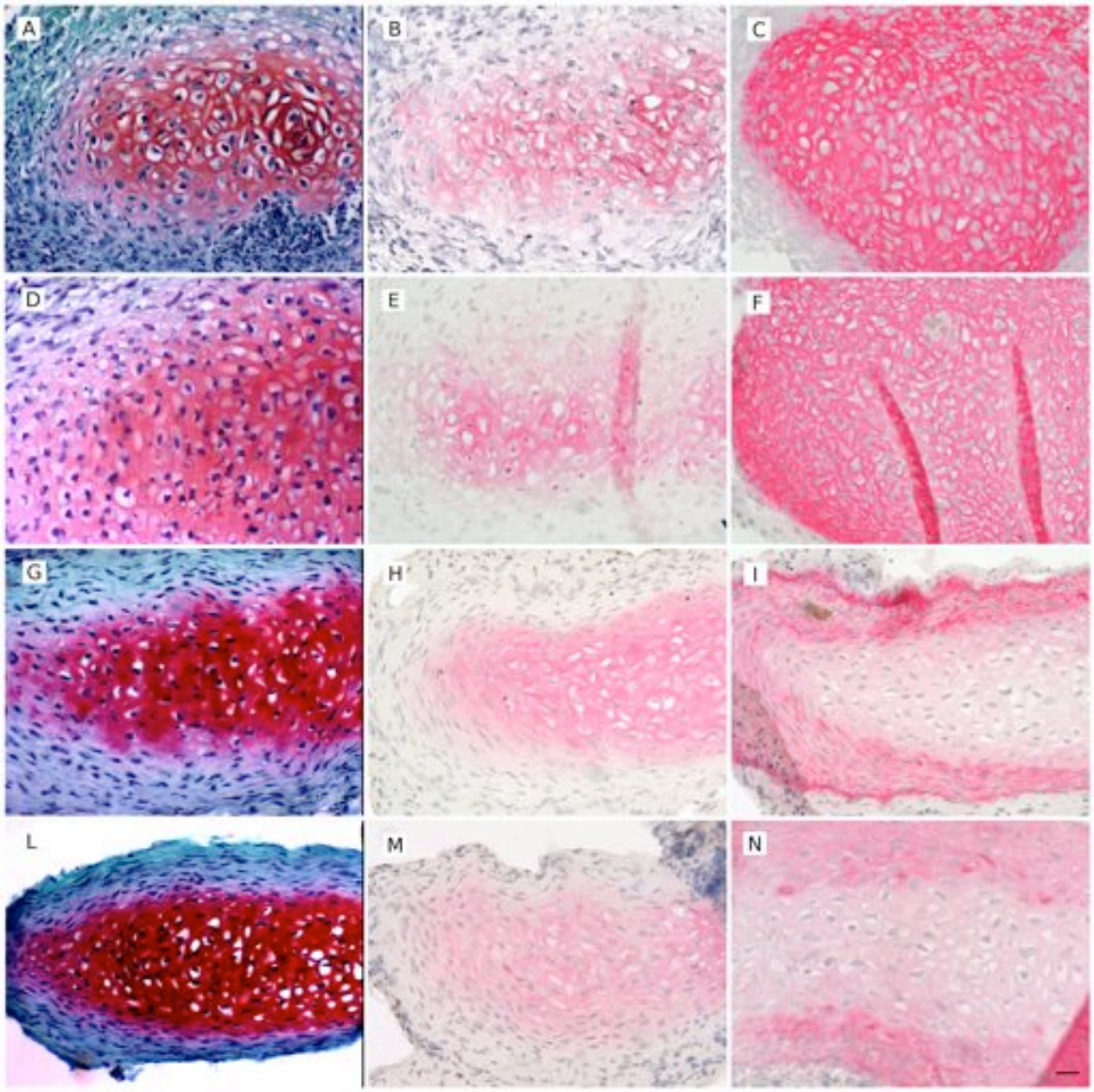

Figure 50. Histological analysis on in vivo samples. Safranin O: a) HA-Fib, 1 week, d) AVA3.75, 1 week, g) HA-Fib, 6 weeks, l) AVA3.75 6 weeks. Immunohistochemistry for Collagen type II: b) HA-Fib, 1 week, e) AVA3.75, 1 week, h) HA-Fib, 6 weeks, m) AVA3.75 6 weeks. Immunohistochemistry for Collagen type I: c) HA-Fib, 1 week, f) AVA3.75, 1 week, i) HA-Fib, 6 weeks, n) AVA3.75 6 weeks

Interestingly, we observed already at only one week upon implantation the formation of a cartilaginous extracellular matrix, positive for Safranin O and type II collagen with typical chondrocytic morphology cells in all the experimental conditions (Figure 50A,B,D,E). After 3 (data not shown) and 6 weeks in vivo the Safranin O positive cartilaginous matrix (Figure 50G,L) became even more uniformly stained for type II collagen whereas type I collagen was expressed only in the outer fibrous tissue. Safranin O staining also indicated

the time lapse between 1 week and 3 weeks time point as the one in which scaffolds degraded. No nectrotic or pycnotic cells were found in the all the constructs.

Immunohistochemical analyses indicated a decrease with the time in culture of the deposition of type I collagen. Type I collagen displayed an intense staining and uniform spatial distribution throughout the whole cartilaginous constructs after 1 week in vivo (Figure 50C,F), in all the groups. At 6 weeks after implantation instead type I collagen was faintly stained in the center cartilaginous matrix and more strongly deposited at the borders of the implant, which corresponds to the fibrous capsule (Figure 50I,N). An opposite trend was instead showed by type II collagen, which was quite strongly deposited in the center cartilaginous part of the implant already at 1 week in vivo (Figure 50B,E). At 6 weeks, type II collagen was more uniformly and intensively present in the center cartilaginous tissue and completely negative in the outer fibrous capsule, surrounding the implant (Figure 50H,M). No major differences were observed when the engineered cartilage was generated with HA-FIB functionalized scaffolds.

Collagen type-X, MMP-13 and bone sialoprotein (BSP), checked in order to assess whether hypertrophy occurred in vivo, resulted all negative in all constructs (data not shown), so confirming to have obtained a stable chondrocytic cell phenotype in all experimental groups overtime.

In order to semi-quantitatively assess the quality of the tissue-engineered cartilage, a histological scoring system was used (Table 5). Statistically significant differences were found in the final score at 3 weeks between AVA5 and HA-Fib ($p<0.05$), and at 6 weeks between HA-Fib and both AVA3.75 ($p<0.001$) and AVA5 ($p<0.01$). This aspect is mainly due to a statistical difference found between the groups with and without Avastin® in the vascularization item at 3 and 6 weeks (Table 6).

Sample	**HA-Fib**			**AVA3.75**			**AVA5**		
Time point	1w	3w	6w	1w	3w	6w	1w	3w	6w
Scoring categories									
1. Intensity	0.82± 0.98	1.82± 0.87	2.70± 0.48	0.67± 0.78	1.82± 0.60	3.00±0. 00	1.00± 1.00	1.91±0. 54	2.64± 0.50
2. Density	0.55± 0.69	1.36± 0.50	2.10± 0.57	1.00± 0.95	1.64± 0.47	2.27±0. 65	1.00± 0.89	1.91±0. 83	2.45± 0.69
3. Morphology	1.27± 1.35	1.82± 0.40	2.50± 0.53	1.08± 1.00	1.73± 0.67	2.91±0. 30	1.36± 1.29	2.00±0. 63	2.55± 0.69
4. Uniformity	0.55±	1.64±	2.20±	0.92±	1.64±	2.55±0.	0.91±	1.36±0.	2.00±

	0.69	0.50	0.63	1.00	0.50	69	0.94	50	1.00
5. Calcifications	3.00± 0.00	3.00± 0.00	2.40± 0.52	3.00± 0.00	3.00± 0.00	2.91±0. 30	3.00± 0.00	3.00±0. 00	3.00± 0.00
6. Vascularization	2.67± 0.71	1.22± 0.67	1.38± 0.74	3.00± 0.00	1.78± 0.67*	2.78±0. 44†	2.78± 0.44	1.89±0. 60*	2.67± 0.50†
Final score	**8.85± 2.06**	**10.86 ±1.39**	**13.28 ±1.43**	**9.76± 1.87**	**11.6± 1.32**	**16.41± 1.13§**	**10.05 ±2.13**	**12.07± 1.41***	**15.3± 1.57†**

Table 6. Histological scoring evaluation (Note: Statistical differences evaluated between the scaffolds with and without Avastin at each time point) * p<0.05; † p<0.01; § p<0.001

The proposed score has been validated calculating the maximum (σmax) and overall (σov) variability. They were found to be 21.43% and 8.16%, respectively.

In order to better investigate the vessels ingrowth inside not reabsorbed constructs and its role for the overall quality of the neo-formed cartilage, immunofluorescence for CD31 has been performed (Figure 51A-D) and data were found to be consistent with the histological score assessment. No CD31+ endothelial cells were found inside the neo-formed matrix at 1 week, but they remained localized in the fibrotic capsule surrounding the tissue (data not shown). However, Figure 51A shows the situation at three weeks, where host vessels are infiltrating inside the construct not loaded with Avastin® (HA-FIB), so leading to a process ending to the breakdown of the tissue-engineered cartilage at later timepoints, as previously indicated in Figure 49. On the other hand, CD31-positive vessels remained confined at the borders of the tissue for AVA3.75 (Figure 51B) and AVA5 (Figure 51C) constructs, so both suggesting the capacity of the eluted Avastin® to effectively inhibit neo-angiogenesis and pointing out the 3 weeks time point as the most critical one. This aspect was quantitatively confirmed by vessels ingrowth quantification (Figure 51D). Indeed, a statistical significant difference ($p<0.05$) was found between HA-Fib constructs and the groups with Avastin®.

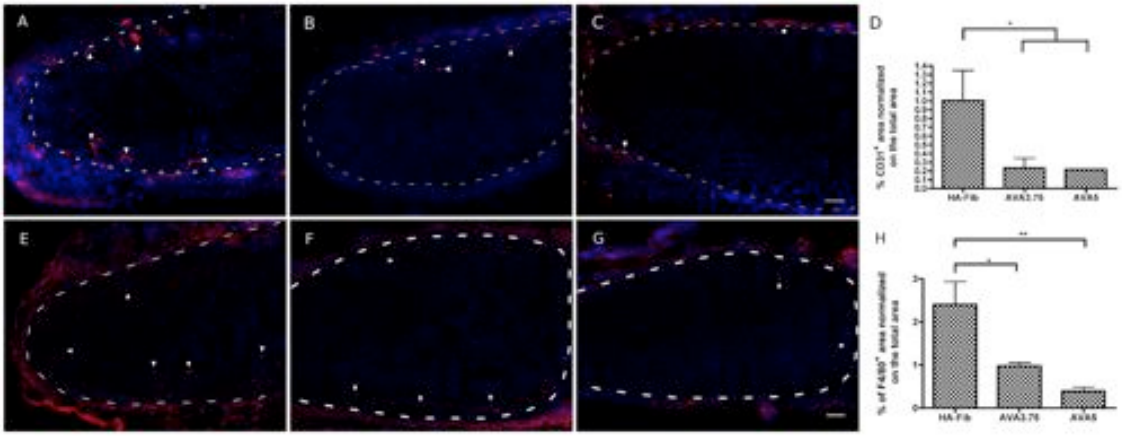

Figure 51. In vivo host vessel ingrowth. Immunofluorescence for CD31 at 3 weeks time point of a) HA-FIB, b) AVA3.75, c) AVA5 samples; d) vessels quantification. Inflammatory response at 3 weeks time point. Immunofluorescence for F4/80 of e) HA-FIB, f) AVA3.75, and g) AVA5 samples; h) migrated monocytes quantification

In order to deeply understand the in vivo degradation process of the constructs, immunofluorescence for F4/80 was performed, particularly focusing on 3 weeks time point. Figure 51E-H displays a higher presence inside the matrix of F4/80-positive murine cells in HA-Fib respect to AVA3.75 and AVA5 construct (Figure 51E-G), meaning that eluted Avastin® is able to inhibit host monocytes migration towards the implanted scaffold and the following differentiation into macrophages. Macrophages invasion inside the construct was correctly calculated quantifying F4/80-positive area respect to the whole section. Figure 51H shows how a statistically significant higher number of F4/80+ cells was found in the construct not loaded with Avastin® (HA-FIB) respect to the AVA3.75 and AVA5 groups.

Effect of the eluted Avastin® and scaffold degradation products on HUVEC proliferation

In order to better understand the process of the in vivo construct resorption, the effect of each scaffold component has been investigated (Figure 52A). Fibrin (FIB) degradation products were found to strongly enhance HUVEC proliferation, 1.71 ± 0.09-fold higher with respect to the positive control of HUVEC cultured in growth medium (GM). The presence of HA to the fibrin in the HA-FIB scaffolds appeared to reduce the proliferative effect of the FIB alone and brought it to the value of the GM (1.02±0.09). This aspect can be explained by the antiangiogenic effect of the high-molecular weight hyaluronic acid (HMW-HA) entrapped and released by the scaffold [Pardue et al, 2008]. Surnatants collected at day 7 for scaffolds composed of FIB and Avastin® showed a reduction of the HUVEC metabolic activity which is similar to that obtained with the HA-FIB composite

scaffolds, and, therefore, similar to the GM control. Noteworthy, degradation products of the AVA3.75 scaffolds (containing both HA and Avastin) showed that already at day one the released HA and Avastin® synergistically contribute to reduce the HUVEC rate of proliferation. At day 7 the degradated HA and the released Avastin® were able to reduce HUVEC proliferation to the one of the negative control, in which HUVEC were cultured with a lower % of FBS (AM) value.

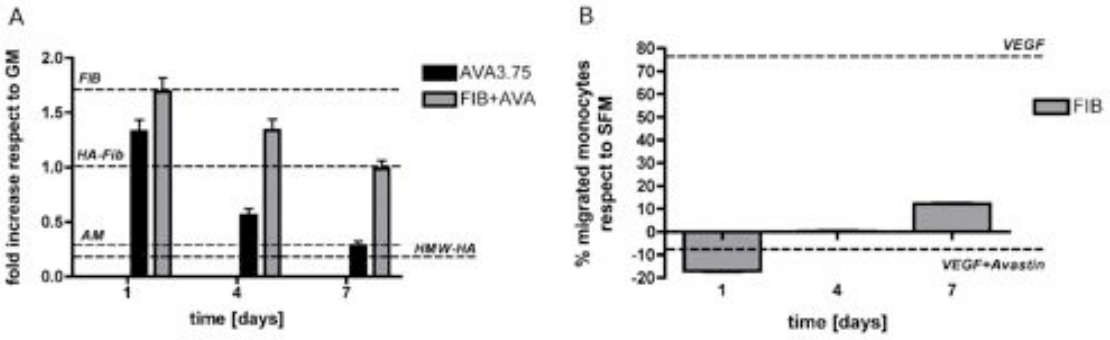

Figure 52. Scaffold components characterization. Single components of the scaffold, such as fibrin either alone (FIB) or with HA (FIB-HA) and high molecular weight HA alone (HMW-HA) were tested in a HUVEC proliferation assay (A) as controls together with the degradation products of scaffolds, made of HA-FIB supplemented with AVA3.75 (AVA3.75) or FIB supplemented with AVA 3.75 (FIB+AVA). Surnatants were collected after 7 days incubation at 37°C and at 5%CO2. HUVEC metabolic activity was shown as fold increase respect to growth medium (GM, positive control) for 1, 4 and 7 days of culture. Monocytes' migration assay (B) was assessed at 1, 4 and 7 days and performed on the degradation products of FIB alone scaffolds. Supplementation of VEGF alone or in combination with Avastin were used as controls

Effect of the eluted Avastin® and fibrin degradation products on monocytes migration

Confirming the results previously obtained by others [Zentilin et al, 2006], VEGF revealed to be a strong chemoattractant for monocytes – i.e 78.07±1.14% of migrated monocytes respect to the serum-free control group (SFM), as shown inFigure 52B. Bevacizumab, by blocking the VEGF signal, could reset this effect. Interestingly, degradation products obtained from FIB scaffolds represented a good stimulus for the migration of monocytes, with 12.28±1.18% of migrated monocytes more respect to SFM at day 7, while not significant differences were found for HA-FIB degradation products.

Discussions and conclusions

In this study, we investigated how the inhibition of angiogenesis could affect engineered cartilage development. Our work demonstrated that blocking of angiogenesis seems to be both essential for the implantation of an immature graft and fundamental in order to

faithfully recapitulate the avascular nature of the articular cartilage, so ensuring the formation of high-quality and stable cartilaginous engineered tissue.

Despite the great results recently obtained from CTE, new strategies are warranted in order to overcome the limitations intrinsic in the extensive, costly and time-consuming in vitro manufacturing process [Pelttari et al, 2009]. One possible approach relies on direct implantation of cell loaded 3D scaffolds, without any in vitro construct pre-conditioning. To this extent, here we proposed a strategy based on two main pillars: (i) the use of a chondrosupportive scaffold that can ensure the differentiation of seeded cells towards a chondrogenic phenotype, and (ii) the inhibition of the host vessels ingrowth in order to preserve the construct in the first phase upon implantation, so paving the way to long-term stability of newly formed cartilage.

First of all, we developed a scaffold based on well-established, FDA-approved materials in the CTE field, i.e. fibrin and HA, mixed in an original way. In this system, fibrin ensured the 3D porous structure and HA represented the chondrogenic stimulus, resulted to be essential for NC re-differentiation, as confirmed by the results from the in vitro differentiation assays. The proposed scaffold displayed a strong chondrosupportive capacity also in vivo, leading to the formation of newly formed cartilage with good quality already after 1 week, as shown by the strong positivity both to Safranin O staining and to immunohistochemistry for collagen type II.

Moreover, we hypothesized that inhibition of host vessel ingrowth in implanted constructs would have been essential in order to obtain stable engineered cartilage, by mimicking the environment of the native tissue. The strategy to block angiogenesis for cartilage regeneration has gained consents in the last few years. However, so far, only gene therapy approaches have been used to reach this goal: progenitor cells could be engineered to over-express autologous anti-angiogenic molecules, such as sFlt-1 [Matsumoto et al, 2009], endostatin [Jeng et al, 2010], and chondromodulin [Klinger et al, 2011]. To our knowledge this is the first time in which this goal has been pursued using a direct and clinically-oriented approach, by means of a drug-eluting scaffold. We fully demonstrated, by specific in vitro and in vivo assays, how the release of VEGF monoclonal antibody – i.e. bevacizumab – from our scaffold is both effective on endothelial cells proliferation and migration and, ultimately, fundamental for the stability of immature grafts upon direct implantation.

The release of Avastin® during the first weeks effectively blocked host vessels ingrowth, as verified by histological score and then further quantified from immunofluorescence for CD31, and resulted in a long-term stability of the construct loaded with Avastin®. Indeed,

ca. 82% of scaffolds without Avastin® (HA-Fib experimental group) completely degraded after 6 weeks in vivo, probably due to the host vessels and monocytes invasion started at the 3 weeks-time point. On the other hand, the presence of bevacizumab inside the constructs (AVA3.75 and AVA5 groups) contributed to strongly delaying construct invasion, so letting NC produce cartilaginous matrix and endogenous anti-angiogenic signals. To this extent, we also showed for the first time that fibrin degradation products strongly enhance the endothelial cell proliferation, so stimulating the unsuitable vascularization of the constructs and the following reabsorption of the implanted construct. This effect has been completely blocked by the combined effect of released bevacizumab and high-molecular weight HA. However, to better understand the role of bevacizumab, further investigations could be performed by using a different support scaffold characterized by inert materials and longer degradation time in order to unmask the effect of fibrin and HA in the system.

The degradation of the engineered constructs could be also explained by the inflammatory response induced post-implantation. Francioli et al [Francioli et al, 2011] and Luo et al [Luo et al, 2009] demonstrated how the level of maturation of cartilaginous tissues generated in vitro is correlated with a different profile of inflammatory chemokines production (e.g. IL-1β), and in particular how the in vitro pre-conditioning can mitigate the post-implantation inflammatory reaction. Thus, blocking the VEGF signaling might be useful to inhibit the infiltration of immune system cells – e.g. monocytes –, so alleviating the post-implantation inflammatory response. Implants in orthotopic and immunocompetent models could better explain these processes.

Finally, the chondrogenic capacity of different types of cells should be also tested in our system, in order to broad the clinical application scenario. It has been recently shown that bone marrow-derived mesenchymal progenitor cells (BMSC) undergo hyperthrophy, followed by formation of micro-ossicles after ectopic transplantation in immunodeficient mice [Pelttari et al, 2007; Henning et al, 2006]. VEGF plays an essential role during hypertrophy and ossification, therefore it could be essential to be able to control VEGF expression in case of mesenchymal progenitor cells, which tend to not have a stable chondrocytic phenotype. Next experiments will investigate whether the blocking of the VEGF signaling could help to overcome the above-mentioned problems and lead BMSC to a terminal differentiation as stable chondrocytes.

References

Ahmed T, Hincke MT, "Strategies for Articular Cartilage Lesion Repair and Functional Restoration",*Tissue Engineering Part B*(**2010**), 16: 305-330

Candrian C, Vonwil D, Barbero A, Bonacina E, Miot S, Farhadi J, Wirz D, Dickinson S, Hollander A, Jakob M, Li Z, Alini M, Heberer M, and Martin I, "Engineered Cartilage Generated by Nasal Chondrocytes Is Responsive to Physical Forces Resembling Joint Loading", *Arthrithis and Rheumatism* (**2008**), 58: 197–208

Davidenko N et al, "Collagen–hyaluronic acid scaffolds for adipose tissue engineering", *Acta Biomater* (**2010**), 6: 3957–3968

Davis HE et al, "Supplementation of Fibrin Gels with Sodium Chloride Enhances Physical Properties and Ensuing Osteogenic Response", *Acta Biomater* (**2010**)

Farndale RW, Buttle DJ, Barrett AJ, "Improved quantitation and discrimination of sulphated glycosaminoglycans by use of dimethylmethylene blue", *Biochim Biophys Acta* (**1986**), 883: 173-177

Francioli SE, Martin I, Sie CP, Hagg R, Tommasini R, Candrian C, Heberer M, Barbero A,"Growth Factors for Clinical-Scale Expansion of Human Articular Chondrocytes: Relevance for Automated Bioreactor Systems", *Tissue Engineering*(**2007**), 13: 1227-1234

Gibson LJ, Ashby MF, "Cellular solids: structure and properties", *2nd ed. Cambridge: Cambridge University Press*, (**1997**)

Grogan SP, Barbero A, Winkelmann V, Rieser F, Fitzsimmons JS, O'Driscoll S, Martin I, Mainil-Varlet P, "Visual histological grading system for the evaluation of in vitro-generated neocartilage", *Tissue Engineering* (**2006**), 12: 2141-2149

Grogan SP, Rieser F, Winkelmann V, Berardi S, Mainil-Varlet P, "A static, closed and scaffold-free bioreactor system that permits chondrogenesis in vitro", *Osteoarthritis and Cartilage* (**2003**), 11: 403-411

Henschen A et al., "Covalent Structure of Fibrinogen", *Ann. N. Y. Acad. Sci.* (**1983**), 8: 28-43

Ho STB, Cool SM, Hui SM, Hutmacher DW, "The influence of fibrin based hydrogels on the chondrogenic differentiation of human bone marrow stromal cells", *Biomaterials* (**2010**), 31: 38-47

Jeng L, Olsen BR, Spector M, "Engineering endostatin-producing cartilaginous constructs for cartilage repair using nonviral transfection of chondrocyte-seeded and mesenchymal-stem-cell-seeded collagen scaffolds", *Tissue Engineering Part A* (**2010**), 16: 3011- 3021

Kim DJ, et al, "Tissue-Engineered Allograft Tracheal Cartilage Using Fibrin/Hyaluronan Composite Gel and Its In Vivo Implantation", *The Laryngoscope*(**2010**), 120

Klinger P, Surmann-Schmitt, Brem M, Swoboda B, Distler J, Carl HD, Von der Mark K, Hennig FF, Gelse K, "Chondromodulin-I stabilizes the chondrocytes phenotype and inhibits endochondral ossification of cartilage repair tissue", *Arthritis & Rheumatism* (**2011**), 63: 2721-2731

Kubo S, Cooper GM, Matsumoto T, Phillippi JA, Corsi KA, Usas A, Li G, Fu FH, Huard J, "Blocking vascular endothelial growth factor with soluble Flt-1 improves the chondrogenic potential of mouse skeletal muscle-derived stem cells", *Arthritis & Rheumatism* (**2009**), 60: 155-65

Marcacci M, Berruto M, Brocchetta D, Delcogliano A, Ghinelli D, Gobbi A, Kon E, Pederzini L, Rosa D, Sacchetti GL, Stefani G, Zanasi S,"Articular cartilage engineering with Hyalograft C: 3-year clinical results",*Clin Orthop Relat Res*(**2005**), 435: 96

Matsumoto T, Cooper GM, Gharaibeh B, Meszaros LB, Li G, Usas A, Fu FH, Huard J, "Cartilage repair in a rat model of osteoarthritis through intraarticular transplantation of muscle-derived stem cells expressing bone morphogenetic protein 4 and soluble Flt-1", *Arthritis & Rheumatism* (**2009**), 60: 1390- 1405

Miot S, Gianni-Barrera R, Pelttari K, Acharya C, Mainil-Varlet P, Juelke H, Jaquiery C, Candrian C, Barbero A, Martin I, "In Vitro and In Vivo Validation of Human and Goat Chondrocyte Labeling by Green Fluorescent Protein Lentivirus Transduction", *Tissue Engineering Part C* (**2010**), 16: 11-21

Nguyen LH, Kudva AK, Guckert NL, Linse KD, Roy K,"Unique biomaterial compositions direct bone marrow stem cells into specific chondrocytic phenotypes corresponding to the various zones of articular cartilage",*Biomaterials*(**2010**), 32: 1327-1338

Nyberg P, Xie L, Kalluri R,"Endogenous inhibitors of angiogenesis", *Cancer Research* (**2005**), 65: 3967-3979

Pardue EL, Ibrahim S, Ramamurthi A, "Role of hyaluronan in angiogenesis and its utility to angiogenic tissue engineering", *Organogenesis* (**2008**), 4: 203-214

Park SH et al, "Potential of Fortified Fibrin/Hyaluronic Acid Composite Gel as a Cell Delivery Vehicle for Chondrocytes", *Artif Org* (**2009**), 33: 439–447

Pelttari K, Wixmerten A, Martin I, "Do we really need cartilage tissue engineering?", *Swiss Med Weekly* (**2009**), 139: 602–609

Spiller KL, Maher SA, Lowman AM, "Hydrogels for the repair of articular cartilage defects", *Tissue Engineering Part B* (**2011**); in press (doi: 10.1089/ten.TEB.2011.0077)

Strobel S, Loparic M, Wendt D, Schenk AD, Candrian C, Lindberg RLP, Moldovan F, Barbero A, Martin I, *Arthritis Research & Therapy* (**2010**), 12: R34

Takita H, Kikuchi M, Sato Y, Kuboki Y, "Inhibition of BMP-Induced Ectopic Bone Formation by an Antiangiogenic Agent (Epigallocatechin 3-Gallate)", *Connective Tissue Research* (**2002**), 43: 520

Tan H et al, "Gelatin/chitosan/hyaluronan scaffold integrated with PLGA microspheres for cartilage tissue engineering", *Acta Biomater* (**2009**), 5: 328–337

Tay AG, Farhadi J, Suetterlin R, Pierer G, Heberer M, Martin I, "Cell yield, proliferation, and postexpansion differentiation capacity of human ear, nasal, and rib chondrocytes", *Tissue Eng* (**2004**), 10: 762–770

Visna P, Pasa L, Cizmar I, Hart R, Hoch J, "Treatment of deep cartilage defects of the knee using autologous chondrograft transplantation and by abrasive techniques—a randomized controlled study", *Acta Chir Belg* (**2004**), 104: 709-14

Wang Y, Fei D, Vanderlaan M, Song A, "Biological activity of bevacizumab, a humanized anti- VEGF antibody in vitro", *Angiogenesis* (**2004**), 7: 335-345

Wu SC, Chang JK, Wang CK, Wang GJ, Ho ML,"Enhancement of chondrogenesis of human adipose derived stem cells in a hyaluronan-enriched microenvironment", *Biomaterials*(**2010**), 31: 631- 640

Zentilin L, Tafuro S, Zacchigna S, Arsic N, Pattarini L, Sinigaglia M, Giacca M, "Bone marrow mononuclear cells are recruited to the sites of VEGF-induced neovascularization but are not incorporated into the newly formed vessels", *Blood*(**2006**), 107: 3546-3554

Zhao H et al, "Fabrication and physical and biological properties of fibrin gel derived from human plasma", *Biomed Mater* (**2008**), 3

4. Ongoing works and future perspectives

Vascular project

Although, we produced a lot of convincing experimental data demonstrating the efficiency of the proposed approach in vascular tissue engineering, important evidences from proper in vivo orthotopic models are still missing. Preliminary results provided by the in vivo rabbit studyon the aorto-aortic bypass model (**par. 2.4**), although not conclusive, were encouraging and paved the way for further dedicated experiments.

Taken together all the data produced under the framework of this project represents a strong substrate for an extensive preclinical study, which could end up in the final validation of these differentiating vascular grafts.

Osteochondral project

After assessing the proof-of-principle of the beneficial effect of blocking angiogenesis with functionalized hyaluronate-fibrin scaffold for formation of a mature cartilage by using a chondrocytic cell type (**par. 3.2**), we now want to apply the same concept to a more clinical relevant cell source, such as mesenchymal progenitor cells. Following our strategy, we identify bonemarrow as a suitable source of mesenchymal progenitor cells for articular cartilage regeneration for its ease of harvesting, which could allow an intra-operative intervention. Moreover, bone marrow-derived stem cells (BMSCs) could be also recruited directly in vivo upon implantation from the bone underlying the cartilage. Due to their high proliferation and multilineage differentiation capacity, BMSCs represent promising candidates for regeneration of tissue and organ systems including cartilage. BMSCs fulfill the demands for a use in tissue engineering of articular cartilage since they can be conveniently manipulated to differentiate towards chondrocytes in vitro.

However, it has been shown in literature by different groups in the last few years that BMSCs undergo to an undesired and premature hypertrophic phenotype leading to a strong in vivo calcification and formation of micro-ossicles after ectopic transplantation in immunodeficient mice, so showing problems in terms of cartilage terminal differentiation. Moreover, other recent results showed that BMSCs also could undergo to an endochondral process by initiating remodeling via the production of specific matrix

metalloproteinases (MMP) and attract blood vessels by releasing VEGF. Looking at this scenario, we hypothesize that blocking the VEGF signaling by releasing a monoclonal VEGF-antibody (i.e. Avastin) from the scaffold could avoid the above-mentioned problems and lead BMSCs to terminal differentiation in chondrocytes.

Future studies will aim at investigating the in vivo chondrogenic differentiation potential of human expanded BMSC directly seeded on a 3D scaffold, without in vitro pre-commitment into a chondrocytic lineage. In particular, we hypothesize that initial blocking of angiogenesis will allow in vivo chondrogenesis and the achievement of a stable chondrocytic phenotype, also in an orthotopic large animal model. This step would finally allow the realization of bilayered scaffolds for osteochondral repair where a single population of BMSCs could differentiate into two separate phenotypes, i.e. osteogenic and chondrogenic lineages.

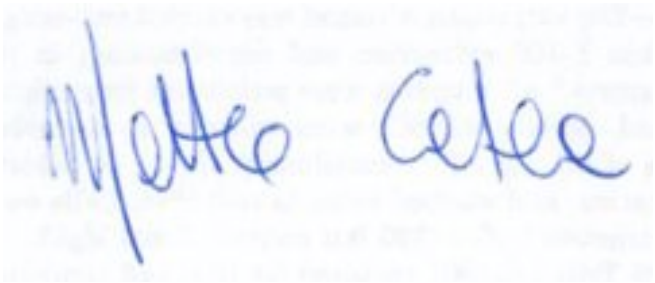

Acknowledgments

Per cercare di trasmettere al meglio i miei sentimenti verso le persone che direttamente o indirettamente hanno contribuito alla stesura di questa tesi, così come al raggiungimento di questo traguardo, questa sezione la scriverò nella mia lingua madre.

Questo lavoro, lo sappiamo, è diverso da tutti gli altri: ti trascina, ti prende, e se ti lasci trasportare rischia di riempire la tua vita. Il laboratorio quindi diventa, vuoi o non vuoi, la tua seconda famiglia, e poter lavorare in un ambiente cordiale e stimolante fa tutta la differenza del mondo. E qui in questi anni, io ho trovato decisamente il mio habitat.

Ovviamente non posso che non iniziare dalla relatrice di questa tesi. Anche se questo termine sminuisce un pò il ruolo che lei ha avuto durante questi 4 anni vissuti fianco a fianco. Nei ringraziamenti della mia tesi di laurea specialistica scrivevo "*[…] La Prof.ssa Trombetta non ha mai smesso di credere in me, dimostrandosi attenta e disponibile in ogni occasione. Basti pensare solamente che vicino al mio letto di ospedale, dopo l'operazione, oltre ai miei genitori e ai miei amici più stretti c'era Lei! Le sue parole di conforto, di insegnamento e a volte di rimprovero mi hanno aiutato a crescere sia come studente che come persona. Penso che ogni studente vorrebbe, o dovrebbe, incontrarLa sulla sua strada*". Non posso che confermare queste parole, e aggiungere anche che, mentre alcune di quelle persone che mi affiancavano vicino a quel famoso "*letto di ospedale*" le ho lasciate per strada, lei è ancora lì…

Un ringraziamento molto sentito per tutto quello che ha saputo darmi nel corso di questi anni va ad Alberto. A volte si fa fatica a ricordarsi come si era, lavorativamente parlando, all'inizio di un percorso. Io so solamente che in questi 4 anni Alberto ha contribuito in maniera a dir poco decisiva a trasformarmi da un semplice ragazzino entusiasta e pieno di passione, in uno scienziato vero (o almeno spero!), trasmettendomi i trucchi del mestiere e una dedizione smodata per questo lavoro. Insomma è stato un vero mentore da cui ho preso a piene mani, e di cui sperodi poter tramandare degnamento "il tocco".

Un grazie con tutto il cuore va a Franca, molto più che una collega, una vera amica. Una di quelle persone di cui con gioia potrò sempre dire che ho avuto la fortuna di incontrare. Se sono arrivato a vedere lo striscione del traguardo è anche merito suo, mi ha sempre spronato, stimolato, aiutato, incitato, confortato, mettendomi spesso davanti anche alle sue di priorità. Ho cercato di non perdere mai l'occasione di trasmetterle la mia stima e il mio affetto, ma in questa sede voglio approfittare per ribadire il concetto…Dai Francaaaaa!!!!

Non posso di certo dimenticarmi delle mie compagne di viaggio, Sara e Liliana, con cui ho condiviso molte molte ore della mia vita. Quello che penso è che questo è un lavoro di equipe e quindi se sono arrivato in fondo il merito è anche delle mie compagne di squadra: grazie per avermi supportato e sopportato!

Uscito dal laboratorio le due facce più gradite del corridoio per un break ristorativo, sono state di certo quelle di Alessio, Max e Nino. Grazie per aver condiviso con me le lamentele, i sogni, la stanchezza, i momenti di gioia, i progetti e i fanta-progetti…siete stati fondamentali.

Una menzione ci tengo a farla anche al Dott. Spadaccio, o meglio a Cristiano, o meglio ancora a Chicchi. Una delle persone più brillanti e appassionate che io conosca, il suo

entusiasmo travolgente e la sua competenza sono state e resteranno per me fonte d'ispirazione. Decisamente un modello da seguire. Daje chicchiiii!!!!!!

Una persona che mi sento di ringraziare, forse sopra a tutti gli altri, è proprio quella che, per sua stessa ammissione, "*non ha contribuito a scrivere nemmeno una parola in questa tesi*". Il BuonT, al secolo Stefano, è stato il compagno di viaggio ideale in questo lungo percorso, un coinquilino perfetto. Sempre presente, sia nei momenti di divertimento e chillin' che, soprattutto, in quelli di difficoltà. Saper di poter contare SEMPRE su un amico è una cosa senza prezzo, e per cui non smetterò mai di ringraziare. Abbiamo condiviso tantissimo in questi 3 anni, le mangiate all'Hard Rock, il gelato da Angelo, gli sfottò a Fabio e agli altri del quartiere, le improvvisate a Perugia e non solo, le serate "alla faccia di Enzetto". Insomma tanti ricordi intensi e meravigliosi, che porterò sempre con me e sono sicuro riusciranno a strapparmi un sorriso anche tra 20 anni. Boomshakalaka BuonT!!!!

La cosa più difficile in questi giorni finali è stata sicuramente lasciare l'appartamento che custodisce gelosamente tantissimi ricordi meravigliosi,ma ringrazierò sempre di aver avuto la fortuna di averli vissuti…anche grazie all'altro mio splendido coinquilino, il Buon Uca. Mi mancherai.

Un terzo del mio periodo di dottorato l'ho trascorso in quel di Basilea. Prima di andarci, sapevo a mala pena dove si trovasse geograficamente, e ricordo ancora l'angoscia dei primi giorni dove tutto solo, mi sono trovato di fronte una città grigia, piovosa e fredda. Ma in quel di Basel, ho trovato davvero una famiglia, un posto che non vedo l'ora di poter chiamare casa. Il mio grazie si estende veramente a tante persone che sono entrate prepotentemente nella mia vita…a cominciare da Anna. Lavorarci insieme ogni giorno fianco a fianco è stato stupendo. Con i suoi modi unici mi ha insegnato l'ABC della tecnica e della teoria, mi ha formato e plasmato. Averla incontrata sul mio percorso è stata una fortuna irripetibile, mi ha dato il carburante necessario per tener viva la mia passione ed il suo approccio quotidiano alla scienza è stato per me un esempio decisivo. Se ci aggiungiamo poi il fatto che è una persona squisita e genuina come poche, si capisce perchè io spero di poter ancora condividere tanto insieme a lei.

Un enorme ringraziamento va ad Ivan. Mi ricordo la prima volta che sono entrato nel suo ufficio, in punta di piedi e con una paura incredibile di fare la classica *brutta figura*. Ma quelle paure sono svanite all'istante: Ivan è l'esempio di come non serva "sentirsi grandi" per esserlo davvero. La sua umiltà e la sua disponibilità, sia da un punto di vista professionale ma soprattutto umano, sono cosa rara a certi livelli. Mi ha accolto come uno dei suoi e mi ha messo nelle condizioni di dare il massimo, illuminandomi letteralmente ogni qualvolta andavo da lui per un consiglio. Il fatto che abbia creduto in me è una cosa che mi riempie di orgoglio, e mi da una carica incredibile per tagliare questo *traguardo…parziale ovviamente!* (….per usare le sue stesse parole….)

Un omaggio particolare a tutti i ragazzi del laboratorio, che mi hanno accolto e coinvolto da subito, dandomi supporto sia dentro che fuori dal laboratorio, facendomi sentire da subito a casa. Quindi grazie ad Elia, Silvia, Paul, Sinan, Prasad, Celeste, Adam, Andrea, Sandra, Clem, Vale, Nunzia, Marianna, Stefano, Francine…e scusatemi se ho dimenticato qualcuno.

Dopodiché ci sono tutti gli altri, la mia famiglia di emigranti. Sarà per colpa del periodo di enormi cambiamenti occorsi nella mia vita, fatto sta che in pochissimo tempo Ema e Fra, O' Professore, Davide, Il Doc e Mina, La Gnappetta, Cate, e tutti gli altri, masoprattutto la mia Small, sono entrati di diritto nella mia vita cambiandola radicalmente. In meglio, si intende! E per questo mi ritengo molto fortunato. Vorrei spendere tantissime parole per ringraziarli a dovere, ma fortunatamente avrò modo di farlo di persona tra poco…

Sicuramente non voglio scordarmi dei miei amici…Dario e Settimio su tutti. Nemmeno le Alpi sono riuscite ad allontanarci veramente, sempre i primi a condividere successi e disavventure. Due persone meravigliose, due amici straordinari.Dopodiché un pensiero ai miei amici storici (Il Praino, Capotio, Matteo, Zio, Dindo, Ciallù, Il Capitano, Palovo, Jaric, Pisellino e DiBi), ci vediamo sempre meno ormai, ma il modo in cui li sento vicini non è cambiato di una virgola. E quando riusciamo a stare insieme le sensazioni sono sempre le stesse. Grazie per non cambiare mai!

Alla fine di tutto, ma di certo non per ordine di importanza, c'è la mia famiglia. Mamma, papà e Roberta. Più passano gli anni e più vi sento vicini, più le cose intorno a me cambiano repentinamente e più voi diventate sempre il mio punto di riferimento. Se sono quello che sono è merito vostro, che avete saputo dare respiro ai miei sogni, che giorno dopo giorno mi avete sostenuto concretamente, che mi amate senza chiedere nulla in cambio. Sentirmi parte di questa famiglia mi inorgoglisce e rassicura…grazie per essere come siete.

Insomma ci siamo. Non nascondo che mentre scrivevo queste righe avevo un perenne ed enorme groppo in gola, dettato dalla consapevolezza che questa splendida esperienza è giunta al capolinea. A peggiorare tutto ciò, c'è un armadio vuoto e una stanza ormai spoglia intorno a me. Ma queste sensazioni sono stupende se si pensa che sono figlie di tantissimi ricordi felici accumulati nel corso di questi anni.

Grazie quindi a tutti voi, compagni inconsapevoli di questo bellissimo viaggio!

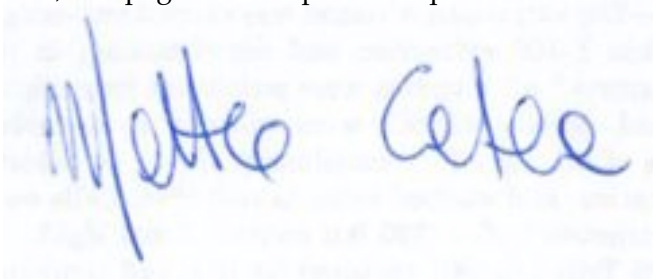

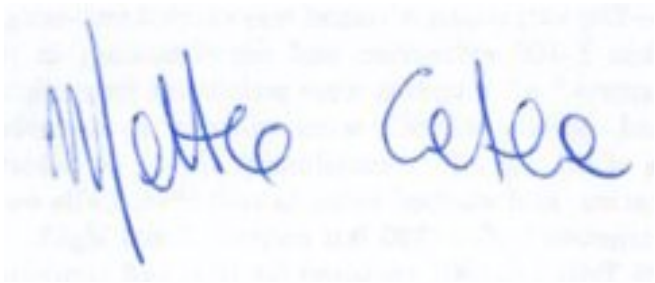

List of Publications

- Rainer A, **Centola M**, Spadaccio C, Gherardi G, Licoccia S and Trombetta M, "Comparative studies of different techniques for the sterilization of poly-L-lactide electrospun microfibers: effectiveness vs. material degradation", International Journal of Artificial Organs 2010, 33 (2): 76-85;
- Spadaccio C, Rainer A, **Centola M**, Trombetta M, Lusini M, Chello M, Covino E, Toyoda Y and Genovese J, "A heparin releasing scaffold for stem cells: a differentiating device for vascular aims", Regenerative Medicine, 2010, 5 (4): 645-655;
- **Centola M**, Rainer A, Spadaccio C, De Porcellinis S, Genovese JA and Trombetta M, "Combining electrospinning and fused deposition modeling for the fabrication of multilayered vascular grafts", Biofabrication 2010, 2 (1) 014102;
- Spadaccio C, Rainer A, Trombetta M, **Centola M**, Lusini M, Chello M, Covino E, Coccia R, De Marco F, Toyoda Y and Genovese JA, "A G-CSF functionalized scaffold for stem cells seeding: a differentiating device for cardiac purposes", Journal of Cellular and Molecular Medicine 2010, 15 (5): 1096-1098;
- Rainer A, **Centola M,** Spadaccio C, De Porcellinis S, Abbruzzese F, Genovese JA and Trombetta M, "A biomimetic three-layered compartmented scaffold for vascular tissue engineering", Conf Proc IEEE Eng Med Biol Soc. 2010, 1: 843-846;
- Spadaccio C, De Porcellinis S, Rainer A, **Centola M**, De Marco F, Chello M, Trombetta M and Genovese JA, "A G-CSF Functionalized PLLA Scaffold for Wound Repair: an In Vitro Preliminary Study", Conf Proc IEEE Eng Med Biol Soc. 2010, 1: 839-842;
- **Centola M**, Giannitelli SM, De Porcellinis S, Vadalà G, Carotti S, Spadaccio C and Rainer A, "Free-form fabrication of biopolymeric scaffolds for osteochondral segment regeneration", Tissue Eng Part A 2010, 16 (8): A1-A29;
- Falavolti C, Rainer A, **Centola M**, Trombetta M, Abbruzzese F, Gidaro S, Sergi F, Buscarini M, "The differentiation of humane adult mesenchimal stem cells of bone marrow (hMSC) into urothelial cells on bio-engineering support (scaffold): preliminary experience of tissue engineering", Urologia 2011, 78 (3): 203-205;
- **Centola M**, Marsano A, Abbruzzese F, Vadalà G, Scotti C, Barbero A, Martin I,

Trombetta M and Rainer A, "Blocking of angiogenesis is required for the successful implantation of an immature graft during neo-cartilage formation", Biomaterials 2012, *submitted*

List of Conference Abstracts

- **Centola M**, Rainer A, Giannitelli SM, Vadalà G and Trombetta M, "Fabbricazione di schiume vetroceramiche bioattive con geometria patient-specific per applicazioni nella medicina rigenerativa", in XVII Congresso Nazionale della Società Italiana di Biomeccanica in Ortopedia e Traumatologia 2009, Firenze
- **Centola M**, Giannitelli SM, De Porcellinis S, Vadalà G, Carotti S, Spadaccio C and Rainer A, "Free-form fabrication of biopolymeric scaffolds for osteochondral segment regeneration" in Bone-Tec 2009, Hannover
- **Centola M**, Rainer A, Spadaccio C, De Porcellinis S, Genovese JA and Trombetta M, "Combining electrospinning and fused deposition modeling for the fabrication of multilayered vascular grafts", in Termis¬-EU 2010, Galway
- **Centola M**, Rainer A, Giannitelli SM, Spadaccio C, De Porcellinis S, Genovese JA and Trombetta M, "Combining electrospinning and fused deposition modeling for the fabrication of a hybrid vascular grafts", in Italian Society for Biomaterials 2010, Genova
- Marsano A, Perugini V, **Centola M**, Güven S, Banfi A, Meikle ST, Guildford AL, Santin M and Martin I, "In vivo chondrogenesis by using antiangiogenic peptides", in European Society for Biomaterials 2011, Dublin
- Spadaccio C, Rainer A, **Centola M**, Chello M, Covino E, Trombetta M and Genovese JA, "Electrospinning of Drug Releasing Three-Layer Vascular Graft: New Alternative in Cardiovascular Tissue Engineering " in Bioprinting and Biofabrication 2009, Bordeaux
- Denaro V, Vadalà G, Rainer A, Loppini M, **Centola M** and Trombetta M, "Smart nanofiber membrane for annulus fibrosus repair and augmentation" in Termis-World Conference 2009, Seoul
- Spadaccio C, Rainer A, **Centola M**, Chello M, Covino E, Trombetta M, Toyoda and Genovese JA, "A Heparin Releasing Scaffold for Stem Cell Seeding: a New Differentiating Device for Vascular Purpose" in Chine-Europe symposium on Biomaterials in Regenerative Medicine 2009, Barcellona

- Denaro V, Vadalà G, Rainer A, Loppini M, **Centola M** and Trombetta M, "Bioactive micro-structured scaffold for annulus fibrosus repair and regeneration", in EFORT 2010, Madrid
- Vadalà G, Rainer A, **Centola M**, Loppini M, Carotti S, Morini S, Trombetta M and Denaro V, "Functionalized PCL surfaces drive Osteo/chondrogenic differentiation of human Bone Marrow Mesenchymal Stem Cells", in Termis-EU 2010, Galway
- Vadalà G, Rainer A, Giannitelli SM, **Centola M**, Trombetta M and Denaro V, "Bioactive glass-ceramic foams seeded with human Mesenchymal Stem Cells generate ectopic bone in vivo", in Italian Orthopedic Research Society 2010, Pavia
- Vadalà G, Rainer A, **Centola M**, Loppini M, Carotti M, Morini S, Trombetta M and Denaro V, "Functionalized PCL Surfaces Drive Osteo/Chondrogenic Differentiation of Human Bone Marrow Mesenchymal Stem Cells", in Italian Orthopedic Research Society 2010, Pavia
- **Centola M**, Rainer A, Spadaccio C, Abbruzzese F, Giannitelli SM, Liverani L, De Porcellinis S, Genovese JA and Trombetta M, "Combining electrospinning and fused deposition modeling for the fabrication of a hybrid vascular grafts", in National Bioengineering Group 2010, Torino
- Giannitelli SM, Rainer A, Vadalà G, **Centola M**, Denaro V and Trombetta M, "Bioactive glass-ceramic foams seeded with human Mesenchymal Stem Cells generate ectopic bone in vivo", in European Society for Biomaterials 2010, Tampere
- Falavolti C, Rainer A, **Centola M**, Trombetta M, Abbruzzese F, Gidaro S and Buscarini M, "La differenziazione delle cellule staminali mesenchimali su supporto di acido polilattico funzionalizzato con fattori di crescita per il differenziamento in un bilayer urotelio-muscolo. Esperienza preliminare", in SIU 2010, Milano
- Giannitelli SM, Rainer A, Accoto D, **Centola M**, De Porcellinis S, Trombetta M and Denaro V, "Un approccio bioispirato per il design e la prototipazione rapida di scaffold per applicazioni ortopediche", in SIOT 2010, Roma
- Vadalà G, Rainer A, Loppini M, **Centola M**, Trombetta M and Denaro V, "Scaffold micro-strutturati bioattivi per la riparazione e la rigenerazione dell'anello fibroso", in SIOT 2010, Roma
- Rainer A, Vadalà G, Giannitelli SM, **Centola M**, Trombetta M and Denaro V, "Schiume bioattive di vetro-ceramica seminate con cellule staminali mesenchimali umane per la produzione di tessuto osseo ectopico in vivo", in SIOT 2010, Roma